

12-2010

CHARACTERIZING AND TREATING THE NEUROPATHOLOGY OF TUBEROUS SCLEROSIS COMPLEX IN THE MOUSE

Sharon W. Way

Follow this and additional works at: https://digitalcommons.library.tmc.edu/utgsbs_dissertations



Part of the [Behavioral Neurobiology Commons](#), [Developmental Neuroscience Commons](#), [Molecular and Cellular Neuroscience Commons](#), and the [Molecular Genetics Commons](#)

Recommended Citation

Way, Sharon W., "CHARACTERIZING AND TREATING THE NEUROPATHOLOGY OF TUBEROUS SCLEROSIS COMPLEX IN THE MOUSE" (2010). *The University of Texas MD Anderson Cancer Center UTHealth Graduate School of Biomedical Sciences Dissertations and Theses (Open Access)*. 103.
https://digitalcommons.library.tmc.edu/utgsbs_dissertations/103

This Dissertation (PhD) is brought to you for free and open access by the The University of Texas MD Anderson Cancer Center UTHealth Graduate School of Biomedical Sciences at DigitalCommons@TMC. It has been accepted for inclusion in The University of Texas MD Anderson Cancer Center UTHealth Graduate School of Biomedical Sciences Dissertations and Theses (Open Access) by an authorized administrator of DigitalCommons@TMC. For more information, please contact digitalcommons@library.tmc.edu.

**CHARACTERIZING AND TREATING THE NEUROPATHOLOGY OF
TUBEROUS SCLEROSIS COMPLEX IN THE MOUSE**

A
DISSERTATION

Presented to the Faculty of
The University of Texas
Health Science Center at Houston
and
The University of Texas
M.D. Anderson Cancer Center
Graduate School of Biomedical Sciences
in Partial Fulfillment

of the Requirements

for the Degree of

DOCTOR OF PHILOSOPHY

by
Sharon Win Way, B.A.

Houston, TX

December 2010

ACKNOWLEDGEMENTS

I owe so much to the following people for making this dissertation possible:

My advisor, Dr. Michael J. Gambello, for being the epitome of the word “mentor”. You have provided so much patience, guidance, encouragement, and support to me throughout these years, despite all my flaws. I am lucky to have had the privilege of being your student.

My committee members, both past and present – Drs. Gil Cote, Seonhee Kim, Pramod Dash, Michael Blackburn, Jacqueline Hecht, and Hope Northrup – I have known most of you throughout my years at graduate school, and you have been unfailingly supportive throughout it all, both personally and professionally. Thank you for being there for me.

My fellow lab members – Jim McKenna, Michelle Reith, Ulrike Mietzsch, and Henry Wu – I could not ask for a better group of people to work with. You are my friends who just happen to share lab space with me, and I could not have come this far without you.

My friends – I’m afraid that I’ll forget to name someone, so you know who you are. I love you all and thank you so much for everything you’ve done for me. Graduate school would not have been anywhere near as fun without each and every one of you.

And finally, my family – both current and future. My parents and brother for being my foundation, and my future family, particularly my fiancé, for being my keystone. I cannot begin to express how lucky I feel to have you all in my life, so I will just keep it simple – Thank you. I love you.

CHARACTERIZING AND TREATING THE NEUROPATHOLOGY OF TUBEROUS SCLEROSIS COMPLEX IN THE MOUSE

Publication No. _____

Sharon Win Way, Ph.D.

Supervisory Professor: Michael J. Gambello, M.D., Ph.D.

Tuberous sclerosis complex (TSC) is a multisystem, autosomal dominant disorder affecting approximately 1 in 6000 births. Developmental brain abnormalities cause substantial morbidity and mortality and often lead to neurological disease including epilepsy, cognitive disabilities, and autism. TSC is caused by inactivating mutations in either *TSC1* or *TSC2*, whose protein products are known inhibitors of mTORC1, an important kinase regulating translation and cell growth. Nonetheless, neither the pathophysiology of the neurological manifestations of TSC nor the extent of mTORC1 involvement in the development of these lesions is known. Murine models would greatly advance the study of this debilitating disorder. This thesis will describe the generation and characterization of a novel brain-specific mouse model of TSC, *Tsc2^{flox/ko};hGFAP-Cre*. In this model, the *Tsc2* gene has been removed from most neurons and glia of the cortex and hippocampus by targeted Cre-mediated deletion in radial glial neuroprogenitor cells. The *Tsc2^{flox/ko};hGFAP-Cre* mice fail to thrive beginning postnatal day 8 and die from seizures around 23 days. Further characterization of these mice demonstrated megalencephaly, enlarged neurons, abnormal neuronal migration, altered progenitor pools, hypomyelination, and an astrogliosis. The similarity of these defects to those of TSC patients establishes this mouse as an excellent model for the study of the neuropathology of TSC and testing novel therapies. We further describe the use of this mouse model to assess the therapeutic

potential of the macrolide rapamycin, an inhibitor of mTORC1. We demonstrate that rapamycin administered from postnatal day 10 can extend the life of the mutant animals 5 fold. Since TSC is a neurodevelopmental disorder, we also assessed *in utero* and/or immediate postnatal treatment of the animals with rapamycin. Amazingly, combined *in utero* and postnatal rapamycin effected a histologic rescue that was almost indistinguishable from control animals, indicating that dysregulation of mTORC1 plays a large role in TSC neuropathology. In spite of the almost complete histologic rescue, behavioral studies demonstrated that combined treatment resulted in poorer learning and memory than postnatal treatment alone. Postnatally-treated animals behaved similarly to treated controls, suggesting that immediate human treatment in the newborn period might provide the most opportune developmental timepoint for rapamycin administration.

TABLE OF CONTENTS

Acknowledgements.....	iii
Abstract.....	iv
Table of Contents.....	vi
List of Figures.....	viii
Abbreviations.....	x
Chapter One: <i>Background and Introduction</i>	1
Introduction.....	2
Clinical Features of Tuberous Sclerosis Complex	3
Neuropathology of Tuberous Sclerosis Complex	4
Genetics of TSC.....	6
Hamartin, tuberin, and the mTORC1 pathway.....	8
Drosophila Homologues of <i>TSC1</i> and <i>TSC2</i>	12
Mouse Models of TSC Neuropathology.....	13
Rapamycin and the PI3K/Akt/mTOR pathway.....	15
Summary.....	18
Chapter Two: <i>Creation and Characterization of the Tsc2^{flx/flx} Mouse</i>	19
Introduction.....	20
Materials and Methods.....	21
Results.....	25
Discussion.....	31
Chapter Three: <i>Creation and Characterization of the Tsc2^{flx/ko}; hGFAP-Cre Mouse</i>	33
Introduction.....	34
Materials and Methods.....	35
Results.....	38
Discussion.....	59
Chapter Four: <i>Rapamycin Treatment of the Tsc2^{flx/ko}; hGFAP-Cre Mouse</i>	68
Introduction.....	69
Materials and Methods.....	72
Results.....	74
Discussion.....	83

Chapter Five: <i>Behavioral Testing of Rapamycin-Treated Tsc2^{flox/ko}; hGFAP-Cre</i>	92
<i>Mouse</i>	
Introduction.....	93
Materials and Methods.....	94
Results.....	99
Discussion.....	105
Chapter Six: <i>Significance and Future Directions</i>	109
Introduction.....	110
mTOR and Neuronal Migration.....	112
Migration and the Cell Cycle.....	112
Migration and the Rho Family Small GTPases.....	115
mTOR and Myelination.....	118
Myelination and Migration.....	118
Myelination and Axonal Surface Molecules.....	119
Myelination and Neuronal Activity.....	120
Model Summary.....	121
Additional Future Studies.....	121
Creation of a tuber-based mouse model.....	121
Further investigation of differentiation and proliferation defects.....	123
Characterization of seizure phenotype.....	125
Conclusion.....	126
Vita.....	152

LIST OF FIGURES

Figure 1.1	The mTOR network.....	9
Figure 2.1	Generation of the <i>Tsc2^{neo}</i> allele.....	22
Figure 2.2	Generation of the <i>Tsc2^{flox}</i> and <i>Tsc2^{ko}</i> allele.....	23
Figure 2.3	Analysis of the <i>Tsc2^{neo}</i> allele.....	26
Figure 2.4	Comparison of organs of wild type vs <i>Tsc2^{flox/flox}</i> mice.....	28
Figure 2.5	Analysis of the <i>Tsc2^{ko}</i> allele.....	30
Figure 3.1	Generation of <i>Tsc2^{flox/ko};hGFAP-Cre</i> mice.....	40
Figure 3.2	Cerebral cortical defects and up-regulation of mTORC1 in cortical neurons and astrocytes in <i>Tsc2^{flox/ko};hGFAP-Cre</i> mice.....	43
Figure 3.3	Hippocampal defects and up-regulation of mTORC1 in hippocampal neurons and astrocytes in <i>Tsc2^{flox/ko};hGFAP-Cre</i> mice.....	45
Figure 3.4	Post-natal developmental analysis of <i>Tsc2^{flox/ko};hGFAP-Cre</i> mice.....	47
Figure 3.5	Lamination defects in the <i>Tsc2^{flox/ko};hGFAP-Cre</i> mice.....	50
Figure 3.6	Cortical neural progenitor pool analysis at embryonic day E14.5.....	53
Figure 3.7	Astrogliosis in the <i>Tsc2^{flox/ko};hGFAP-Cre</i> mice.....	55
Figure 3.8	Postnatal developmental analysis of hypomyelination and oligodendrocytes in the mutant.....	58
Figure 4.1	Rapamycin treatment cohorts.....	71
Figure 4.2	Postnatal rapamycin dosage of 0.1 mg/kg attenuates mTORC1 expression.....	75
Figure 4.3	Comparison of rapamycin treatment cohorts.....	77
Figure 4.4	Rapamycin reduces cortical thickness, cell size, and alleviates lamination defects.....	80
Figure 4.5	Prenatal rapamycin treatment alleviates cortical layer defect.....	82
Figure 4.6	Pre+postnatal rapamycin treatment rescues lamination defects in the mutant.	84
Figure 4.7	Postnatal rapamycin rescues myelin defect and astrogliosis.....	86
Figure 5.1	Combined pre+postnatal rapamycin treatment of <i>Tsc2^{flox/ko}; hGFAP-Cre</i> mice impairs spatial learning and memory.....	100
Figure 5.2	Combined pre+postnatal rapamycin treatment of <i>Tsc2^{flox/ko}; hGFAP-Cre</i> mice impairs contextual learning and memory.....	102

Figure 5.3 Rapamycin-treated *Tsc2^{fllox/ko}*; *hGFAP-Cre* mice display anti-anxiety behavior..... 104

Figure 5.4 Short-term memory is intact in all rapamycin-treated cohorts..... 106

ABBREVIATIONS

4E-BP1	eukaryotic initiation factor 4E (eIF4E)-binding protein 1
5'-TOP	5'-terminal oligopyrimidine tract
AMPK	AMP-dependent protein kinase
BBB	blood brain barrier
BPC	basal progenitor cell
ECM	extracellular matrix
ERK	extracellular signaling-regulated kinase
GAP	GTPase-activating protein
H&E	hematoxylin and eosin
LAM	lymphangioleiomyomatosis
LOH	loss of heterozygosity
MBP	myelin basic protein
mTORC1	mammalian target of rapamycin complex 1
MWM	Morris Water Maze
RGC	radial glial cell
Rheb	Ras homolog enriched in brain
RSK	p90 ribosomal protein S6 kinase
S6K1	p70 ribosomal protein S6 kinase-1
SEGA	subependymal giant cell astrocytoma
SEN	subependymal nodule
SLM	stratum lacunosum-moleculare
SVZ	subventricular zone
TSC	tuberous sclerosis complex
VZ	ventricular zone

Chapter One:

Background and Introduction

Introduction

In 1879, the pediatrician Désiré-Magloire Bourneville performed an autopsy on a 15-year old mentally handicapped girl named L. Marie who had died in a psychiatric hospital:

She had suffered seizures most of her life, at first partial and, after the age of 2 years, generalized...at the age of 3 years, she suffered frequent episodes of status epilepticus and developed a right spastic hemiplegia. ...Pathologic examination of the brain disclosed raised, opaque, and sclerotic areas in some of the cerebral convolutions... [and] what appeared to be white nodular tumors embedded in the corpus striatum and protruding into the lateral ventricles.” Bourneville coined the term *tuberous sclerosis of the cerebral convolutions* for this unique potato-like consistency, hence the adjective *tuberous*. Notably, Bourneville also found small yellowish white tumors in the kidneys, protruding 3 to 5 mm over the surface, which he thought were unrelated to the cerebral pathology. He concluded that Marie’s partial seizures originated in an extensive sclerotic area, indeed a large tuber...(1).

Though similar characteristics had been previously described by other physicians (1), it was not until Bourneville’s detailed account and naming of this disease that it was brought from relative obscurity into common medical knowledge. Thanks to his contributions and that of the many physicians, scientists, and patients who followed, we now have a better understanding of the intricacies of tuberous sclerosis complex (TSC), including the genetic etiology and some of the major pathways that are affected. This in turn has allowed for the creation of cell lines and animal models with which the pathophysiology of the disease continues to be more clearly elucidated. Though much still remains unknown nearly a century and a half after Bourneville’s initial report, the TSC field has advanced to the point that clinical trials targeting the biochemical disease pathways are under way. In the following chapters, I will discuss the main features of TSC, some of the significant

advances made within the past ten years, and the contributions of our laboratory to the growing body of knowledge regarding this disease.

Clinical Features of Tuberous Sclerosis Complex

Tuberous sclerosis complex is an autosomal dominant tumor suppressor disease with an incidence of approximately 1 in 6000 live births (2). It is characterized by hamartomas, or benign tumors, which can occur in various organ systems, most notably the skin, heart, lungs, kidneys, and brain (3). While TSC is a highly penetrant disease, the clinical manifestations vary greatly from patient to patient and may occur at different developmental timepoints (4).

Skin lesions, for example, may be detected at all ages and are found in almost 90% of patients with TSC. These lesions are often found as small growths on the face (facial angiofibromas), as discolored (hypopigmented macules) or raised areas (shagreen patches) along the back or extremities, or as thickened growths along the finger or toenails (ungual fibromas) (5). Aside from seizures, skin lesions are one of the most common reasons TSC patients come to medical attention (4). Though they are a cosmetic nuisance, this manifestation of TSC usually has little clinical impact on patients.

Cardiac lesions are detectable in nearly 50-70% of infants with TSC (6). They are considered one of the less serious aspects of TSC for a majority of those affected, though they may cause severe problems in a small number of afflicted patients. Cardiac rhabdomyomas are the most common tumor diagnosed *in utero* and are useful for prenatal diagnoses of TSC, though for the most part they spontaneously disappear later in life (7). However, cardiac rhabdomyomas may cause a number of critical defects in infancy, such as heart failure or complete heart block (8).

Pulmonary manifestations of TSC are usually found in early adulthood and specifically in women, at a rate of 26-39% (9). The sex-specific nature of lymphangioleiomyomatosis (LAM), characterized by a proliferation of defective smooth muscle growth, has led to theories regarding the role of estrogen in the formation of these lesions. Though many of these women are asymptomatic, a study by the Mayo Clinic of 49 TSC-related deaths cited 4 as the result of LAM (10), making it the third most frequent cause of death after kidney and brain lesions.

The renal manifestations of TSC are pathologically heterogeneous and may occur from childhood through adulthood. About 55-75% of patients are affected with renal angiomyolipomas, or benign tumors composed of vascular, fat, and smooth muscle elements, which are often bilateral. The abnormal vasculature of these tumors makes spontaneous life-threatening bleeding a serious concern. Presence of epithelial renal lesions, usually found in the form of cysts, renal cell carcinomas, or polycystic kidney disease, may also lead to hypertension and renal failure (11).

Though tumor presence in other organs may be devastating, the brain abnormalities of TSC are the cause of the most severe morbidity and mortality of this disease (12). The pathophysiology of these brain lesions remains largely unknown, and treatment remains inadequate. Through the creation, characterization, and treatment of a unique animal model, my dissertation elucidates some of these pathophysiologic mechanisms.

Neuropathology of Tuberous Sclerosis Complex

Nearly 95% of patients with TSC exhibit some form of brain pathology, which often leads to a wide range of neurological and behavioral abnormalities such as epilepsy, cognitive dysfunction, mental retardation, and autism. These features are usually detectable

in early childhood and are often resistant to existing therapies (13). Although the classification of TSC as a "prototypical neurodevelopmental disorder (14)" is well accepted in the field, little is known regarding the development of TSC neuropathology or how it contributes to brain dysfunction.

The most common brain lesions found in TSC patients are cortical tubers, subependymal nodules (SENs), and subependymal giant cell astrocytomas (SEGAs) (15). Cortical tubers are present in over 80% of patients and are likely intimately related to the neurobehavioral abnormalities found in TSC. Tubers are firm, "potato-like" growths of variable size that occur most often at the gray-white junction. Histologically they demonstrate a loss of cortical lamination, where the distinct organization of the six-layer cortex is disrupted. A proliferation of disordered and dysplastic neuronal and glial cells are also found in tubers, including "giant cells," or cytomegalic cells of mixed neuronal and astrocytic lineage (16). Increased tuber burden is strongly predictive of infantile spasms (17), a characteristic seizure condition of TSC with a typical onset between 4-8 months, in which the body abruptly bends forward and the arms and legs stiffen (18). This epileptic syndrome is often associated with poor neurologic prognosis and severe mental retardation, and occurs in roughly 20-30% of infants with TSC (19). It is unknown whether neurological dysfunction may be attributed to the presence of tubers alone or as a result of seizures caused by tuber presence (20).

SENs are small growths that may be partially or completely calcified. They are typically asymptomatic and line or protrude into the lateral and third ventricles (21). Like tubers, they are mainly composed of dysplastic astrocytes and mixed-lineage neuronal or astrocytic cell components. SEGAs, or giant-cell tumors, are thought to derive from SENs and occur in about 10% of TSC patients. Though they do not become malignant glial tumors, SEGAs

may enlarge over long periods of time and cause obstruction of cerebrospinal fluid pathways, hydrocephalus, endocrinopathy, and even death (16).

The development of these brain lesions and what role they play in subsequent brain dysfunction is not well understood. However, other histologic features of TSC, such as heterotopic neuronal aggregates and varying degrees of cortical cytoarchitectural disorganization, suggest that the disease may be thought of more cohesively as a neuronal migration disorder (22) that is also characterized by aberrant cellular proliferation and differentiation. Though establishment of the neurodevelopmental nature of the disorder has greatly assisted studies in determining the best approaches to modeling and studying TSC, it was not until the discovery of the genetic etiology of the disease that advances in experimental research could be made.

Genetics of TSC

Several decades passed following Bourneville's initial account of TSC before some physicians began noticing a trend in TSC patient families. In 1910, Kirpicznik first recognized TSC as a genetic condition when he investigated a family consisting of three generations of affected individuals and described the disease in identical as well as fraternal twins. Gunther and Penrose noticed in 1935 the dominant inheritance pattern of the disease and suggested that a high mutation rate was "causal" in TSC (23).

The genes responsible for the disease, *TSC1* and *TSC2*, were eventually identified using linkage analysis and positional cloning in 1997 and 1993, respectively (24, 25). *TSC1*, located on chromosome 9q34, encodes a 23-exon transcript that results in a 130 kDa protein named hamartin. *TSC2*, identified on chromosome 16p13, is associated with a 200 kDa protein named tuberin and encodes a 41-exon transcript.

TSC is caused by inactivating mutations in either *TSC1* or *TSC2* (26). The prevailing hypothesis regarding lesion formation states that inactivation of both alleles of either gene, or loss of heterozygosity (LOH), is required, in accordance with Knudson's two-hit tumor suppressor gene model (27). Studies showing LOH in lesions including SEGAs but not the surrounding normal tissue have supported this hypothesis (28-30), and this finding has been observed in most types of hamartomas found in TSC patients. However, LOH is observed more consistently in some lesion types than others, with only rare observances in cortical tubers (31, 32). Recent studies have suggested that loss of tuberin function in tubers does not primarily occur as the result of a second hit event, but rather as a consequence of Erk (extracellular signaling-regulated kinase) phosphorylation of tuberin, which suppresses its biochemical and tumor-suppressor functions (33). This hypothesis is supported by findings that hyperactivation of Erk is frequently observed in tubers (34-36). The exact mechanism by which tuber formation occurs is therefore the subject of ongoing debate.

Though mutations within either gene give rise to TSC pathology, the locations and types of mutations vary widely. Over 900 unique allelic variants have been reported for both genes, representing large and small deletions, rearrangements and insertions, nonsense, missense, and spliced mutations (37-40). Interestingly, the frequency of mutations found in *TSC2* is higher than that of *TSC1*, such that over 65% of sporadic cases, which represent 66% of all TSC cases reported, are *TSC2*-based (26). *TSC2*-based cases also have a more debilitating form of the disease. It is speculated that this disparity in frequency may be the result of increased germline and somatic mutations in *TSC2* compared to *TSC1*, though why *TSC2* mutations result in more severe disease is not clearly understood (41). Recent studies have suggested this effect may be attributed to the distinct functions of the proteins hamartin and tuberin (42).

Hamartin, tuberin, and the mTORC1 pathway

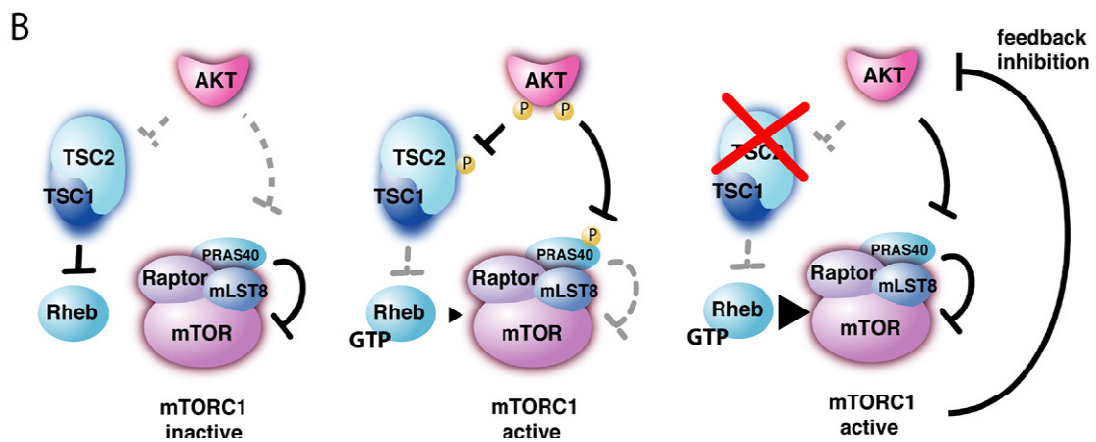
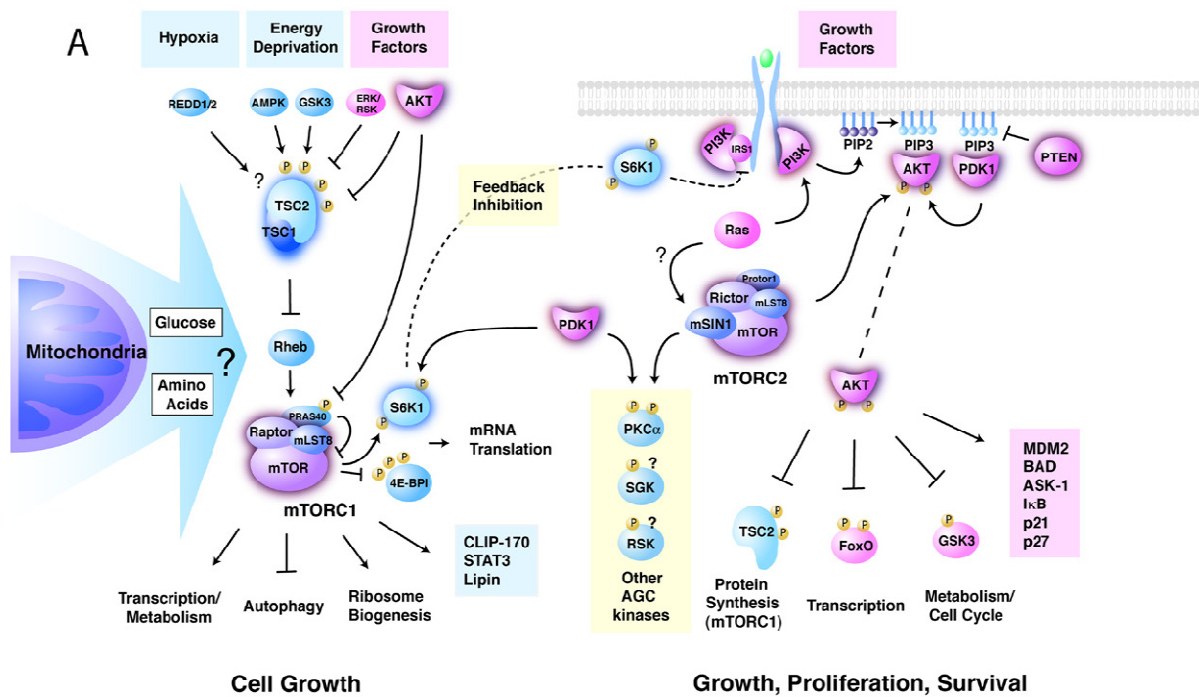
Though it was clear that hamartin and tuberin must either be binding partners or work closely in the same biochemical pathway (43), it was not until later that the correct relationship was elucidated. In a landmark study, tuberin was found to contain a binding domain on its N-terminus with high affinity for a similar domain on hamartin (44, 45). In fact, tuberin and hamartin form a heterodimeric coiled-coil complex, henceforth called the "TSC complex," in which it is thought that the main function of hamartin is to stabilize tuberin (46, 47), whereas tuberin's major known role lies in its GTPase-activating protein (GAP) domain (25).

The most well-characterized function of the TSC complex is its inhibition of Rheb (Ras homolog enriched in brain) via the GAP function of tuberin (48). Tuberin's GAP domain is located near its C-terminus and is indirectly responsible for hydrolyzing the conversion of the Ras-related small G protein Rheb from its active GTP-bound state to its inactive GDP-bound form (49) (Fig 1.1). Inactivation of Rheb, in turn, inhibits its ability to activate mammalian target of rapamycin complex 1 (mTORC1), a distinct GβL/raptor (*regulatory associated protein of mTOR*)-bound structure of the large serine-threonine protein kinase mTOR (50). This process is achieved by antagonizing mTORC1's endogenous inhibitor FK506-binding protein 38 (FKBP38) in a GTP-dependent manner (51). The TSC complex therefore negatively regulates mTORC1 activation through Rheb.

It does so in response to four major signals – nutrient availability, growth factors, energy status of the cell, and hypoxia. As amino acids are the building blocks of proteins, mTORC1 activity is heavily regulated by amino acid sensing, as demonstrated in a study in which withdrawal of amino acids from *Drosophila* and mammalian cells resulted in attenuated mTORC1 signaling (52). However, recent work by Smith et al. (53) showed that

***Fig 1.1. The mTOR network.** (A) The mTOR kinase is the catalytic component of two distinct multiprotein complexes called mTORC1 and mTORC2. (Left) In addition to mTOR, mTORC1 contains RAPTOR, mLST8, and PRAS40. mTORC1 drives cellular growth by controlling numerous processes that regulate protein synthesis and degradation. Diverse positive and negative growth signals influence the activity of mTORC1, many of which converge upon the TSC1/2 complex. (Right) mTORC2 also contains mLST8, but instead of RAPTOR and PRAS40, mTORC2 contains the RICTOR, mSIN1, and PROTOR proteins. (B) Model of mTORC1 co-regulation by RHEB and PRAS40. (Left) When AKT is inactive, TSC1/2 inhibits RHEB while PRAS40 inhibits mTORC1. (Middle) Upon activation, AKT promotes mTORC1 activity by phosphorylating both TSC1/2 and PRAS40. This results in GTP-loading of RHEB, which directly activates mTORC1 and release of mTORC1 from PRAS40 repression. (Right) In *tsc2* null cells, RHEB strongly activates mTORC1. This in turn inhibits AKT by way of the negative feedback loop. Even though PRAS40 is dephosphorylated in this state, its ability to repress mTORC1 is overrun by the greatly elevated Rheb activity.

* Figure and legend taken from (54). Legend has been slightly modified by deletion of sentences that do not apply to my work. Permission to reproduce this figure in this thesis has been requested and received from Elsevier, license number 2554090654204 to Sharon Way.



amino acid withdrawal can affect mTORC1 signaling in cells lacking Tsc2, albeit to a lesser degree than in a wild type cell. While this study revealed that amino acid sensing may occur independently of TSC2, the TSC complex is one node by which nutrient signaling to mTORC1 occurs.

Growth factor signaling to mTORC1, on the other hand, is closely regulated by the TSC complex via phosphorylation of TSC2 by Akt, a major serine/threonine kinase involved in multiple cellular processes. Akt is itself activated by PI3K, a signal transducer enzyme which responds to insulin and growth factor presence in cell surface receptors (55, 56). Binding of growth factors therefore results in phosphorylation of TSC2, which hinders the function of the TSC complex in inhibiting mTORC1 via a mechanism that is still being debated (57). In addition to Akt, Erk may also stimulate mTORC1 activity in response to growth factors and cytokines via phosphorylation of TSC2 by RSK (p90 ribosomal protein S6 kinase), which results in dissociation of TSC1 and TSC2 (58, 59).

Meanwhile, the TSC complex also plays an important role in energy and oxygen sensing. When energy in the form of ATP is low, intracellular levels of AMP are increased and bind to AMPK (AMP-dependent protein kinase) (60), which is then activated via upstream kinases such as LKB1, a tumor suppressor associated with Peutz-Jeghers syndrome. Activated AMPK then phosphorylates downstream targets such as TSC2 to decrease energy-depleting processes (59, 61). Hypoxia has also been shown to downregulate mTORC1 activity via AMPK (62), as well as through REDD1. REDD1, a stress response gene, was first identified when its orthologues in *Drosophila* (*scylla* and *charybdis*) were found to suppress an overgrowth phenotype caused by overactivation of Akt (63). Later studies suggested that REDD1 inhibits mTORC1 activity by reversing Akt-mediated inhibition of the TSC complex through removal of 14-3-3 (64), a signaling regulator thought to be involved in Akt phosphorylation. By integrating these various

signals, the TSC complex functions as a “central hub of signal transduction within the cell (57)” to control mTORC1 activity.

The evolutionary-conserved mTORC1 pathway modulates a number of major downstream processes that regulate cell growth and proliferation such as mRNA translation, ribosome biogenesis, nutrient metabolism, and autophagy. Protein translation is regulated by mTORC1 through phosphorylation of at least two known translational regulatory proteins: the activation of p70 ribosomal protein S6 kinase-1 (S6K1) and inhibition of eukaryotic initiation factor 4E (eIF4E)-binding protein 1 (4E-BP1) (65). S6K1 regulates cell size via phosphorylation of 40S ribosomal protein S6, which is important in translational control of mRNAs that contain a 5'-terminal oligopyrimidine tract (TOP). 4E-BP1, on the other hand, inhibits eIF4E, which recruits 40S ribosomal subunits to the 5' end of mRNAs. Phosphorylation of 4E-BP1 by mTORC1 hence activates mRNA translation (66). Mutations in either *TSC1* or *TSC2* therefore lead to constitutive activation of the mTORC1/4E-BP1/S6K1 signaling pathway, resulting in dysregulated translation.

Drosophila Homologues of *TSC1* and *TSC2*

Much of the knowledge regarding the functions of the *TSC1* and *TSC2* genes was first elucidated from studies of the fruit fly, *Drosophila melanogaster*. The cells of the *Drosophila* eye progress through the cell cycle in a continuum from anterior to posterior (67), making it an excellent subject for study of the cell cycle. During a genetic screen to identify new mutations affecting eye structure, Ito and Rubin (68) isolated several mutations that produced enlarged cells and identified them as allelic to the previously characterized *gigas* gene, a homolog of *TSC2*. Characterization of these alleles revealed that though they undergo normal differentiation, cells undergo S phase without entering M phase and are enlarged due to this cell cycle defect. Similar results were found in mutants of the

Drosophila homolog of *TSC1* in two independent studies (69, 70), both of which also suggested a role for *TSC1/2* in the insulin signaling pathway given the similarities between mutants of each group. These and similar studies using *Drosophila*, like those described previously, significantly advanced the understanding of the functions of *TSC1* and *TSC2* and served as a comparison for later findings in mammalian models of TSC.

Mouse Models of TSC Neuropathology

With the newfound understanding of the *TSC1* and *TSC2* genes from *Drosophila* studies, researchers were eager to better understand the brain and other pathologies of TSC using a mammalian model system by creating *Tsc1* and *Tsc2* knockout mice. The importance of the mTORC1 pathway in prenatal development was quickly underscored, however, when homozygous KO mice for both genes were found to be embryonic lethal. Characterization of the *Tsc1* KO mice revealed they died from liver hemangiomas, a symptom both *Tsc1* (71) and *Tsc2* (72, 73) heterozygous KO mice exhibited, along with kidney lesions. In addition, both heterozygotes were found with increased numbers of astrocytes (74), suggesting a role for both hamartin and tuberin in astrocyte proliferation. However, as little other brain pathology was seen, a conditional knockout allele was eventually created of the *Tsc1* gene using the Cre-loxP system.

This *Tsc1*-based conditional knockout (*Tsc1* CKO) mouse has been independently used to study two cell groups affected in TSC neuropathology: astrocytes and neurons. In the astrocyte-specific *Tsc1* CKO mouse (75), hamartin is deleted using a *GFAP-Cre* driver beginning embryonic day 14.5 (E14.5) (76). These mice developed clinically obvious seizures by 2 months of age and die by 22 weeks. These mice also displayed an increase in brain size, increased astrocyte proliferation, abnormal neuronal organization in the

hippocampus, and mTORC1 activation. The astrocyte-specific Tsc1 CKO mouse does not, however, exhibit pathology similar to that seen in cortical tubers.

A neuron-specific Tsc1 CKO was created using a *synapsin-Cre* driver that deletes hamartin beginning E13.0 (77). These mice exhibit a much more severe phenotype than that seen in the astrocyte-specific Tsc1 model. They display neurological abnormalities such as hyperactivity, enhanced startle response, and high-frequency trunk and limb tremor as early as postnatal day 10 (P10). Neuron-specific Tsc1 CKO mice also display a failure to thrive phenotype with a median survival of 35 days. Spontaneous and provoked seizures were also observed, with some seizures ending in a fatal tonic phase. Compared to the astrocyte-specific model, these mice also exhibit a more severe histologic phenotype in the form of abnormal brain cytoarchitecture, enlarged and dysplastic neurons showing activated mTORC1, and reduced myelination.

The astrocyte- and neuron-specific Tsc1 CKO mouse models have provided the TSC field with valuable insight into TSC brain pathology, as they both exhibit features similar to those seen in humans. In particular, the neuron-specific Tsc1 CKO provided support for the LOH model of tumor formation in the TSC brain, as it models the human condition of one general deletion of *Tsc1* in all cells, with knockout of the second allele only in post-mitotic neurons. Given the higher frequency and more severe nature of *TSC2*-based disease, however, our laboratory sought to use a similar method to create a *Tsc2*-based conditional allele with which TSC neuropathology might be studied. The creation and characterization of this *Tsc2*-based conditional allele is the subject of Chapter 2 in this thesis.

Using this conditional allele, we also sought to establish a *Tsc2*-based mouse model of the development of TSC neuropathology. Cortical tubers have been detected as early as 19-20 weeks in a human fetus, evidence that they are developmental lesions (78, 79). Tubers also contain cells of mixed neuronal and glial lineage with loss of cortical lamination

(16), suggesting that they arise from a neuronal-glial precursor that failed to properly differentiate and migrate (80, 81). Radial glial cells are neuroglial progenitors that give rise to the majority of neurons and astrocytes in the cortex. In addition, they form radial fibers along the width of the developing cortex which are crucial to neuronal migration (82). We therefore hypothesized that loss of *TSC1* or *TSC2* in radial glial cells may be a major mechanism of TSC neuropathology. Using a radial-glia specific Cre driver, *hGFAP-Cre* (83, 84), we have tested this hypothesis in a *Tsc2*-based CKO mouse. This experiment is discussed in depth in Chapter 3 of this thesis.

Rapamycin and the PI3K/Akt/mTOR pathway

Since inhibition of mTORC1 is the most well-characterized role of the TSC complex, researchers speculated that treatment of patients with an mTORC1 inhibitor might rescue formation of TSC pathology. The macrolide rapamycin, also known as sirolimus, was suggested as a candidate. Originally used to probe mTOR (*mammalian Target Of Rapamycin*) biology and crucial in elucidating the function of the mTOR pathway (85, 86), rapamycin is an FDA-approved drug used as an immunosuppressant for kidney transplants (87). Rapamycin inhibits mTORC1 via a mechanism similar to that of FKBP38 by forming a complex with the intracellular binding protein FKBP12 (88). FKBP12 then binds to mTORC1's FKBP12-rapamycin binding domain to inhibit the ability of the kinase to signal to its downstream effectors (89).

The ability of rapamycin to inhibit TSC-related pathology was first demonstrated in the Eker rat. The Eker rat model of TSC harbors a spontaneous mutation that inactivates *Tsc2* and is characterized by hereditary renal cell carcinoma (90). Immunohistological staining of primary tumors from these rats demonstrated increased phospho-4E-BP1 and pS6K, indicators of activated mTORC1 (91). Short-term treatment of the Eker rats with rapamycin

resulted in induction of apoptosis and reduction of cell proliferation (92). Follow-up studies addressing the pituitary tumors found in 58% of adult Eker rats showed that long-term treatment with rapamycin reversed weight loss and abnormal gait while prolonging lifespan. However, withdrawal of treatment resulted in further clinical deterioration of these rats. Despite this potential drawback, these initial preclinical studies demonstrated that rapamycin was a promising agent for the pharmacologic treatment of TSC. Preclinical rapamycin treatment studies have been conducted in both the astrocyte- (93) and neuron-specific (94) Tsc1 CKO mouse models. In the former, early and late treatments with rapamycin were tested. Early treatment, given from 2 to 7 weeks of age, was found to prevent the development of epilepsy and premature death. Late treatment, given from 6 weeks to 9 weeks of age, was able to suppress seizures and prolonged survival in mice that had already developed epilepsy. Rapamycin treatment also inhibited the mTORC1 activation, astrogliosis, megalencephaly, and neuronal disorganization initially reported. Similar findings were observed in the neuron-specific Tsc1 CKO. Rapamycin treatment resulted in improvement of the neurofilament abnormalities, cell enlargement, and myelination defects, though the dysplastic features and abnormal dendritic spine density and length originally described in the neurons were unaffected.

Taken together, these results suggest that rapamycin may have a large therapeutic impact on TSC brain pathology. However, the latter findings regarding the minimal impact rapamycin had on dendrites and neuronal morphology are particularly interesting. Though the inhibitory role of the TSC complex on mTORC1 is well characterized, a number of studies suggest that hamartin and tuberlin have additional functions, both as a complex and as individual proteins (42). While it is unknown how these alternate roles contribute to TSC pathology, a steadily increasing body of findings such as those previously described suggests mTORC1 alone cannot be solely responsible for all manifestations of TSC.

For example, recent studies have shown that the TSC complex is also required for proper activation of mTORC2 (95), a distinct, rapamycin-insensitive complex of the mTOR protein that consists of the rictor/GβL-bound structure of the mTOR protein. mTORC2 activates Akt, giving it a firm role in the regulation of actin cytoskeleton and cell morphology (96). As previously described, the Akt pathway is a key component of the insulin/PI3K signaling pathway which modulates cell survival, actin formation, and proliferation. It has also been identified as a major regulator of neuronal polarity, including axon and dendrite formation (97, 98). Given that rapamycin had minimal impact on neuronal morphology and dendritic spine density in the neuron-specific *Tsc1* CKO mouse, it follows that these aspects of TSC brain pathology might function through mTORC2 rather than mTORC1. However, the downstream target of mTORC1, S6K1, is a known inhibitor of PI3K (99), suggesting that increased mTORC1 signaling might also attenuate Akt signaling and affect dendritic growth. In addition, prolonged treatment of rapamycin has been shown to inhibit mTORC2 assembly and Akt signaling (100). The complex interplay between these two pathways suggest that distinguishing between mTORC1 and mTORC1-independent pathways may be more difficult than previously thought.

We have investigated some of these issues by examining the effects of low dosage rapamycin treatment in our *Tsc2*-based mouse model. In addition to establishing whether rapamycin is equally effective in *Tsc2*-mediated pathology, we have sought to explore the impact of dosage as well as pre- versus postnatal administration of rapamycin. By treating with rapamycin at different stages, we hoped to better understand the effects of drug treatment on defects that occur prenatally or postnatally. As TSC is a neurodevelopmental disorder, we were especially interested in assessing whether *in utero* rapamycin administration might rescue defects that occur before birth. Given the complexities of the PI3K/Akt/mTOR pathway as described above, we also hoped to determine the degree of

mTORC1-specific involvement in the various aspects of TSC brain pathology using rapamycin as a direct inhibitor of mTORC1. The histologic outcomes of these experiments are further explored in Chapter 4 of this thesis. The same treatment schemes are then used in these mice to determine the functional impact of rapamycin rescue, as described in Chapter 5.

Summary

From the first descriptions of TSC in the late 19th century to the relatively recent discovery of the main pathway in which the TSC proteins function, our understanding of TSC has increased exponentially. However, significant gaps still exist in our knowledge regarding the pathophysiology of the disease. In this thesis, we sought to address some of these unknowns through the creation and characterization of a novel neuro-glial conditional knockout of the *Tsc2* gene, which recapitulates many aspects of TSC neuropathology. We then used this model to test the therapeutic potential of rapamycin to treat TSC brain defects while elucidating the degree of mTORC1 involvement in formation of these lesions. Chapter 2 will detail the creation of the *Tsc2*-based conditional allele and its characteristics. Chapter 3 will describe the creation and characterization of our mouse model of TSC neuropathology in which *Tsc2* is deleted in radial glial cells. Chapter 4 will examine the effects of treatment at different timepoints of these mice with rapamycin. These studies will continue in Chapter 5, where functional rescue of TSC pathology following rapamycin treatment will be examined via behavioral testing of these mice. Together, these studies have contributed greatly to our current knowledge regarding the formation, characteristics, and effects of treatment of TSC pathology in the brain.

Chapter Two:
Creation and Characterization of the Tsc2^{flox/flox} Mouse

Introduction

It was well established that tuberlin and hamartin formed a heterodimer to regulate mTORC1, a function that was thought to be the main role of the two proteins and a major mechanism of TSC pathology formation. However, much less was understood regarding the functions of these proteins when individually bound to the other partners both were shown to have (42). The fact that both tuberlin and hamartin had other binding partners strongly emphasized the need to investigate the individual contributions of both *Tsc1* and *Tsc2* to TSC pathology. As characterization of *Tsc1*-based mouse models of TSC were under way, researchers began attempts to create a *Tsc2*-based model for future investigation.

Tsc2^{+/-} mice (77) and Eker rats (101) demonstrated limited brain pathology with no associated clinical phenotype. Similar to *Tsc1* null mice (71), *Tsc2* null mice were found to be embryonic lethal (72, 73) and could not be used for study of advanced brain pathology. However, study of *Tsc2* null murine neuroepithelial progenitor cells (NEPs) demonstrated that these cells displayed aberrant differentiation and represented giant cells found in tubers, suggesting that biallelic inactivation of *Tsc2* in the brain could provide a good model system for the study of tuber pathogenesis (102). The need for a model in which *Tsc2* could be conditionally knocked out in the brain was therefore clear. Our laboratory therefore set out to create and characterize such a model.

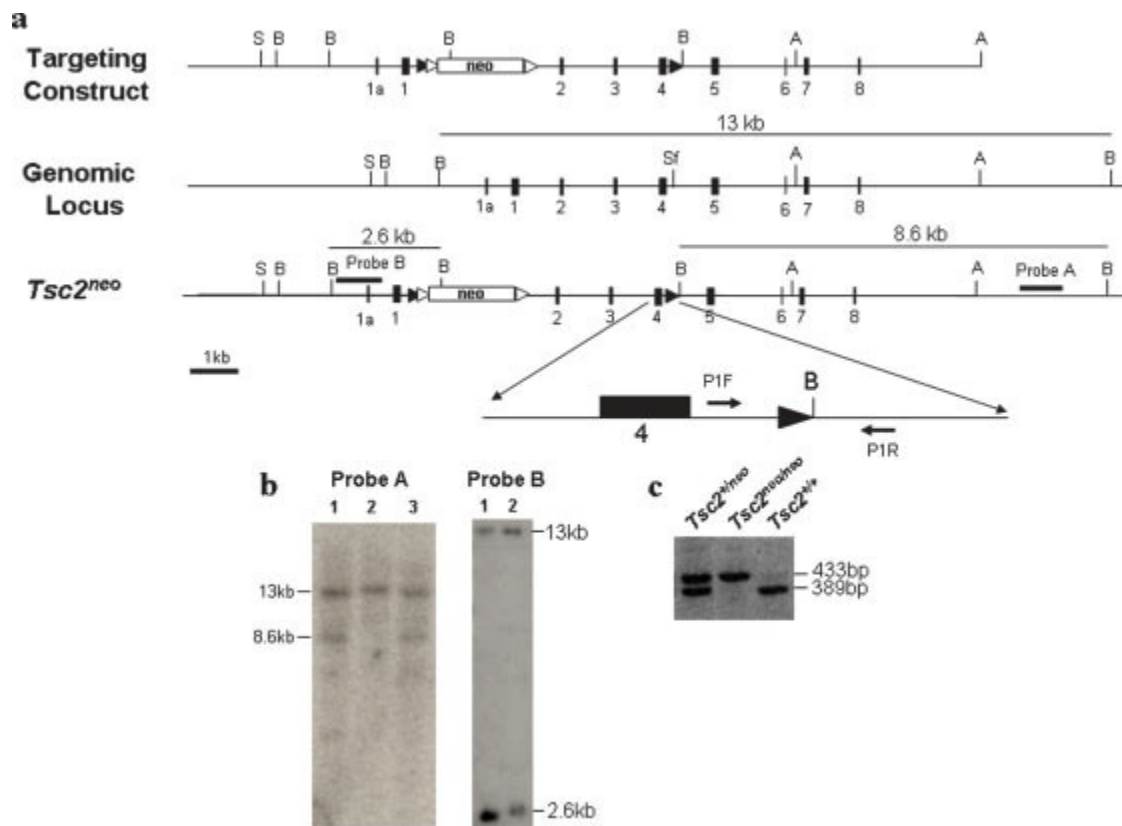
When I began my doctoral studies, the laboratory had already created the *Tsc2*^{flox} mouse. Nonetheless, I helped characterize and establish that this strain would be a useful reagent for cell specific Cre-mediated deletion (103). In the following chapter, I will summarize previously conducted work in the methods section, while the work that I contributed to in characterizing this *Tsc2*-based conditional knockout mouse will be presented in the results section.

Materials and Methods

Generation of a Conditional Disruption of the *Tsc2* Gene – As described in Hernandez et al. (103), the *Cre-loxP* and *Flp-frt* systems were used to create a floxed *Tsc2* allele.

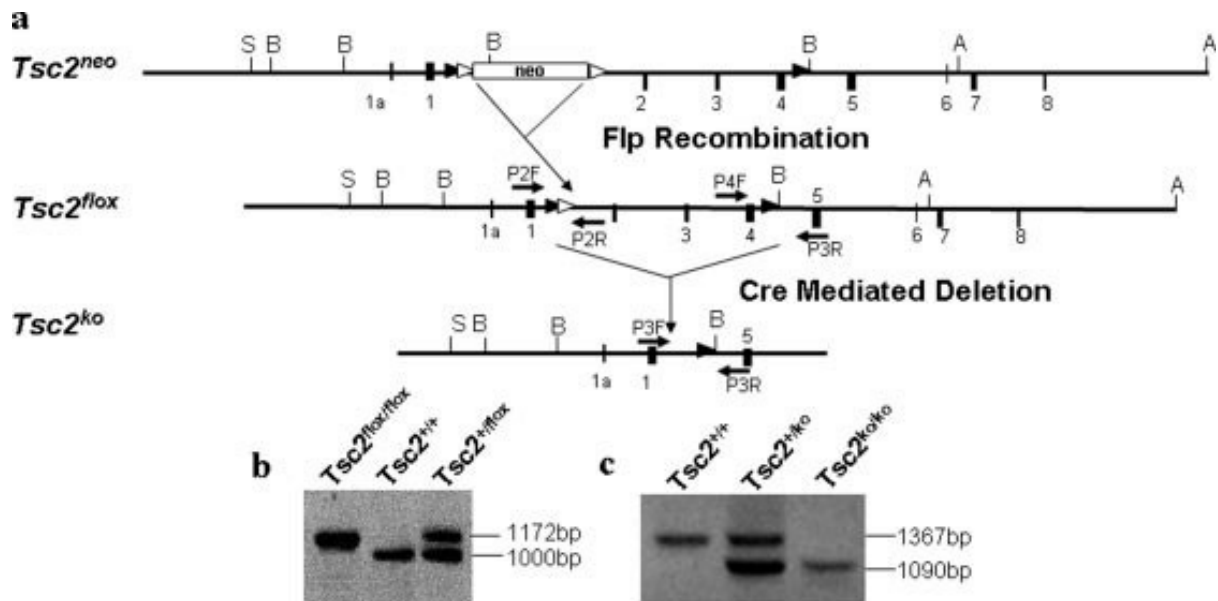
...We made a *Tsc2*^{neo} targeting vector by inserting a *loxP-BamHI* site into intron 4 and a *loxP-frt-neo-frt* cassette into intron 1 (Fig 2.1a). To screen for neomycin resistant ES cells we used the 3' external and 5' internal probes indicated. Seven of 180 clones demonstrated 13 kb wildtype and 8.6 kb mutant bands on Southern blot when the genomic DNA was digested with *BamHI* and probed with the external probe (Fig 2.1b). After Southern analysis of *BamHI*-digested DNA using the internal probe demonstrated the correct 13 kb wildtype and the 2.6 kb mutant bands (Fig 2.1b), two of the clones were selected for blastocyst injection. Only one chimera demonstrated germline transmission as demonstrated by PCR genotyping for the presence of the loxP-BamHI site (Fig 2. 1c). ...To generate a conditional allele of *Tsc2* that would be useful for modeling the multiorgan pathology of TSC in the mouse, we removed the neomycin gene by mating the *Tsc2*^{+/neo} to FLPe transgenic mice (Fig 2.2a) (104). We confirmed that the neomycin gene was removed by PCR detection of the *loxP-frt* site that remains after Flp recombination (Fig 2.2b). To demonstrate that the *Tsc2*^{flox} allele could be converted to a null allele by Cre recombination, we mated the *Tsc2*^{flox/flox} mice with a CMV-Cre transgenic mouse (Fig 2.2a). Complete deletion of exons 2–4 was demonstrated by PCR genotyping (Fig 2.2c). (100)

Embryo and Adult Organ Analysis – All animal procedures were approved by the University of Texas Health Science Center Animal Welfare Committee. For embryonic analysis, the day the vaginal plug was found was considered embryonic day 0.5. Dams were anesthetized using 2.5% avertin and killed via cervical dislocation before embryos



†Figure 2.1. Generation of the *Tsc2*^{neo} allele. (a) Gene-targeting construct. Exons are indicated by black boxes labeled with exon numbers. *LoxP* sites are marked by black triangles and *frt* sites by white triangles. The *loxP-frt-neo-frt* cassette was inserted in intron 1 and a *loxP-BamHI* site in intron 4. External and internal probes used for ES cell screening are indicated. PCR primers P1F and P1R were used to confirm germline transmission of the *Tsc2*^{neo} allele. B, *BamHI*; A, *AflIII*; S, *SbfI*. (b) Southern blot analysis of genomic DNA digested with *BamHI* from *Tsc2*^{+/+} and *Tsc2*^{+/neo} ES cell clones and probed with the external probe (Probe A). Positive clones (Lanes 1, 3) demonstrate the shorter 8.6 kb band because of the introduced *BamHI* site. Hybridization using the internal probe (Probe B) shows 13 and 2.6 kb fragments for both *Tsc2*^{+/neo} clones (Lanes 1,2). (c) PCR product from mouse DNA using Primers P1F and P1R. Lane 1 shows a heterozygote *Tsc2*^{+/neo} with a 433bp *loxP-BamHI* allele and a 389bp wild type allele; Lane 2, homozygous *Tsc2*^{neo/neo} embryo DNA; Lane 3 wild type.

†Figure and legend taken from (103). All figures and legends in this chapter are taken from a previous publication in which I was the second author. Guidelines from this journal do not require permission to reproduce manuscript content as part of a thesis, as described in this website: (http://authorservices.wiley.com/bauthor/faqs_copyright.asp#1.7)



†Figure 2.2. Generation of the *Tsc2*^{lox} and *Tsc2*^{ko} alleles. (a) The *Tsc2*^{neo} allele was converted to a floxed allele by mating with a FLPe transgenic mouse. Heterozygous and homozygous *Tsc2*^{lox} mice were obtained at the expected Mendelian frequencies, and homozygous mice were viable and fertile. A *Tsc2*^{ko} allele was generated by mating the *Tsc2*^{lox} mice with a general Cre-deletor strain. (b) PCR of tail DNA from conditional knockout mice using primers P2F and P2R. The 1172bp band indicates the presence of the *loxP-flr* site while the 1000bp band represents a wildtype allele. (c) PCR of tail or embryo DNA using primers P4F, P3R, and P3F to detect the wild type and the *Tsc2*^{ko} alleles. The 1090 bp band represents the null allele. Homozygous *Tsc2*^{ko/ko} genotypes were only identified at embryonic time points due to the lethality of the null phenotype (Lane 3).

†Figure and legend taken from (103).

were extracted and placed into cold 1 x PBS. Yolk sacs or a small part of each body were taken for genotyping. Embryos were then fixed for 4-6 hours in 4% paraformaldehyde (PFA) and stored in 70% ethanol prior to staging. Adult mice were transcardially perfused with ice-cold 1 x PBS followed by 4% PFA. Organs were extracted and post-fixed overnight in 4% PFA before storage for a minimum of one day in 70% ethanol. Organs were then dehydrated, embedded in paraffin and sectioned at 5 μ m on a microtome. Slides were rehydrated and stained with hematoxylin and eosin then protected with a coverslip. Organ sections were visualized with an Olympus BX51 light microscope while all images were captured using a SPOT RT digital camera.

Immunoblotting – Embryos were extracted from dams as described above and the yolk sac or a hindlimb taken for genotyping. Embryos were then snap frozen in liquid nitrogen, and following genotype identification, pooled by genotype and homogenized with 10 volumes of RIPA buffer and protease inhibitor (Sigma) in a dounce homogenizer. Lysates were centrifuged for 10 min at 4°C, sonicated to ensure complete homogenization, and frozen until use. A BCA reagent kit (Pierce) was used to determine protein concentration. Samples were diluted using Laemmli SDS-sample buffer and separated by electrophoresis on a 4-12% bis-tris gel (Invitrogen) before being transferred to a nitrocellulose membrane. The same membrane was sequentially probed with three different antibodies with a stripping step in between each probe. Antibodies used, in order, were tuberin (1:1000, Cell Signaling), hamartin (1:1000, Santa Cruz), and phosphorylated (Ser 240/244) S6 (1:2000, Cell Signaling). Secondary antibodies were conjugated with horseradish peroxidase and visualization of proteins was conducted using the Amersham ECL kit.

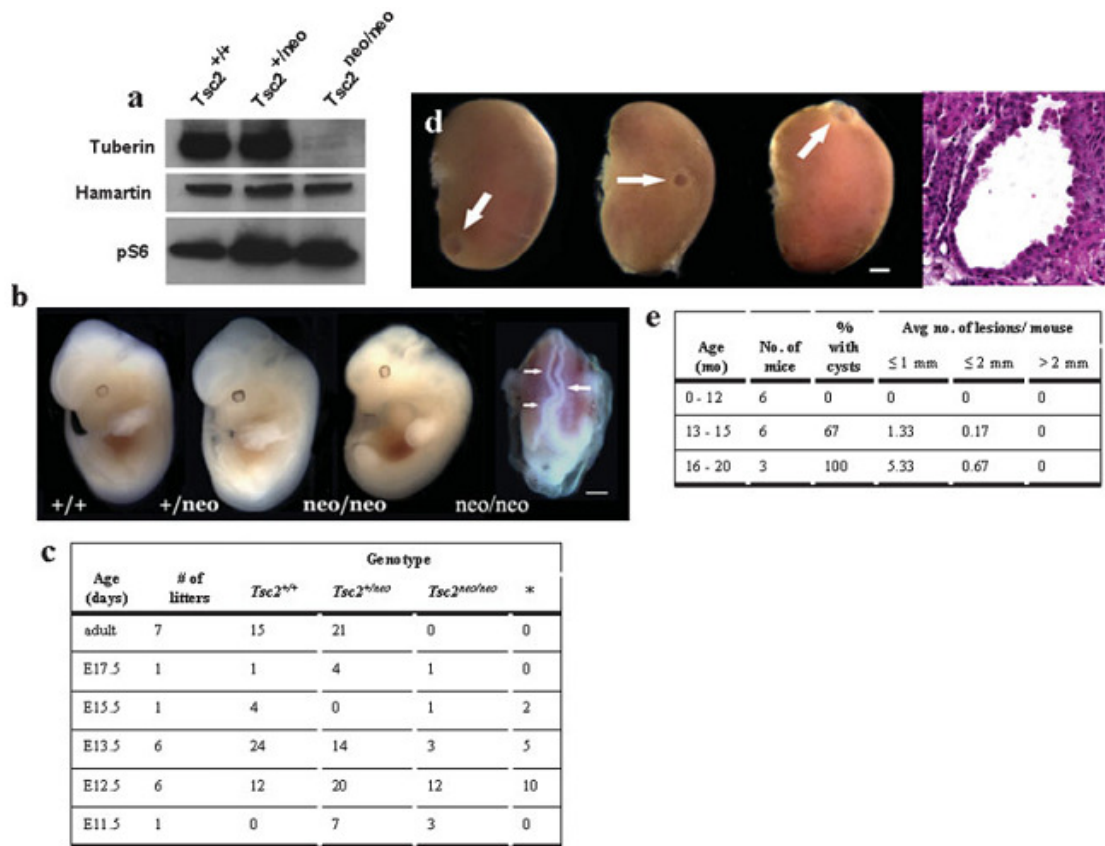
Results

***Tsc2*^{neo/neo} mice are embryonic lethal**

Tsc2^{+/^{neo}} mice were initially generated as an intermediate step before producing the desired *Tsc2*^{+/^{flox}} mice. However, though *Tsc2*^{+/^{neo}} mice were viable and fertile, matings between *Tsc2*^{+/^{neo}} mice did not generate any liveborn *Tsc2*^{neo/neo} pups, indicating that the homozygous state was lethal. Initial studies at embryonic day 12.5 (E12.5) revealed a number of embryos that were smaller, paler, and less developed than their littermates, as well as a number of resorptions. One of these smaller embryos was even found with an open neural tube (Fig 2.3b). Though the resorptions did not yield enough DNA to genotype, the smaller embryos were mainly found to be *Tsc2*^{neo/neo}. Further characterization of litters at E11.5, 12.5, 13.5, 15.5, and 17.5 established that *Tsc2*^{neo/neo} mice were embryonic lethal around E12.5 (Fig 2.3c).

The *Tsc2*^{neo} allele is hypomorphic

The above results are similar to those found in other *Tsc2* null mutants. Onda et al. (72) demonstrated that their *Tsc2* null mouse mutants died at E9.5-12.5, though they did not find any null embryos after E12.5. Meanwhile, *Tsc2* null mutants generated by Kobayashi et al. (73) died around E10.5, with no null embryos found after E13.5. Given that we were able to find *Tsc2*^{neo/neo} mutants up until E17.5, we suspected that the *Tsc2*^{neo} allele might be hypomorphic. This hypothesis was confirmed biochemically using immunoblots. Western analysis of whole embryos at E12.5 (Fig 2.3a) confirmed that expression of the *Tsc2* protein tuberin was significantly decreased, but not completely lost, in the *Tsc2*^{neo/neo} embryos as compared to the *Tsc2*^{+/^{neo}} or *Tsc2*^{+/⁺}. However, expression of pS6, an indication of mTORC1 activation, was similar between the homozygous and heterozygous alleles,



†Figure 2.3. Analysis of *Tsc2*^{neo} allele. (a) Western analysis of lysates from E12.5 embryos. Note the low level of tuberlin antigen in the *Tsc2*^{neo/neo} lane. Hamartin levels are unaffected. Phosphorylated S6 is increased in both *Tsc2*^{+/neo} and *Tsc2*^{neo/neo} lysates. (b) Comparison of embryos at E12.5. *Tsc2*^{neo/neo} embryos were slightly smaller than wildtype and were distinctly underdeveloped and pale. Most noticeable is the lack of digitation of paws and the head size. Note the open neural tube indicated by the arrows. (c) Genotype frequency of *Tsc2*^{+/neo} crosses demonstrating the lethality of *Tsc2*^{neo/neo} embryos. Asterisk (*) denotes nongenotypable resorptions. (d) Kidneys from *Tsc2*^{+/neo} mice at various ages demonstrating cysts, and an H and E histology of a simple cyst, demonstrating renal cyst. Bar represents 1 mm for gross kidney photographs. (e) Table characterizing the kidney cyst phenotype. Note that no cysts developed in the first year of life, most cysts were 1 mm or less. No tumors were detected.

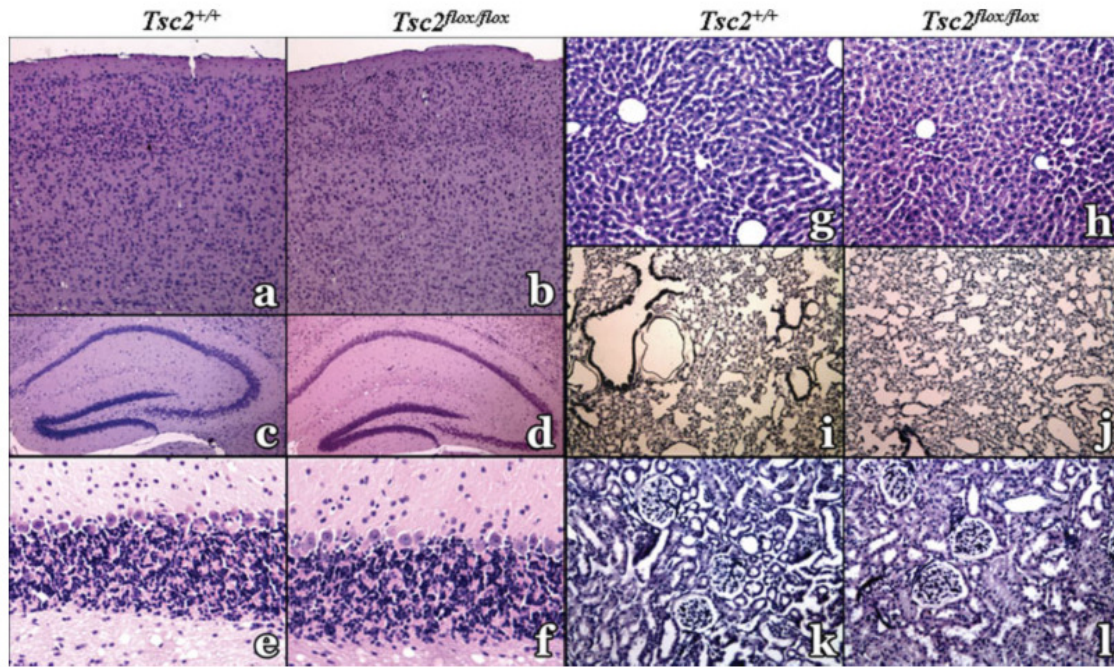
†Figure and legend taken from (103).

suggesting that presence of the neo cassette on *Tsc2* was sufficient to disrupt its inhibition of mTORC1, verifying that the *Tsc2^{neo}* allele was indeed hypomorphic.

***Tsc2^{+neo}* mice develop renal cysts but not carcinomas**

Kobayashi et al. (73) reported that their *Tsc2^{+KO}* mice displayed renal carcinomas (RCs) that were mainly cystic as early as 14 weeks and in almost all mice by 6 months. The *Tsc2* heterozygous allele studied by Onda et al. (72) displayed multiple bilateral renal cystadenomas, or lesions containing solid adenomas and pure cysts, with 100% penetrance by 15 months of age. Though these cysts progressed to RCs in only 10% of the mice, the group found an average of 100 cystadenomas per kidney in 15 month old mice. However, outbreeding this allele to a different mouse strain resulted in a less severe phenotype, which may explain the differences in renal lesion severity found between these two groups.

We sought to compare the renal phenotype of our *Tsc2^{+neo}* mice to those reported. Though older *Tsc2^{+neo}* mice appeared healthy, we noticed that a majority had renal cysts (Fig 2.3d) after one year of age (Fig 2.3e). These cysts mainly appeared as single lesions on each kidney, though mice 16 months and older demonstrated multiple lesions that were larger than those found in younger mice. Systematic analysis of kidneys of 15 mice of different ages revealed that the number and size of cysts were indeed increasing with age in the *Tsc2^{+neo}* mice (Fig 2.3e). We did not find any frank renal tumors in these mice before the study ended at 20 months of age. Cysts were also not detected in any *Tsc2^{+/+}* mice. The presence of a milder renal phenotype in our *Tsc2^{+neo}* mice provides further evidence that the *Tsc2^{neo}* allele is hypomorphic.



†**Figure 2.4.** Comparison of organs of wild type vs *Tsc2flox/flox* mice. *Tsc2*^{+/+}: a,c,e,g,i,k; *Tsc2*^{flox/flox}: b,d,f,h,j,l. (a,b) Cerebral cortex. (c,d) Hippocampus. (e,f) Cerebellum. (g,h) Liver. (i,j) Lung. (k, l) Kidney. Magnification: 40x (a-d); 200x (e-l).

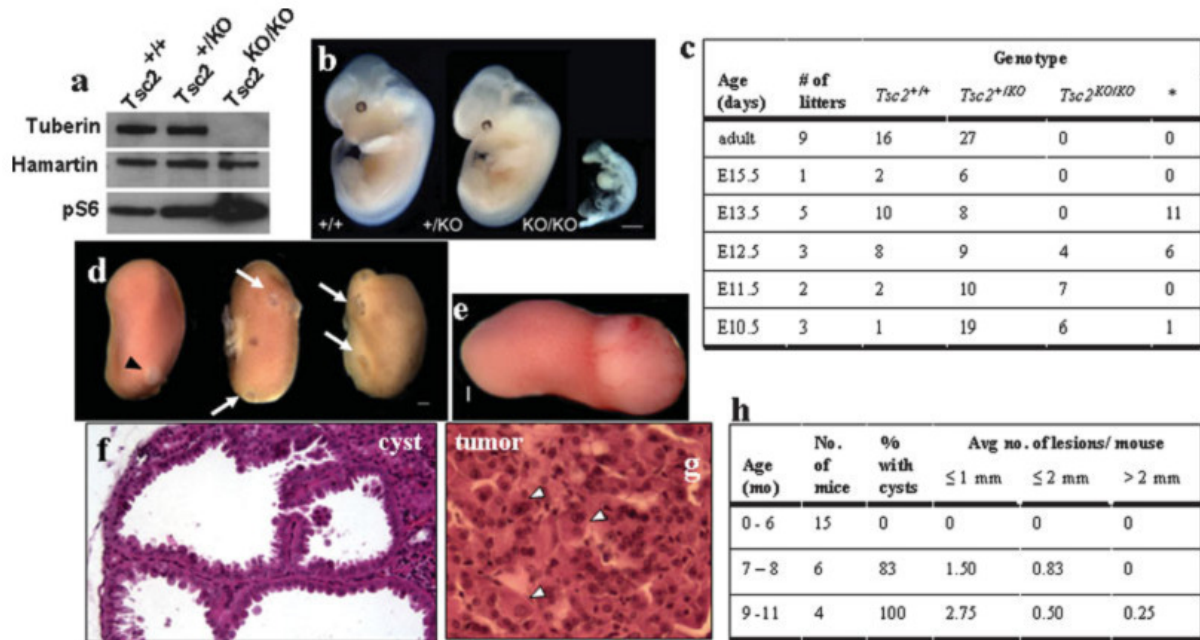
†Figure and legend taken from (103).

***Tsc2*^{flox/flox} mice are viable, fertile, and pathologically indistinguishable from wildtype mice**

The *Tsc2*^{flox} allele was generated by mating the *Tsc2*^{+/neo} mouse with an *FLPe* transgenic mouse, resulting in excision of the neomycin cassette. Heterozygous *Tsc2*^{+/flox} and homozygous *Tsc2*^{flox/flox} mice were viable, fertile, and born in the expected Mendelian ratios. To establish that the presence of loxP sites, located upstream of exon 1 and downstream of exon 4, did not affect major organs, we studied 5 µm paraffin-embedded sections of the *Tsc2*^{flox/flox} cortex, hippocampus, cerebellum, liver, lung, and kidneys that were routinely stained with H&E. As we found no noticeable differences compared to similar tissue samples from *Tsc2*^{+/+} littermates (Fig 2.4), we concluded that the *Tsc2*^{flox/flox} mouse could be used for future studies using organ or tissue-specific Cre-mediated deletion with confidence.

Embryonic and renal phenotypes in *Tsc2* KO mice are similar to those previously reported

To verify that the loxP sites were functional and would generate a null allele following Cre recombination, we mated the *Tsc2*^{flox/flox} mouse with a CMV-Cre transgenic mouse that expresses Cre in all cell types. *Tsc2*^{KO/KO} mice demonstrated midgestation lethality (Fig 2.5c) like the *Tsc2*^{neo/neo} mice, though at the earlier timepoint of E10.5-E11.5. While *Tsc2*^{KO/KO} embryos were still detectable at E12.5, they were severely underdeveloped compared to *Tsc2*^{+/KO} and *Tsc2*^{+/+} littermates. Comparison of the *Tsc2*^{neo/neo} (Fig 2.3b) and *Tsc2*^{KO/KO} embryos at this timepoint underscores the hypomorphic status of the *Tsc2*^{neo} allele as well as the importance of *Tsc2* in development. Western blot analysis of E12.5 *Tsc2* null embryos confirmed absence of tuberlin and significant expression of pS6, while



†Figure 2.5. Analysis of the Tsc2^{ko} allele. (a) Western analysis of E12.5 embryo lysates. Note the absence of tuberlin in Tsc2^{ko/ko} lysates, with the preservation of hamartin levels in all genotypes. Phosphorylated S6 is increased in Tsc2^{+/ko} and even more so in the Tsc2^{ko/ko} lysates, demonstrating activation of the mTOR pathway. (b) Comparison of embryos at E12.5. Wildtype and Tsc2^{+/ko} mice are virtually identical. The Tsc2^{ko/ko} mouse is severely growth retarded. (c) Genotype frequency of Tsc2^{+/ko} crosses demonstrating the lethality of Tsc2^{ko/ko}. Asterisk (*) denotes non-genotypable resorptions. (d) Kidney phenotype. Note the multicyst development (white arrows) in Tsc2^{+/ko} mice. A small tumor is indicated by the black arrowhead. (e) A large tumor was found in a Tsc2^{+/ko} mouse at 11 months of age. (f) Histology of a complex cyst. (g) Histology of tumor shown in panel e. Note the presence of giant cells and nuclei (white arrowheads). (h) Table characterizing the kidney phenotype. Note that cysts as well as tumors were detected within the first year of life, much sooner than with the Tsc2^{neo} phenotype.

†Figure and legend taken from (103).

Tsc2^{+/*KO*} samples also demonstrate a slight increase in pS6 levels compared to the *Tsc2*^{+/*+*} (Fig 2.5a).

Analysis of *Tsc2*^{+/*KO*} kidneys revealed a more severe phenotype than that seen in *Tsc2*^{*neo/neo*} mice, with multicyst formation found in a majority of mice as early as 7 months of age (Fig 2.5d). By 9 months, the renal cyst phenotype was 100% penetrant (Fig 2.5h). Though cystadenomas made up the majority of renal lesions found (Fig 2.5f), several small tumors were found in various kidneys with one large tumor (Fig 2.5e) found in an 11 month old mouse. Histologic analysis of this tumor revealed enlarged cells and nuclei (Fig 2.5g). Taken together, these kidney and embryo findings are similar to those demonstrated in *Tsc2*^{+/*KO*} mice characterized by Onda et al. (72) and Kobayashi et al. (73), confirming that the *Tsc2*^{*fllox*} allele may be used for Cre-mediated deletion of *Tsc2*.

Discussion

Our lab has created and characterized a novel *Tsc2* conditional allele using the *Cre-loxP* system (103). We have shown that the *Tsc2*^{*fllox/fllox*} mice are viable, fertile, and histologically similar to wild type mice. We have also demonstrated that the *Tsc2*^{*fllox*} allele is effectively converted to a null mutation upon *Cre*-mediated recombination, as evidenced by the similarities between *Tsc2*^{+/*KO*} mice generated using our *Tsc2*^{*fllox/fllox*} and previously reported *Tsc2*^{+/*KO*} phenotypes. This *Tsc2*^{*fllox/fllox*} allele will be a valuable tool for determining the role of tuberin in various organ systems, as well as for comparing the individual roles of hamartin and tuberin in TSC pathology.

In the process of creating this *Tsc2* conditional allele, we have also generated a hypomorphic allele, *Tsc2*^{*neo*}, in which a neomycin cassette is present between exons 1 and 2 of the *Tsc2* gene. Although the neo cassette is present in intronic space, presence of this

cassette has been shown to disrupt normal splicing patterns or cause premature transcript termination (105-108). These events often result in attenuation of gene expression or function, as evidenced in the *Tsc2^{+/-neo}* mice, which demonstrate a milder version of similar clinical manifestations compared to *Tsc2^{+/-KO}* mice. These *Tsc2^{+/-neo}* mice may be particularly useful for the study of a milder form of TSC found in patients, which has been associated with *Tsc2* missense mutations (109-111). A number of *Tsc2* missense mutations result in the expression of a stably expressed mutant form of tuberin which can still form a complex with hamartin and appears to have partial function (37, 112). Investigation of the *Tsc2^{+/-neo}* mice may establish a role for hypermorphic alleles with partial function in causing a milder clinical form of TSC (113).

Chapter Three:

Creation and Characterization of the Tsc2^{flox/ko}; hGFAP-Cre Mouse

All figures, legends, and the methods section of this chapter are taken or modified from a previous publication in which I was the first author. Guidelines from this journal do not require permission to reproduce manuscript content as part of a thesis, as described in this website: (http://www.oxfordjournals.org/access_purchase/publication_rights.html)

Introduction

Following the creation of the *Tsc2*-based conditional knockout allele (see Chapter 2), we sought to develop a *Tsc2*-based model of TSC neuropathology. Previous studies in mouse models showed that conditional deletion of *Tsc1* in mature astrocytes resulted in increased brain size, proliferation of astrocytes, abnormal neuronal organization, and clinically obvious seizures, with a median survival of 11-12 weeks (75). Meanwhile, deletion of *Tsc1* in post-mitotic, mature neurons using the same conditional allele resulted in a much more severe phenotype, including megalencephaly, enlarged, dysplastic, and ectopic neurons, reduced myelination, spontaneous or provoked seizures, and a median survival of 35 days (77). Taken together, both models replicate a number of important features of TSC brain pathology in humans. However, individually, neither fully recapitulate the main characteristics of the disease.

This finding may be due to the fact that the deletions generated in these mouse models were all in post-mitotic, differentiated cells. As TSC is a developmental disease and “...the cytoarchitecture of cerebral cortex surrounding tubers is typically normal,” it is likely that “...tubers result from a developmental defect that affects a restricted population of *neuronal precursor cells* during corticogenesis (21) (emphasis added).” Indeed, given that cortical tubers and subependymal nodules (SENs) contain semi-differentiated cells that contain both astrocytic and neuronal markers (16), inactivation of *Tsc1* or *Tsc2* likely occurs pre-differentiation in a neuronal-glial precursor cell.

In 2001, Noctor et al. (82) established that radial glial cells, long thought to be glial progenitors that were mainly used as scaffolding for migrating neurons generated elsewhere (114), were in fact neuroglial progenitor cells. Their study also confirmed the presence of a “lineage relationship between neurons and proliferative radial glia” in which “local clonal relationships in the embryonic ventricular zone can be translated into functional

columnar units in the adult neocortex (82).” As radial glia are progenitor cells that produce both neurons and glia, defects in the differentiation process in these cells may result in daughter cells that are semi-differentiated. Migrational defects in both neuronal and glia populations may also result should problems with the radial glial fibers that form the scaffolding for migration occur. Finally, as radial glial daughter cells form the columnar units found in the neocortex, issues with the mother cell may result in structural problems for the entire columnar unit. Taken together, these findings strongly indicate that radial glial cells are an excellent candidate for the origin of tubers, and perhaps other TSC brain lesions.

To test the neuroglial hypothesis of TSC neuropathology, we crossed an *hGFAP-Cre* (human glial fibrillary acidic protein) transgenic mouse (83, 84), in which Cre expression is confined to radial glial cells, with our floxed *Tsc2* allele (described in Results). The resulting *Tsc2^{flox/ko};hGFAP-Cre* mouse models many prominent features of TSC brain pathology, including defects in cell size, migration, myelination, and astrogliosis. Compared to the *Tsc1*-based astrocyte- and neuron-specific models, our *Tsc2^{flox/ko};hGFAP-Cre* mouse has a more severe phenotype with greater representation of human TSC characteristics. Therefore, this model demonstrates a likely role for radial glia as an origin of TSC brain pathology and provides a good model for the study of TSC neuropathology.

Materials and Methods (taken from (115))

Mice and genotyping – All animal experimentation was approved by the UTHSC Animal Welfare Committee. Mice were in a mixed 129 and C57/Bl6 background. *Tsc2^{+flox}*, *Tsc2^{+/-ko}* and *hGFAP-Cre* mice have been previously described (83, 84, 103). Mice were genotyped for *Tsc2* alleles using three primers in one PCR reaction: KO1: 5'-GCAGCAGGTCTGCAGTGAAT-3', KO2: 5'-CCTCCTGCATGGAGTTG-AGT-3'; WT2: 5'-CAGGCATGTCTGGAGTCTTG -3'. Band sizes were

wild-type (390 bp), *Tsc2^{fllox}* (434 bp) and *Tsc2^{ko}* (547 bp). Cre primers: CreF: 5'-GGACATGTTTCAGGGATCTCCAGGC-3', CreR: 5'-CGACG-ATGAAGCATGTTTAGCTG-3', RapA: 5'-AGGACTGGGTGGCTTCC-AACTCCCAGACAC-3', RapB: 5'-AGCTTCTCATTGCTGCGCGCCAG-GTTCAGG-3'. Band sizes were Cre (219 bp) and Rap (590 bp) as a positive control band. Cre and Rap primers were generously provided by the laboratory of Richard Behringer.

Histological studies – Adult mice were deeply anesthetized before undergoing transcardiac perfusion with PBS and then with 4% paraformaldehyde (PFA). Mouse brains were post-fixed in PFA overnight and stored in 70% ethanol prior to embedding in paraffin. Paraffin blocks were sectioned at 5 μ m. For embryo analysis, the day the vaginal plug was seen was considered embryonic day 0.5. Dams were anesthetized with 2.5% avertin and killed by cervical dislocation before embryos were dissected into cold PBS and staged. A small piece of the embryo was used for genotyping. Embryos were fixed in PFA 4–6 h and washed in 1xPBS before being stored in 70% ethanol and embedded in paraffin. Slides were rehydrated, stained with routine H&E, and protected with a coverslip. Immunofluorescence was performed by blocking in 10% serum from animal in which secondary antibody was raised and 0.05% Triton X-100 in 1 x PBS for 1 h. Primary antibody was allowed to incubate overnight at 4°C. Sections were washed in 1 x PBS followed by secondary antibody incubation for 1 h. Tissue was directly visualized for fluorescence-conjugated secondary antibodies. For adult BrdU analysis, pregnant dams were injected at E15.5 with 10 mg/ml of BrdU dissolved in 0.01 M NaOH in dH₂O. Brains from resulting pups were isolated and embedded as described above. Immunohistochemistry was also performed as described, though sections were incubated for 20 min in 2 N HCl prior to blocking, and visualization was achieved using a Vectastain Elite ABC Kit (Vector Labs, Burlingame, CA) followed by incubation in SigmaFAST DAB metal enhancer (Sigma, St. Louis, MO). For BrdU pulse-labeled

embryos, pregnant dams were injected 30 minutes before embryo extraction, and BrdU was visualized via immunofluorescence. Tissue images were examined using an Olympus BX51 or IX81 microscope and captured with a Qimaging RETIGA-2000RV digital camera or a Bio-Rad 1024 MP confocal microscope. Digital images were then processed using Adobe Photoshop (Version 6.0, San Jose, CA, USA).

Antibodies – The antibodies used for immunohistochemistry were as follows: Pax6 (1:2000, Developmental Studies Hybridoma Bank, Iowa City, IA, USA), phosphorylated (Ser 240/244) S6 (1:100, Cell Signaling Technology, Bedford, MA, USA), Cux-1 (1:50, Santa Cruz Biotechnology, Santa Cruz, CA, USA), FoxP2 (1:4000, Abcam, Cambridge, MA, USA), BrdU (1:50, Becton Dickinson, San Jose, CA, USA), GFAP (1:400, Sigma), CC1 (1:5, Calbiochem, Gibbstown, NJ, USA), S100 (1:100, DakoCytomation, Denmark and 1:500, Abcam), PCNA (1:50, Santa Cruz) and NeuN (1:100), Tbr2 (1:2000), Tbr1 (1:500) and MBP (1:200) from Millipore, Billerica, MA, USA. Prolong Gold antifade reagent with DAPI (Invitrogen, Eugene, OR, USA) was used for DAPI staining and coverslipping of post-natal tissue. Embryonic tissue was stained with Hoechst 33258 (Invitrogen) after removal of the secondary antibody and coverslipped using Fluoromount-G (SouthernBiotech, Birmingham, AL, USA). The antibodies used for immunoblotting were: tuberin (1:1000), hamartin (1:1000), pS6 (1:2000) and α -tubulin (1:1000), from Cell Signaling.

Quantitative analysis – Two or three serial sections from each mouse were used for analysis unless otherwise noted. For post-natal cell counts, equal-sized images spanning the thickness of the somatosensory cortex were taken at the same lateral distance from the midline. Count results were corrected to represent a percentage of cells in the cortex in order to account for differences in total cortex size. For embryo counts, equal-sized images spanning most of the length of the lateral ventricles were used. Marker-labeled cells with visible nuclei

were manually counted using Photoshop and ImageJ (v1.38x, W. Rasband, National Institutes of Health, Bethesda, MD, USA). For neuron cell size determination, the cortex was divided into five equal bins from the bottom of Layer I to the bottom of Layer VI. In one section each from three pairs of control and mutant mice, 50 NeuN-labeled neurons from Bin 3 were outlined and filled using Photoshop and area was analyzed in micrometers using ImageJ. For DG area calculation, one section each from three pairs of mice were stained with H&E. DG cell images were captured using a 60x objective and cells near the midline of the DG were outlined for area calculation in the same manner. Data were analyzed using repeated-measures ANOVA in SPSS (Version 16.0.2, Chicago, IL, USA) and Microsoft Excel (Version 2003, Seattle, WA, USA).

Protein analysis – Whole cell lysates were made from P21 cerebral cortex and hippocampus that were quick-frozen in liquid nitrogen. Samples were homogenized in a dounce homogenizer with 10 volumes of Ripa buffer with protease inhibitor cocktail and phosphatase inhibitor cocktail (Sigma). Lysates were centrifuged at 4°C, sonicated and frozen until use. Protein concentrations were determined with a BCA reagent kit (Pierce, ThermoFisher Scientific, Rockford, IL, USA). Equal amounts of protein were separated on a denaturing 4–12% gradient gel (Invitrogen) and transferred to nitrocellulose. The membrane was cut into sections and each section probed with different antibodies using a stripping procedure after each experiment if necessary. Secondary antibodies were horseradish peroxidase conjugated. Visualization was conducted with an ECL kit (Amersham, Piscataway, NJ, USA). (115)

Results

Generation of *Tsc2^{fllox/ko};hGFAP-Cre* mice

Tsc2^{flox/ko};hGFAP-Cre (mutant) mice were generated by mating male *Tsc2^{+/-};hGFAP-Cre* mice with previously characterized *Tsc2^{flox/flox}* females (103). This mating scheme was chosen to better model *Tsc2* deletion in TSC patients, in whom inactivation of one allele of *Tsc2* occurs in all cells and a second hit is thought to be necessary for pathology formation in a given organ (4). In our model, mice are born with one inactivated allele of *Tsc2* in all cells throughout the body, while the second somatic cell loss occurs only in radial glial cells where Cre is expressed. Cre expression begins at embryonic day 12.5 (E12.5) in the hippocampal anlage, as extensively characterized by Zhuo et al. (83) and Maletesta et al. (84). Though these studies found that Cre activity begins at E13.5 in the cortex, further studies have since demonstrated that Cre may be present as early as E12.5 in cortical neurons and glia (Seonhee Kim, unpublished observations). Radial glial cells and their progeny, which include the majority of neurons and glia in the cortex and hippocampus (82), are therefore the only cells in this mouse with complete loss of *Tsc2*. Though loss of heterozygosity (LOH) has been previously demonstrated in most TSC-associated lesions in the heart, kidneys, and lungs (4, 116), little evidence of LOH in cortical tubers has been found (31, 32, 117). Investigators have hence suggested that tuber formation may not require loss of both alleles or that "only a subgroup of cells within a tuber is affected by a second hit (4)." Characterization of this mouse model therefore also serves to demonstrate whether LOH may lead to formation of TSC-like neuropathology.

***Tsc2^{flox/ko};hGFAP-Cre* mice exhibit a failure-to-thrive phenotype and die of seizures by P23**

Tsc2^{flox/ko};hGFAP-Cre mice were born in the expected Mendelian ratio and appeared healthy until about post-natal day 8, when their weight gain slowed compared with littermate controls (Fig 3.1A). By weaning, *Tsc2^{flox/ko};hGFAP-Cre* mice were severely runted (Fig 3.1B) and died

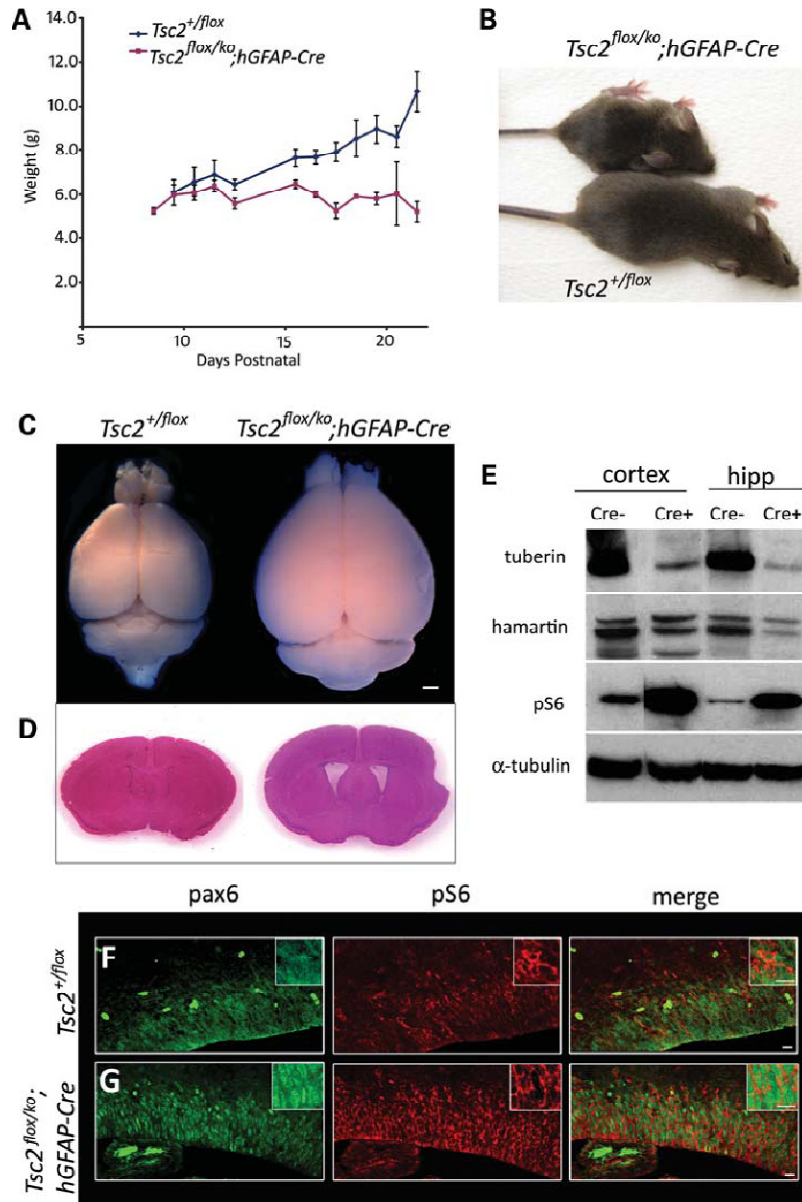


Figure 3.1. Generation of $Tsc2^{flox/ko};hGFAP-Cre$ mice. (A) Weight curves of mutant ($Tsc2^{flox/ko};hGFAP-Cre$) mice (red, n=17) compared with the control ($Tsc2^{+/flox}$) mice (blue, n=15) demonstrating the retarded growth of the mutant animals. (B) A runted mutant, 21-day-old (P21) mouse compared with a control littermate. Note the domed head and splayed feet in the mutant animal. (C) The brain of the mutant mouse (right) was noticeably larger than the control (left). (D) Ventricles in the mutant mouse were dilated (right). (E) Immunoblot analyses of cortical and hippocampal lysates from mutant ('Cre+') mice demonstrated a marked decrease of tuberin, slightly decreased levels of hamartin and large increase in pS6 levels compared with the control ('Cre-'). α-Tubulin was used as the loading control. (F and G) Pax6 and pS6 immunohistochemistry in E15.5 control (F) and mutant (G) mice showed increased activation of mTORC1 in the radial glial cells of the developing cortex. Scale bars, C, 1 μm; F and G, 10 μm.

Figure and legend taken from (115).

between 3 and 4 weeks, likely from seizures, as we observed several mice seizing (n=6) and the majority of dead mice were found in extensor posturing. The *Tsc2^{flox/ko};hGFAP-Cre* mice had splayed feet, domed heads, and were often tremulous and generally less active than littermate controls (115).

Though the mutant mice failed to gain weight after postnatal day 8 (P8), they had milk in their stomachs as neonates and were seen suckling after P8. Though the actual amount of food eaten was not measured, they were also observed feeding normally as late as P21, suggesting the weight issue was not due to lack of food intake. By weaning at P21, most mutant mice were sick-looking and spent the majority of their time hunched over. Interestingly, no mutants were observed having seizures that did not end in death, which occurred at a median age of P23 (n=20). Due to the lethality soon after weaning, all analyses were carried out at P21 unless otherwise specified.

***Tsc2^{flox/ko};hGFAP-Cre* mice have enlarged brains that demonstrate loss of tuberin**

Gross examination of the *Tsc2^{flox/ko};hGFAP-Cre* mouse brains revealed that they were enlarged compared to control brains (Fig 3.1C). Low magnification coronal sections through the lateral ventricles (Fig 3.1D) demonstrate a visible increase in thickness of the cortex, though the increase in brain width appears to be more dramatic posteriorly. Enlargement of the ventricles is also noticeable, suggestive of hydrocephalus.

To demonstrate extensive loss of tuberin, western analysis of cell lysates from P21 cortex and hippocampus of the *Tsc2^{flox/ko};hGFAP-Cre* and control mice was performed and demonstrated significant loss of tuberin antigen (Fig 3.1E). Hamartin levels were also slightly decreased in experimental lysates, reflecting the dependence of its stability on the presence of its binding partner tuberin (46). Loss of tuberin antigen

was accompanied by an expected activation of the mTORC1 pathway based on increased levels of phosphorylated (Ser 240/244) S6 (pS6). We then demonstrated that mTORC1 was activated in radial glia by performing immunohistochemistry on E15.5 brains using antibodies against the radial glial marker Pax6 and pS6 (Fig 3.1F, G) (118). In the mutant embryonic brains, more intensely red pS6 staining was seen surrounding the green Pax6-labeled nuclei of radial glial cells in the ventricular zone compared with the control. This increased pS6 expression in radial glial cells demonstrated activation of mTORC1 caused by loss of *Tsc2*. (115)

Loss of *Tsc2* in radial glia causes cortical enlargement, lamination defects, and increased cell size in *Tsc2^{flox/ko};hGFAP-Cre* mice

Closer histological examination of coronal sections of the control and mutant mouse brains confirmed that the mutant cortices were significantly thicker compared to the control (Fig 3.2A, B; 1.91 mm vs 2.65 mm, $P < 0.0005$). Lamination defects were also pronounced in the mutant, in which the normally clearly-demarcated cortical layers were blurred. This finding is most noticeable in the usually cell-sparse and well-defined marginal zone adjacent to the pial surface, also known as Layer I, which is poorly delineated in the mutant cortex.

Higher magnification of H&E-stained sections revealed significantly enlarged cells (Fig 3.2C-E, $P < 0.005$) in the mutant compared to the control. Though the nuclei of these cells appeared larger, closer observation also revealed enlarged vacuoles (data not shown), a possible indication of increased autophagy. The cells in the mutant cortex also appeared less densely packed compared to the control, suggesting an increase in extracellular matrix.

The loss of *Tsc2* in radial glia should have activated mTORC1 in all their neuronal and glial progeny, similar to what has been observed in human TSC lesions (119, 120). To assess cortical neuronal and

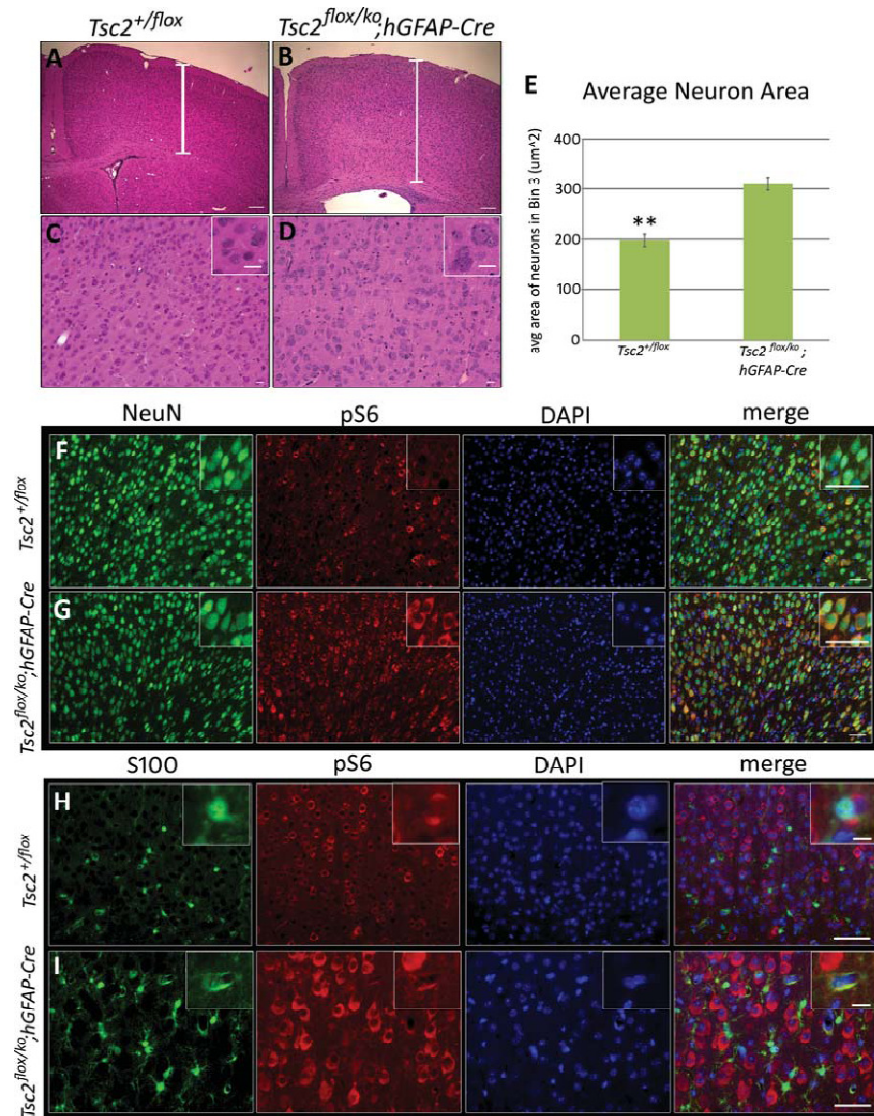


Figure 3.2. Cerebral cortical defects and up-regulation of mTORC1 in cortical neurons and astrocytes in *Tsc2*^{flox/ko};hGFAP-Cre mice. All sections were taken from P21 mice. **(A and B)** The cortex of the mutant (B) was thicker than the control (A) and displayed lamination defects, blurring between the gray–white junction, and a much less-defined molecular layer (Layer I). **(C and D)** Higher magnification revealed enlarged cells in the cortex of the mutant (D) and more extracellular matrix between the cells compared with the control (C). **(E)** Comparison of the areas of NeuN-labeled neurons from mutant and control cortex revealed that mutant neurons are significantly larger (**P<0.005, n = 6) than control neurons. **(F and G)** NeuN-labeled neurons in the mutant cortex (G) displayed substantial increase in pS6 expression compared with the control (F), indicating elevated mTORC1 activation. **(H and I)** S100-labeled astrocytes in the mutant cortex (I) also showed notable increase in pS6 expression compared with the control (H). Scale bars, A and B, 100 μm; C and D, 20 μm; F and G, 50 μm; H and I, 40 μm, inset 10 μm.

Figure and legend taken from (115).

astrocyte mTORC1 activation, we performed double immunohistochemistry against NeuN, a neuronal marker, or S100, an astrocyte marker, and pS6. In the rostral cerebral cortex, almost all NeuN-positive cells in the mutant demonstrated increased pS6 antigen (Fig 3.2F,G). Similarly, the S100-positive astrocytes in the rostral cortex of mutant mice were larger and expressed more pS6 than those of control animals (Fig 3.2H,I). (115)

Loss of Tsc2 in radial glia causes hippocampal organizational defects and neuronal hypertrophy in *Tsc2^{flox/ko};hGFAP-Cre* mice

Coronal sections of the mutant hippocampus revealed organizational defects of the pyramidal layer. Defects in lamination were most severe in the CA1 and CA3 regions (Fig 3.3B, F), in which the usually well-ordered and densely-packed neuronal layer, as seen in the control (Fig 3.3A, E), was disrupted. In fact, as most evident in the CA1 region (Fig. 3B), the ectopic, often enlarged (Fig 3.3G, black arrowhead) neurons seemed to form an almost distinct separate layer in the stratum oriens (SO). Though the defects in organization were less severe in the dentate gyrus (DG) of the mutant hippocampus (Fig 3.3C, D), many enlarged granule cells seemed to line the structure. A number of spherically-organized ectopic cells (seen as ring heterotopias) also dominated the stratum lacunosum molecular (SLM) of the mutant hippocampus (Fig 3.3H). Though these ring heterotopias mainly consisted of post-mitotic NeuN-labeled neurons with a few S100-labeled astrocytes (Fig 3.3I, J, white arrowheads), some cells were present that did not stain for either marker (black arrowhead). These NeuN-/S100- cells may represent Tsc2 null cells in which the process of differentiating into a neuronal or glial cell may have been disrupted.

Increased activation of the mTORC1 pathway was demonstrated by greater pS6 expression in both NeuN-labeled neurons (Fig 3.3K, L) and S100-labeled astrocytes (Fig

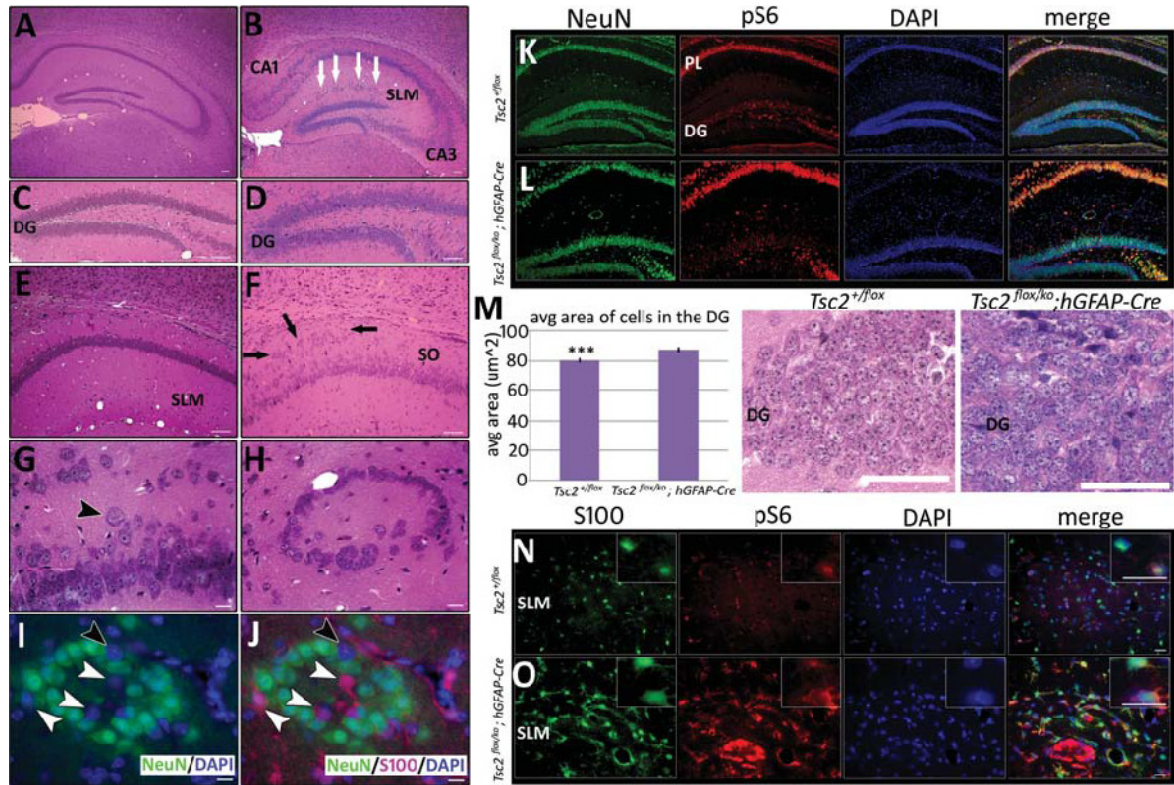


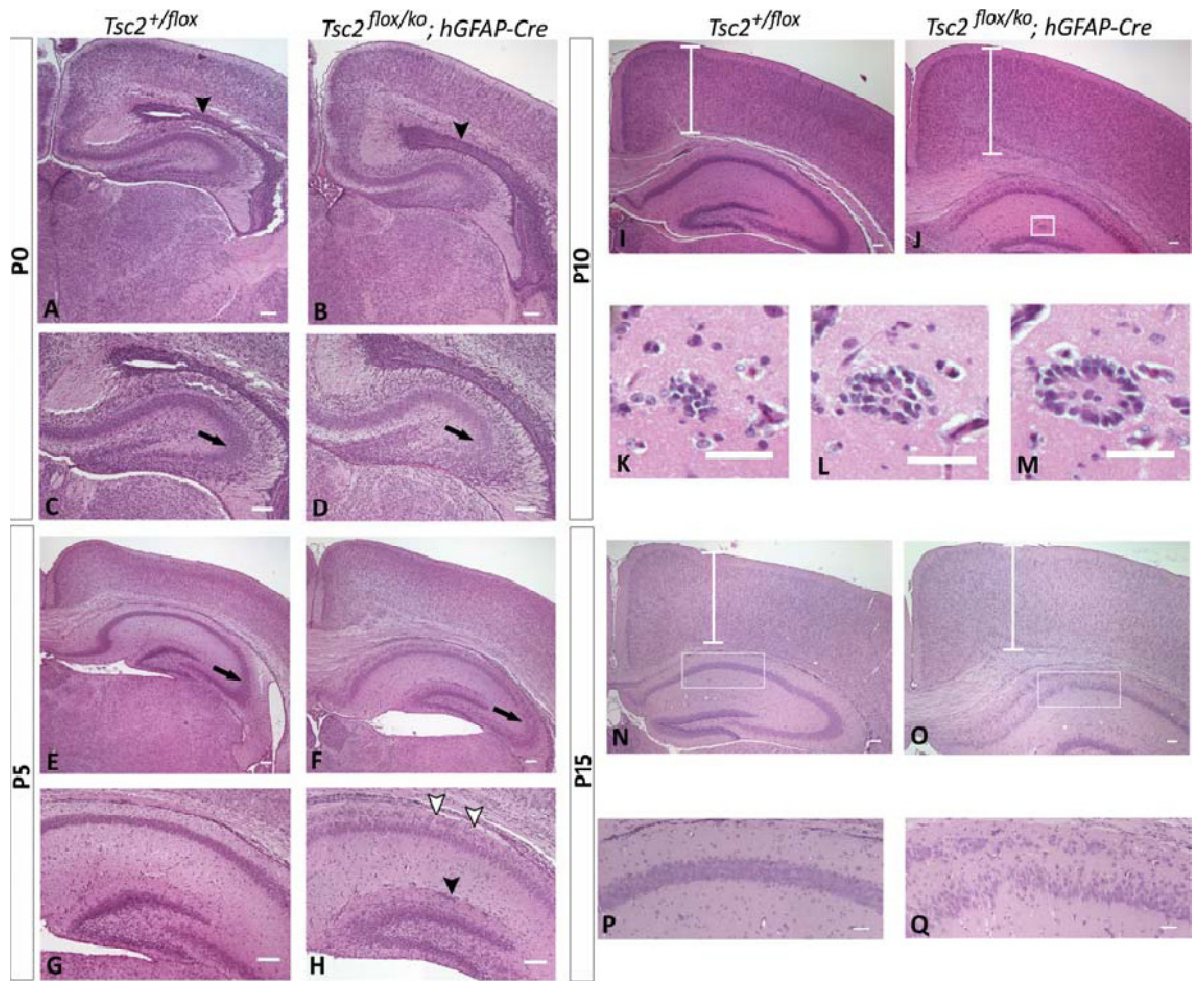
Figure 3.3. Hippocampal defects and up-regulation of mTORC1 in hippocampal neurons and astrocytes in *Tsc2^{flox/ko};hGFAP-Cre* mice. All sections were taken from P21 mice. **(A and B)** Severe lamination defects in the mutant mouse (B) were apparent in H&E-stained sections of the hippocampus, especially in the CA1 and CA3 regions. White arrows represent ring heterotopias that were evident throughout the SLM. **(C and D)** The DG was lined with large, ectopic granule cells in the mutant (D). **(E–G)** Numerous ectopic neurons (F, black arrows) and enlarged cells (G, black arrowhead) were also present in the SO of the mutant hippocampus (F), in contrast to the tight, well-organized pyramidal layer in the control (E). **(H–J)** High power magnification of a ring heterotopia demonstrated that they were mainly composed of NeuN-positive neurons (green cells) with some S100-positive astrocytes (I, J, red cells, white arrowheads), though some cells do not stain for either marker (I, J, black arrowheads). **(K and L)** NeuN-labeled neurons in the hippocampus of the mutant (L) displayed greater pS6 expression than the control (K). However, expression of pS6 in the DG of both the mutant and the control is reduced compared with their respective PL. **(M)** Despite low immunohistochemical pS6 expression in the mutant DG, average cell area of cells in the DG of the mutant was significantly larger (*** $P < 0.0005$) than the control ($n = 6$). **(N and O)** S100-labeled astrocytes in the hippocampus of the mutant (O) had increased pS6 expression. The SLM region of the hippocampus is shown. Scale bars, A–F, 50 μm ; G–J, 10 μm ; K and L, 100 μm ; M, 50 μm ; N and O, 20 μm .

Figure and legend taken from (115).

3.3N, O) in the hippocampus. However, expression of pS6 was not noticeably increased in the DG of the mutant hippocampus (Fig 3.3L), though previous characterization of the *hGFAP-Cre* transgenic mouse using a *Rosa-26* reporter confirmed Cre expression in this structure (83, 84). As increased mTORC1 activity often results in increased cell size, we quantitated the area of cells within the DG and found that the average area of cells in the mutant was significantly greater ($P < 0.0005$) than those of the control (Fig 3.3M), confirming upregulation of mTORC1 activity in the mutant DG despite our inability to detect increased pS6 expression.

Developmental analysis of *Tsc2^{flox/ko};hGFAP-Cre* mice reveals post-natal cerebral enlargement and possible migration defects.

To analyze the development of the cerebral abnormalities seen at P21, we examined hematoxylin and eosin (H&E) stained sections from E16.5–P15 (Fig 3.4). At E16.5, we observed no notable difference in thickness of the developing cortex between mutant and control (data not shown). At P0, the difference in thickness of the cerebral cortex was also minimal, though the ventricular zone appeared thicker in the mutant (Fig 3.4A, B). In the hippocampus, defects in organization of the CA3 layer of the mutant were already apparent (Fig. 3.4C, D). By P5, the difference in cortical thickness became more pronounced while the lamination abnormalities in CA1 and CA3 and ectopic neurons in the SO were evident. In the hippocampal fissure, there were several ectopic clusters of cells in the mutant brains (Fig 3.4E–H). These clusters appeared to be the site of origin of the future ring heterotopias. By P10, the mutant cortex was noticeably thicker than control and the ring heterotopias were becoming more obvious (Fig 3.4I–M). By P15, the mutant brains were similar histologically to brains analyzed at P21 (Fig 3.4N–Q). (115)



‡Figure 3.4. Post-natal developmental analysis of *Tsc2^{flox/ko};hGFAP-Cre* mice. H&E-stained sections from P0 to P15. **(A–D)** At P0, the size of the cerebral cortex was comparable between the control and the mutant. The ventricular zone (arrowheads) appeared thicker in the mutant and lamination abnormalities in CA1 and CA3 (arrows) were beginning to develop. **(E–H)** At P5, an increase in the cortical thickness of the mutant (F) was more apparent. The layering abnormalities in CA3 (arrow) were more pronounced. There were many ectopic cells in the SO of the mutant (H, white arrowheads) compared with the control. There was also the appearance of clusters of cells in the hippocampal fissure (black arrowhead). **(I–M)** By P10, the cerebral cortex of the mutant had continued to enlarge, and the layering was indistinct compared with the control. The ring heterotopias in the SLM were evident (inset J). The corpus callosum was also noticeably thicker. Sectioning through a heterotopia **(K–M)** demonstrated that they represent a nodule of ectopic cells. **(N–Q)** By P15, the same abnormalities were present as those seen at weaning. Scale bars, A, B, E–J, N, O, 100 μ m; C, D, K–M, P, Q, 50 μ m.

‡Figure and legend taken from (115).

Loss of Tsc2 in radial glia disrupts cortical lamination

To gain better insight into the lamination abnormalities identified with H and E staining in the mutant mouse, we performed immunohistochemistry using layer-specific antibodies to visualize individual cortical layers. Cux-1, a transcription factor that is expressed almost exclusively in the later-born neurons of Layer II-IV of the cortex (121), was used as a marker to reveal these well-defined layers in the control. In the mutant cortex, however, Cux1-labeled cells were not clearly restricted to Layers II-IV (Fig 3.5A). Although the majority of these labeled cells were in the appropriate cortical layers, they appeared disperse, with poor demarcation of the bottom of Layer IV. Most notably, a number of Cux1-labeled cells were also present in the lower cortical layers, further indication of a defect in cortical migration. As Reelin is essential for proper neuronal positioning and cortical layer formation (122), we examined Reelin-secreting Cajal-Retzius cells at E14.5 and found no notable difference in their numbers or Reelin expression (Fig 3.5I), suggesting the observed migration defect was Reelin-independent. To assess whether the ectopic cells were the result of aberrant proliferation, we quantitated the number of Cux1-labeled cells in the control and mutant and did not find a significant difference in density of the cells (Fig 3.5D). The migration defect was further investigated using BrdU labeling at E15.5. BrdU is a thymidine analog that is incorporated into dividing cells during S phase (123), and is therefore widely used to visualize proliferating cells at a given timepoint. By labeling with BrdU during neurogenesis and examining BrdU⁺ cell populations at P21, we were able to determine the final destination of cells born at E15.5 or immediately after (Fig 3.5F). Division of the cortex into 10 horizontal bins allowed us to quantitate the number of BrdU⁺ cells in each bin. This analysis demonstrated that mutant mice had increased ectopic cells in the lower layers of the cortex compared to the control, despite the similar birthdates of these labeled cells (Fig 3.5G). No significant difference was found between the total number of BrdU-labeled cells in

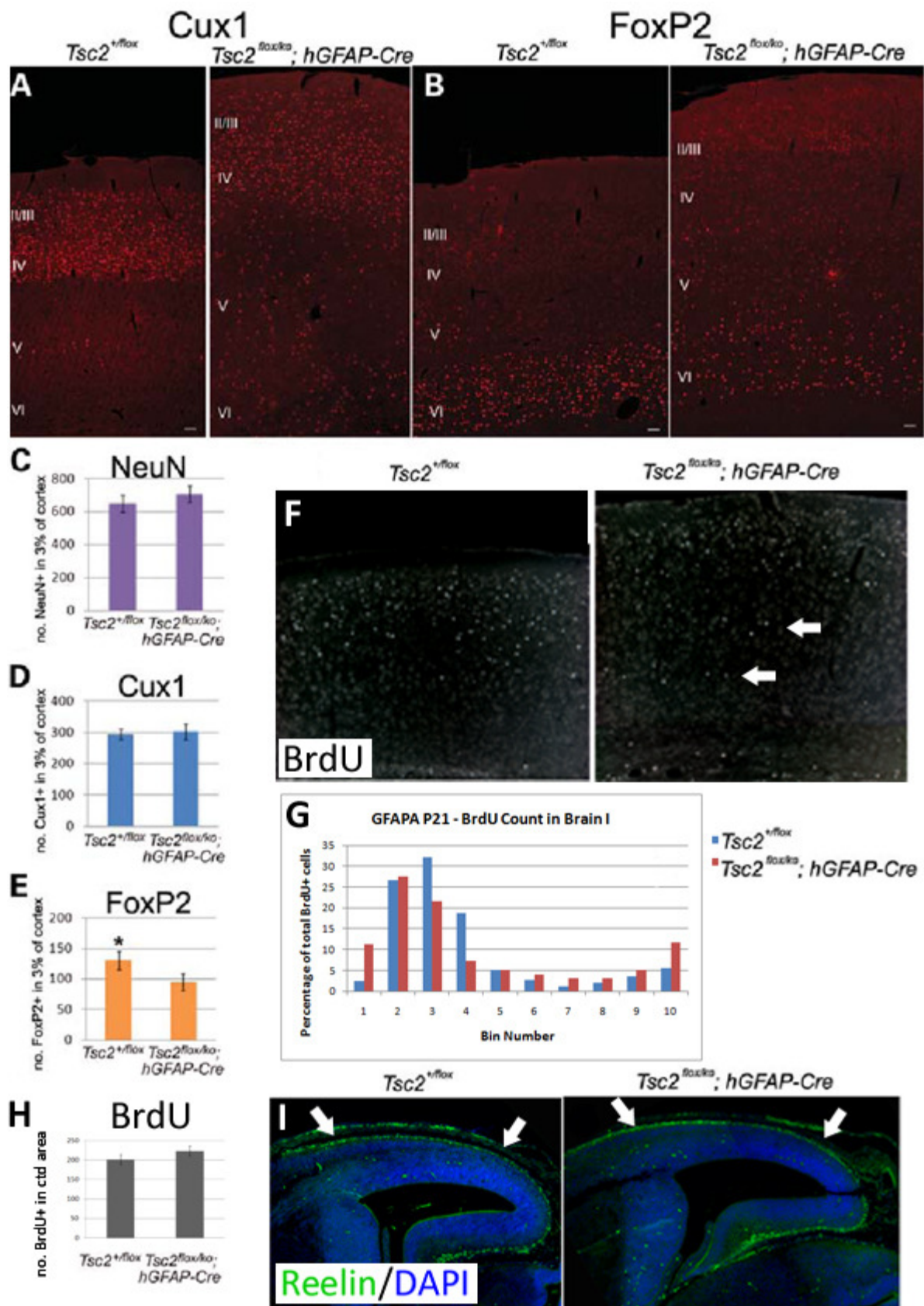
the control compared to the mutant (Fig 3.5H), supporting the Cux1 findings that migration was disrupted in these mice, with no evidence of a proliferation defect. This conclusion was further demonstrated by quantitation of all post-mitotic cortical neurons using NeuN, which showed no significant difference in total neuron density between the control and mutant animals (Fig 3.5C), while staining with PCNA, a marker for proliferation, at P10 showed no visible discrepancies between cell number (data not shown). Though we attempted to investigate cell death using TUNEL and cleaved caspase 3 (CC3) staining in embryonic day 16.5 (E16.5) and P10 sections, few cells in either the control or mutant appeared labeled in our hands. We therefore concluded that the lamination defect was most likely due to aberrant, Reelin-independent migration rather than abnormal proliferation.

Antibody against FoxP2, a transcription factor expressed exclusively in Layer VI in the mammalian neocortex (124), was used to further examine layering defects of early-born neurons. Interestingly, FoxP2-labeled cells remained in Layer VI in the mutant animal, though they too appeared poorly-organized and disperse within this layer (Fig 3.5B), as previously noted with Cux1-labeled cells. Since there seemed to be fewer FoxP2-labeled cells in the mutant cortex, we questioned whether this disperse effect was due to lower cell numbers or a defect in migration. In fact, density of FoxP2-labeled cells was significantly decreased ($P < 0.05$) in the mutant cortex (Fig 3.5E), with no evidence of labeled cells remaining in the ventricular zone (VZ), which if seen would indicate defective migration.

Taken together, the findings described above suggest that a proliferation defect is not present in the mutant cortex, while migration of the later-born neurons is somewhat defective. Furthermore, aberrations in cell layer populations might exist, given that fewer FoxP2-labeled cells are found with no difference in total neuron or Cux1-labeled density, total BrdU-labeled cell number, or evidence of cell death. Although attempts to quantitate

‡Figure 3.5. Lamination defects in the *Tsc2*^{flox/ko};*hGFAP-Cre* mice. All sections and counts conducted in P21 mice. **(A and B)** Cux1 (A), a Layer II –IV marker, and FoxP2 (B), a Layer VI marker, were used to assess lamination defects (n = 6 and 4, respectively). The Cux1-labeled cells of the control resided mostly in their designated layers, whereas the labeled cells of the mutant were scattered throughout the cortex. FoxP2-labeled cells were generally in Layer VI for both control and mutant. **(C–E)** Although density of NeuN-labeled neurons (C) and Cux1-labeled cells (D) were not found to be significantly different in the cortex, there were significantly less FoxP2-labeled cells in the mutant (E, P =0.05). **(F,G)** Cells born and labeled with BrdU at E15.5 mainly settle in the upper layers of the cortex, as seen in the control. Mutant mice display ectopic BrdU+ cells in the lower cortical layers (white arrows). **(H)** Total number of BrdU-labeled cells is not significantly different between the control and mutant. **(I)** Reelin staining at E14.5 demonstrates no observable difference between control and mutant Reelin expression of Cajal-Retzius cells in the developing brain.

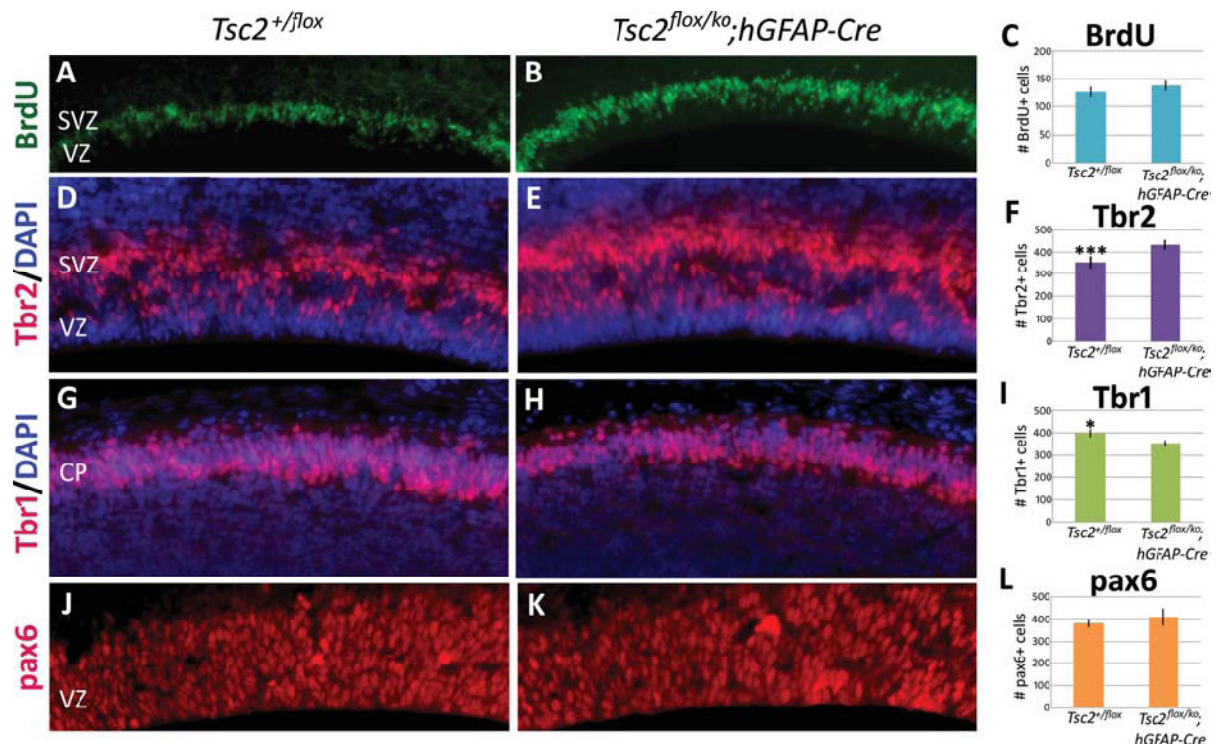
‡Figure and legend modified from (115).



neurons in the remaining Layer V using ER-81 were unsuccessful in our hands, our results indicate that more neurons displaying Layer V markers likely exist in the mutant.

***Tsc2^{flox/ko};hGFAP-Cre* mice exhibit altered cortical neural progenitor pools with no evidence of aberrant proliferation**

Though it is well known that the mTORC1 kinase and its downstream effectors are highly involved in proliferation (125), we found no significant difference in numbers of NeuN-labeled neurons in the mutant cortex. TUNEL and CC3 staining at E16.5 and P10 also revealed no noticeable increase in cell death in the mutant compared to the control (data not shown), suggesting that our equal cell numbers were not due to proliferation then subsequent death of cells. As cell death detection requires precise timing, we decided to instead confirm these results by investigating proliferation using BrdU pulse-labeling at E14.5, soon after *Tsc2* deletion occurs in radial glial cells. Quantitation of BrdU-labeled cells undergoing S phase following 30 minute pulse-labeling showed no significant difference between control and mutant animals (Fig 3.6A-C). We therefore concluded that defects in neuronal progenitor proliferation were not present in the mutant cortex. Though aberrant proliferation was not observed in the *Tsc2^{flox/ko};hGFAP-Cre* mouse, we wanted to further characterize the mechanism of the lamination defect by examining developmental formation of cortical layers. We had previously found a significant decrease in early-born FoxP2-labeled neurons in Layer VI of the mutant compared to the control, with no evidence that density of later-born Cux1-cells or total neuron density was different in the cortex. We therefore hypothesized, in the absence of evidence of cell death, that there must be an increase in Layer V neurons, and hence a defect in generation of neurons for specific layers. We investigated this phenomenon using markers for two major populations of cells at this mid-neurogenesis timepoint, Tbr1 and Tbr2. During radial glial cell (RGC)-mediated



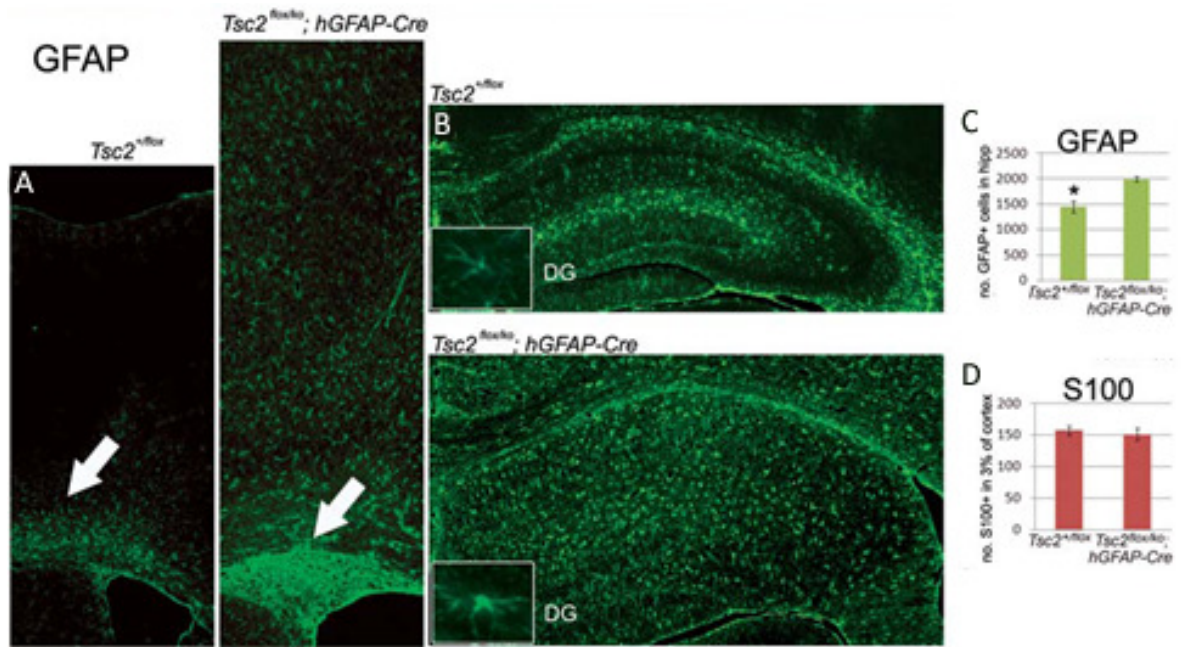
‡Figure 3.6. Cortical neural progenitor pool analysis at embryonic day E14.5. (A–C) BrdU pulse-labeling failed to detect any significant proliferative differences along the ventricles of the control and mutant embryos at E14.5 ($n = 6$). (D–F) Significantly more (F, *** $P < 0.0005$) Tbr2-labeled basal progenitor cells were found in the subventricular zone of the mutant (E) compared with the control (D) ($n = 6$). (G–I) The number of post-mitotic Tbr1-labeled neurons was significantly decreased (I, * $P < 0.05$) in the control (G) ($n = 6$). (J–L) Radial glia numbers (L), as labeled by pax6, were not found to be significantly different between the control and the mutant (J) ($n = 4$). CP, cortical plate, SVZ, subventricular zone, VZ, ventricular zone. A, B, G and H taken at 20x magnification, D, E, J and K taken at 40x.

‡Figure and legend taken from (115).

neurogenesis, neurons may arise directly from asymmetric division of RGCs (126) and become post-mitotic, thereby expressing Tbr1. Alternatively, RGCs may produce basal progenitor cells (BPCs) that express Tbr2, which in turn give rise to post-mitotic Tbr1-expressing neurons (118) in a process that produces the majority of neurons in the cortex. Since the process of neuron production via BPCs is less direct, the majority of Tbr1-labeled neurons at E14.5 should be the direct progeny of RGCs. Interestingly, we found a significant ($P<0.05$) decrease of Tbr1-labeled post-mitotic neurons at E14.5 (Fig 3.6G-I), accompanied by a highly significant increase ($P<0.0005$) of Tbr2-labeled BPCs (Fig 3.6D-F). This data suggests that deletion of *Tsc2* in RGCs caused an imbalance in the production of postmitotic neurons and BPCs, where instead of directly generating neurons, a number of RGCs generated BPCs. Then again, to replenish the neuroprogenitor pool, RGCs may also undergo symmetric divisions and generate more RGCs, which may explain the subsequent increase in BPCs. No significant difference in pax6-labeled RGC numbers was found, however. Taken together, this data indicates that symmetric RGC division is not disrupted following *Tsc2* deletion, though asymmetric division into neurons or BPCs is altered. The finding of less early-born Tbr1-labeled cells in the mutant supports our results for fewer early-born FoxP2-labeled neurons. However, the notable increase in BPCs which generate the majority of later-born neurons does not translate into increased Cux1-labeled cell density by P21.

***Tsc2^{flox/ko};hGFAP-Cre* mice exhibit astrogliosis**

Astrogliosis, in which astroglia become “active” in response to CNS injury and disease, is characterized by cellular hypertrophy, abnormal astrocyte proliferation, and an increase of intermediate filament proteins such as GFAP (127). As TSC tubers and subependymal nodules often present with astrogliosis (119, 128), we examined the *Tsc2^{flox/ko};hGFAP-Cre*



‡**Figure 3.7. Astrogliosis in the *Tsc2^{flx/ko};hGFAP-Cre* mice.** (A and C) Immunostaining of GFAP in the cortex (A) revealed substantial increase of GFAP-expressing astrocytes in the cortex compared with the control. Intense GFAP expression was also seen in the mutant ventricular zone of the lateral ventricle (white arrows). As quantification of GFAP+ cells in the cortex was difficult in the control, S100 (D) was used to label cortical astrocytes. No significant difference was found in S100+ cells between the mutant and the control. (B and D) GFAP expression was notably higher in the mutant hippocampus where astrocytes had larger cell bodies but shorter, thicker processes compared with the control (B). Significantly more GFAP-labeled cells (C) were present in the mutant hippocampus.

‡Figure and legend modified from (115).

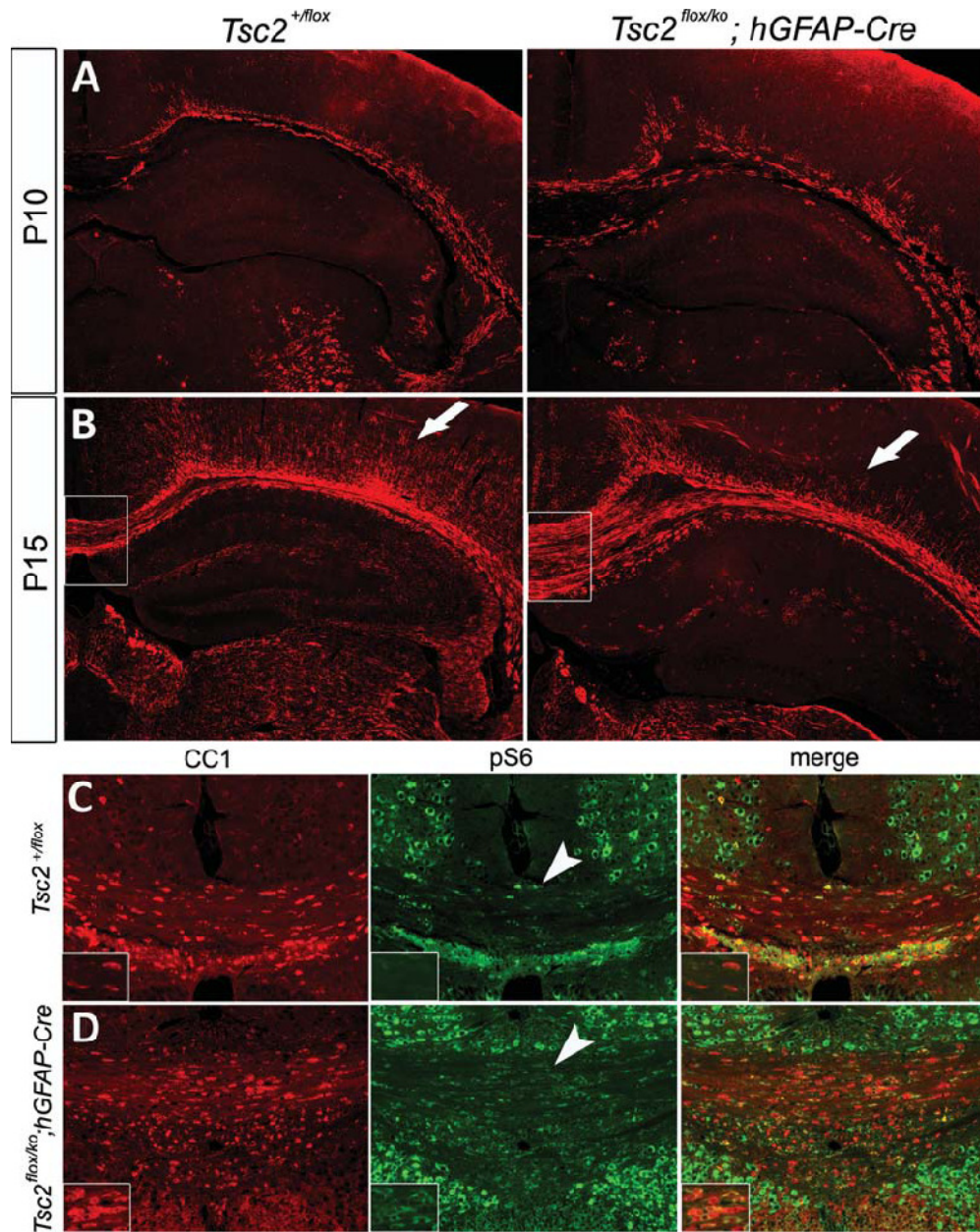
mutant cortex to determine whether it displayed an astrogliosis. Immunohistochemical analysis using GFAP revealed a substantial increase in GFAP expression in the mutant cortex, where particularly intense GFAP expression was found in the ventricular zone of the lateral ventricle, suggestive of disrupted migration of glia (Fig 3.7A, white arrows). GFAP expression was also increased in the mutant hippocampus (Fig 3.7B), where astrocytes displayed signs of being “active” with enlarged cell bodies and shorter and thicker processes. Abnormal proliferation of GFAP-expressing astrocytes was found to be significant in the mutant hippocampus (Fig 3.7C). Since endogenous expression of GFAP in the cortex is too low for detection, we used antibody against S100, a mature astrocyte marker, to quantitate astrocyte numbers in the cortex. Interestingly, we did not find a significant increase of S100-labeled cells in the cortex (Fig 3.7D), despite augmented GFAP expression. These results indicate that astrogliosis is present in both the mutant cortex, where it is characterized only by astrocyte activation, and the hippocampus, where it is characterized by astrocyte activation and proliferation.

Loss of *Tsc2* in radial glia results in defective myelin progression despite increased numbers of mature oligodendrocytes

Advances in MRI imaging techniques have identified a variety of white matter defects in the brains of TSC patients (129, 130). Diffusion tensor MRI, which detects the direction and magnitude of water diffusion in tissues, has even identified microstructural defects in normal-appearing white matter from TSC patients (130). Some of the most common white matter lesions identified in the brains of TSC patients were gliosis and hypomyelination. The neuron-specific *Tsc1* mouse model demonstrated significant hypomyelination (77). (115)

We sought to investigate defects in white matter in our mutant mice by performing immunohistochemistry for myelin basic protein (MBP), a major component of and a common marker for the myelin sheath. By P10, myelin within the corpus callosum is notable in both control and mutant animals (Fig 3.8A), though several areas display only patchy expression of MBP in the mutant. By P15, however, the control animal contains a large number of myelinated fibers in the lower layers of the cortex, in stark contrast to the relatively sparsely myelinated cortex of the mutant (Fig 3.8B). The myelination patterns seen at P15 were similar to those seen in P21. By examining myelination progress at these different stages of postnatal development, we concluded that the hypomyelination finding was not due to demyelination but rather a defect in myelin progression in the lower cortex.

Since the production of myelin requires differentiation from oligodendrocyte progenitor cells to mature oligodendrocytes (131, 132), we sought to explain the hypomyelination defect by examining mature oligodendrocytes using a marker called CC1. Surprisingly, we found a significant increase in CC1-labeled mature oligodendrocytes in the corpus callosum of the mutant mouse compared to the control (Fig 3.7C, D, $n=4$, $665 \text{ cells/mm}^2 \pm 46$ versus $532 \text{ cell/mm}^2 \pm 35$, $P = 0.05$), while immunostaining with pS6 and CC1 revealed that a number of oligodendrocytes also demonstrated upregulated mTORC1 activity. In spite of the increase in oligodendrocytes, however, myelination does not progress. It is unclear whether the increase in mature oligodendrocytes with upregulated mTORC1 activity contributed to the hypomyelination in the mutant mice, or if the myelin defect is unrelated to the oligodendrocytes findings.



‡Figure 3.8. Postnatal developmental analysis of hypomyelination and oligodendrocytes in the mutant. (A and B) Immunostaining of MBP at P10 (A) and P15 (B) demonstrated a defect in myelin formation in the mutant cortex (arrows). **(C and D)** Oligodendrocyte analysis using CC1 revealed a 1.25-fold increase in CC1-labeled cells in the mutant ($n = 4$, data not shown) compared with the control. Colocalization of pS6 and CC1 (arrowheads) showed that most oligodendrocytes in the mutant had up-regulated mTORC1 activity.

‡Figure and legend taken from (115).

Discussion

We have generated a mouse model in which *Tsc2* is conditionally ablated from radial glial cells, which are neuroglial progenitors involved in migration that produce the majority of neurons and glia in the cortex and hippocampus. These *Tsc2^{flox/ko};hGFAP-Cre* mutant mice fail to gain weight by P8 and are severely runted and sick-looking by P21, subsequently dying of seizures at a median age of P23. They develop a postnatal megalencephaly with dilated ventricles, cell hypertrophy and lamination defects in the cortex and hippocampus, and ring heterotopias. Immunoblots and immunohistochemistry using pS6, an indicator of mTORC1 activation, confirm that tuberin function is lost and mTORC1 is upregulated in most neurons and glia of the cortex and hippocampus. These mice also demonstrate evidence of abnormal cell division of radial glia during neurogenesis, in which the early-born neuron pool was significantly decreased while the intermediate progenitor pool was significantly increased. Mutant mice also demonstrate an astrogliosis and defects in myelin formation, though there is an increase in mature oligodendrocytes within the corpus callosum. Taken together, these data demonstrate that our mouse model recapitulates many aspects of TSC brain pathology and will be very useful in studying this disease.

Loss of heterozygosity as a mechanism of TSC neuropathology formation

TSC is considered a tumor suppressor disease in which loss of heterozygosity (LOH) has been readily demonstrated in almost all lesions except tubers (4, 128). This has led to questions regarding the necessity of LOH in the formation of TSC brain pathology. One of our goals in generating this mouse using a two-hit strategy was to determine whether LOH would result in TSC-like neuropathology. The similarity of characteristics between our *Tsc2^{flox/ko};hGFAP-Cre* mouse and human TSC lesions demonstrate that LOH of *Tsc2* can lead to TSC-like neuropathology, lending support to the two-hit hypothesis for brain lesion

formation. Establishment of LOH as a mechanism for TSC neuropathology formation could be further supported by comparing the *Tsc2* heterozygous littermates of our mutant mouse, the *Tsc2^{+/ko};hGFAP-Cre*, with the mutant itself to determine if inactivation of one allele of *Tsc2* alone can generate TSC-like neuropathology. The presence of Cre in the same radial glial cells as the mutant is necessary in this case to control for Cre as a possible variable. Though we have not thoroughly characterized the brain of the *Tsc2* heterozygote, gross examination suggests these mice are not distinguishably different from the control. Characterization of other *Tsc2^{+/-}* mice has also yielded little observation of brain pathology aside from an astrogliosis (72), suggesting that both alleles of *Tsc2* must be inactivated to generate the TSC-like neuropathology observed in our mutant mouse.

*What causes the megalencephaly in *Tsc2^{flox/ko};hGFAP-Cre* mice?*

The presence of “giant” cells is a main characteristic of TSC brain pathology, while association with hemimegalencephaly is considered one of the aspects of TSC brain lesions (16). We have found that enlarged cells in the cortex and dentate gyrus as well as postnatal megalencephaly are also major features of the *Tsc2^{flox/ko};hGFAP-Cre* mouse. Studies regarding the effects of *TSC2* deletion in *Drosophila* (67-70) have established increase in cell size as a major consequence of mTORC1 activation, which we have confirmed in the cortical and hippocampal neurons and astrocytes of the *Tsc2^{flox/ko};hGFAP-Cre* mouse. The cause of the increased brain size, however, is less clear. Megalencephaly is typically thought to result from one of three events: 1) an increase in cell number (133), 2) an increase in extracellular matrix (ECM), or 3) an increase in cell size. While we did not find a significant difference in density of post-mitotic neurons and astrocytes in the P21 cortex, on average more cells were actually present in the larger mutant cortex. Further characterization of this possible defect must be conducted to determine whether increase in

cell number causes the increase in brain size (see Ch 6 Discussion for details), especially as quantitation of cells undergoing S-phase at E14.5 has provided no evidence of a defect in proliferation in the developing mutant cortex. We have also investigated possible contributions to brain size from proliferation of cortical interneurons, which are not produced from radial glia and therefore do not demonstrate Cre expression (84) but, like all other cells in the mutant body, are heterozygous for the *Tsc2* deletion. Quantitation of interneuron populations using calretinin and calbindin showed no significant increase in numbers of these cells (data not shown). Meanwhile, closer examination of the mutant and control cortex, as seen in Fig 3.2C-D, suggests that the mutant cells are more sparse, which may be indicative of an increase in extracellular matrix. While we have not directly characterized this possibility, the similar density of cells in the control versus mutant indicates a proportional increase of ECM with increase in cell number, suggesting a combination of the two defects may be occurring in the mutant. In addition, we have previously shown that the percentage of increase in neuronal cell area is similar to the percentage of increase in cortical thickness. While more thorough investigation of all possible causes is needed, the proportional increases in brain size to cell size suggest cell size may also contribute to the megalencephaly.

Why do $Tsc2^{flox/ko};hGFAP-Cre$ mice fail to thrive?

Though the brains of the mutant mice are enlarged, the mice are runted and display a failure to thrive phenotype. While this symptom is typically caused by inadequate caloric intake (134), we have tentatively ruled out starvation as a reason for this effect given that milk is routinely seen in the stomachs of mutants, they have been observed suckling beyond the time they stop gaining weight, and even in their sickened, hunched-over state around P21, they still have observed feeding normally. Actual caloric intake must be

measured before it may be formally ruled out as a reason for starvation. Possibilities other than restricted caloric intake might also explain why the mice fail to gain weight even with feeding. For example, though the mice may be feeding normally, signals converting this intake into actual growth may have been disrupted. It is well-established that the mTORC1 pathway plays an important role in nutrient-sensing. Its major known role, as reviewed in Chapter 1, is to integrate a number of signals derived from growth factors, energy status, oxygen, and amino acids to set overall growth rates via cell cycle-coordinated growth and division (135). By altering basic mTORC1 function via deletion of one of its major regulators, we are directly disrupting a sensory pathway that is crucial for proper development and growth. Though failure-to-thrive is not a common phenotype in TSC patients, understanding of this side effect of *Tsc2* deletion in our mutant mouse may provide further insight into the role of *Tsc2* and mTORC1 in gross development and growth.

Potential causes of the neuronal migration defect

Migration of neurons to their appropriate positions is critical for proper brain function. In the mammalian brain, migration is a highly complicated process that involves a number of signaling factors that are susceptible to influence from environmental and genetic factors (136). Though TSC brain lesions are characterized by proliferation and differentiation defects as well, di Mario (16) suggested in 2004 that TSC neuropathology should be considered more cohesively as a neuronal migration disorder:

This is justified because in tuberous sclerosis complex, histologic features exist that are characteristically identified in neuronal migration disorders in general...[such as] (1) abnormal number, size, and thickness of cortical gyri; (2) heterotopic neuronal aggregates; and (3) variable degrees of cortical cytoarchitectural disorganization and aberrant columnar and laminar arrangement. (16)

The severe defects in migration found in the *Tsc2^{flox/ko};hGFAP-Cre* cortex and hippocampus model the characteristics described above. Basic H&E staining revealed blurred cortical layering in the cortex, most obviously in the usually clearly-demarcated marginal zone that is poorly defined in the mutant. Immunostaining with layer markers provided further evidence of lamination defects, including a number of ectopic cells stuck in the lower layers of the cortex despite their expression of upper-layer markers. Problems with migration were particularly notable in the hippocampus, in which an almost entirely separate layer of ectopic cells existed above the dispersely-organized pyramidal layer. Ring heterotopias were common in the SLM region of the mutant hippocampus as well, which developmental studies suggest may be formed by cells stuck along the hippocampal fissure. This finding is interesting given that *TSC2* has been found to play a critical role in cell spreading, polarization, and migration. For example, fibroblast cells deficient in *TSC2* were “impaired in their ability to spread and to alter actin cytoskeleton upon stimulation with IGF-1 (137).” The majority of cells in the cortex and hippocampus of the mutant mouse seem to exhibit only mild migration defects, as evidenced by the large number of *Cux1* cells present, though not well organized, in their designated layers and the formation of an at least recognizable pyramidal layer in the hippocampus. However, a number of the defects in the mutant seen do appear to be due to inhibited migration, suggesting that a contributing factor to this effect may be *Tsc2* deletion in these “stuck” cells that changes their ability to reorganize the actin cytoskeleton efficiently.

On the other hand, the presence of less mobile cells may be due to inhibited migration of their progenitor, the radial glial cell. The mouse mutant of the lissencephaly gene, *Lis1*, exhibits a very similar pattern of hippocampal disorganization compared to our mutant mouse. Studies in this mouse revealed that *Lis1* RNAi blocked interkinetic nuclear migration in radial glial cells (138). Radial glial cells migrate from the subventricular zone

(SVZ) during S phase to the apical surface (AS) along the ventricle during M phase (139), and studies have suggested that radial glia must reach the AS if mitosis is to occur (140). If deletion of *Tsc2* in radial glia affects *Lis1* expression or a gene of similar function, the observed “stuck” cells could conceivably be radial glia that had reached the AS and generated similarly immobile neurons and glia. This hypothesis could also explain the semi-differentiated “giant” cells found in TSC brain lesions as immobile radial glia that had not been able to reach the AS to differentiate.

Meanwhile, *Lis1* RNAi was also found to block conversion of cells generated in the SVZ by basal progenitor cells (BPCs) into their bipolar, migratory form (138). These cells would be post-mitotic neurons that were unable to migrate to their proper layer, another possible origin of the ectopic cells found in our mutant mouse. Indeed, about 38.8% of cortical neurons were found to display aberrant polarity in the neuron-specific *Tsc1* CKO (77), suggesting an impact on *Lis1* or a protein of similar function by *Tsc1/2*.

As the radial fiber tracts produced by radial glia are essential for proper radial migration and columnar organization (141), the disruption of these tracts via *Tsc2* deletion alone may explain the migration defects we see in the mutant. Interestingly, however, both the neuron- (77) and astrocyte-specific (75) *TSC1* CKO mice exhibit defects in migration as well, suggesting the aforementioned, radial-glia independent explanation may be more likely. In the neuron-specific mouse, cortical lamination is mainly disrupted with little disturbance in the hippocampus. In the latter, hippocampal organization is severely altered, with no demonstration of neocortical lamination defects. Surprisingly, disorganization of the hippocampus was not observed until 3 weeks of age in the astrocyte-specific *Tsc1* CKO, with progressive disruption occurring over the next 5 weeks. This is contrary to our observations in the *Tsc2^{flax/ko};hGFAP-Cre* mutant, in which migration defects in the hippocampus seem to be present from birth (Fig 3.4). Uhlmann et al. (75) suggest the

progression of aberrant neuronal migration in the hippocampus may be closely related to the astrogliosis they too observe in their mutant, where the increase in astrocytes “displaces” the neurons. However, since they see regional specificity of the neuronal migration though the astrocytosis occurs throughout the brain, they also suggest the possibility that new neurons are being generated from the nestin-positive, immature astrocytes which may be “progenitors.” Finally, they also discuss the important but still poorly-understood relationship between astrocytes and neurons, and the possible ways astrocytes may influence neuronal migration. Since our mouse model also displays a reactive astrogliosis, exploration of these suggestions may yield interesting insight into the contributions of astrocytes to TSC brain pathology. Further discussion of other possible mechanisms behind the migration defect may be found in Chapter 6.

Astrogliosis and hypomyelination

Reactive astrogliosis, in which astrocytes undergo changes in molecular expression and morphology, has been traditionally thought to occur in response to CNS injury (127). Despite lack of direct injury, however, astrogliosis has been repeatedly observed in tubers and subependymal nodules (119). *Tsc2^{fllox/ko};hGFAP-Cre* mutant mice also demonstrate an astrogliosis throughout the cortex and hippocampus, though proliferation of GFAP-labeled astrocytes is only seen in the hippocampus. It is unclear what role astrogliosis plays in TSC pathophysiology. Recent studies have indicated that astrogliosis is not an all-or-nothing response, and in fact involves a “finely gradated continuum of progressive changes in gene expression and cellular changes” (142). As such, mild-to-moderate forms of astrogliosis may result in hypertrophy of the astrocyte and its processes, while more severe forms may involve proliferation of astroglia to initiate scar formation (142). Severity of the reaction is therefore dependent on the severity of the insult. As the role of astroglia under normal

conditions is to “maintain the integrity of the blood-brain barrier, provide neurotrophic support for neurons, and contribute to neurotransmitter and extracellular ion homeostasis...(143)”, it is thought that disruption of these processes triggers astrogliosis as a rescue mechanism. Studies have shown that ablation of reactive astrocytes significantly increased neuronal death, exacerbated tissue degeneration, and impaired blood brain barrier (BBB) repair (127) following injury.

Hence, the presence of moderate to severe reactive astrogliosis in our mutant mice may indicate that deletion of *Tsc2* in radial glia has resulted in enough insult that this mechanism is triggered. Indeed, a majority of enlarged and reactive astrocytes are found surrounding giant cells, or hypertrophic cells of mixed neuronal and astrocytic lineage, in human tubers (119). Although we do not see giant cells in our mouse model per se, enlarged cells and ring heterotopias are common, and may contribute to causing the resulting astrogliosis.

We also observe a defect in myelin progression in the cortex of our mutant, despite presence of mature oligodendrocytes and myelin presence in the corpus callosum. Though it is unclear whether the increase in oligodendrocytes number has an effect on the hypomyelination observed in our mouse, it is known that myelination of axons requires proper signaling from the neuron (Sher 2008). This suggests the defect in myelin progression may be indicative of damage to the neuronal axons (143), another trigger of astrogliosis. However, in the neuron-specific TSC1 CKO mouse, astrogliosis is not observed, despite neuronal hypertrophy and myelination defects (77). On the other hand, astrogliosis with increased proliferation over time is seen in the astrocyte-specific TSC1 CKO (75), and aberrant mTORC1 activation has been demonstrated in reactive astrocytes in TSC tubers (119). These studies indicate that the astrogliosis found in our mutant mouse may simply be the result of *Tsc2* deletion in these astrocytes, rather than a response

mounted by the body to address insult. Further characterization of this mechanism will be required to determine whether either process or a combination of both events lead to the astrogliosis observed in our mutant mouse.

Understanding of the process by which the astrogliosis occurs will be particularly interesting given that “hypertrophy of astrocytes during the process of epileptogenesis has been observed before the development of seizures and in the absence of other pathological change (144).” If reactive astroglia might significantly contribute to epileptic activity, as a study by Tian et al. (145) indicates, inhibition of the astrogliosis alone may alleviate seizure activity in our mice as well as patients. However, while the neuron-based TSC1 CKO mouse did demonstrate seizure activity, reactive astrogliosis was not seen (77), encouraging further investigation into the role of astrogliosis in TSC pathophysiology as well as seizure activity.

Conclusions

In this study, we have generated and characterized a novel model of TSC brain pathology by deleting *Tsc2* in radial glial cells in the mouse. The *Tsc2^{flox/ko};hGFAP-Cre* mouse exhibits a number of characteristics observed in TSC brain lesions and will provide valuable insight into TSC-related defects as well as mammalian neurodevelopment. As both neurons and astrocytes of this mouse display highly upregulated mTORC1 kinase activity, future work will assess the effect of mTORC1 inhibitors such as rapamycin on the various TSC-like defects discussed. These efforts will significantly increase our understanding of TSC pathology while elucidating the roles of mTORC1 and other pathways in TSC neuropathology formation.

Chapter Four:

Rapamycin Treatment of the Tsc2^{flox/ko}; hGFAP-Cre Mouse

Introduction

The *Tsc2^{flox/ko}; hGFAP-Cre* mouse recapitulates many characteristics of human TSC neuropathology, including megalencephaly, cell hypertrophy, defects in lamination, hypomyelination, and astrogliosis. These similarities make it an excellent model with which to test novel therapies. As the main known role of the hamartin-tuberin TSC complex is to inhibit the mTORC1 kinase, preclinical animal studies and human studies have been initiated to determine whether rapamycin, a macrolide that also inhibits mTORC1, might be able to “replace” the function of the lost TSC complex. Treatment in TSC1 CKO mouse models indicate that rapamycin is able to decrease brain and cell size, inhibit seizures, and alleviate myelin defects and astrogliosis (93, 94). Human studies have shown that treatment with rapamycin results in reduction of subependymal giant cell astrocytoma (SEGA) size, though it appears to have little impact on tubers (146). Though these studies demonstrate substantial benefits of rapamycin use on TSC-related defects, full rescue of the neuropathology has not been achieved. Continuous treatment with rapamycin was also needed in both human and mouse studies to prevent resurgence of the disease state.

These preliminary findings of the effects of rapamycin on TSC neuropathology have raised a number of considerations regarding the potential of rapamycin for the treatment of TSC. First, the aforementioned studies all began treatment postnatally, with the earliest mouse treatment beginning at P7 (94). As TSC is a developmental disorder, however, the majority of defects in the brain are believed to be initiated during prenatal neurodevelopment. Tubers have been detected as early as 19-20 weeks in a human fetus (78, 79). Therefore, by the time rapamycin is administered postnatally, the majority of TSC defects have already formed. We hypothesized that rapamycin rescue might be more effective if administered during fetal and early development. We therefore designed a series of treatment regimens that would compare and contrast prenatal, postnatal, and combined

pre- and postnatal rapamycin treatments. The prenatally treated group was administered rapamycin at E12.5, when *Tsc2* is deleted, until birth in pregnant dams as the “prenatal” or “pre rap” treatment cohort (Fig 4.1). We then withdrew treatment and allowed the mice to live until P21, at which point we examined their brains for comparison to the untreated mutant. Characterization of this cohort not only determined the extent of rapamycin’s ability to rescue prenatal defects, but tested whether prenatal rescue can inhibit formation of postnatal defects such as megalencephaly and hypomyelination.

Neurodevelopment continues throughout the postnatal period, as evidenced by the several defects in the *Tsc2^{flax/ko}; hGFAP-Cre* mice that developed postnatally. We therefore hypothesized that immediate postnatal treatment might also be more effective than treatment from P7. Though prenatal rapamycin treatment seems ideal to rescue developmental defects, the immunosuppressive properties of rapamycin as well as its general effect of suppressing translation and anabolic processes may limit its practicality for similar use in a clinical setting. We therefore treated a second “postnatal” or “post rap” cohort from P0-P21 with rapamycin to determine whether simply including neonatal treatment may result in greater rescue than later postnatal initiation. Finally, as the role the mTORC1 pathway plays in TSC pathology formation is not well understood, there is a possibility that rapamycin alone may not be sufficient to rescue all TSC defects. We explored the role of mTORC1 in TSC pathology by ensuring rapamycin presence throughout the life of the mouse from E12.5-P21 in a “pre+post” cohort, such that alleviation of any defects could be attributed solely to rapamycin involvement. Examination of the effects of rapamycin in each of these cohorts allowed us to determine the potential of rapamycin to inhibit different defects found in TSC neuropathology.

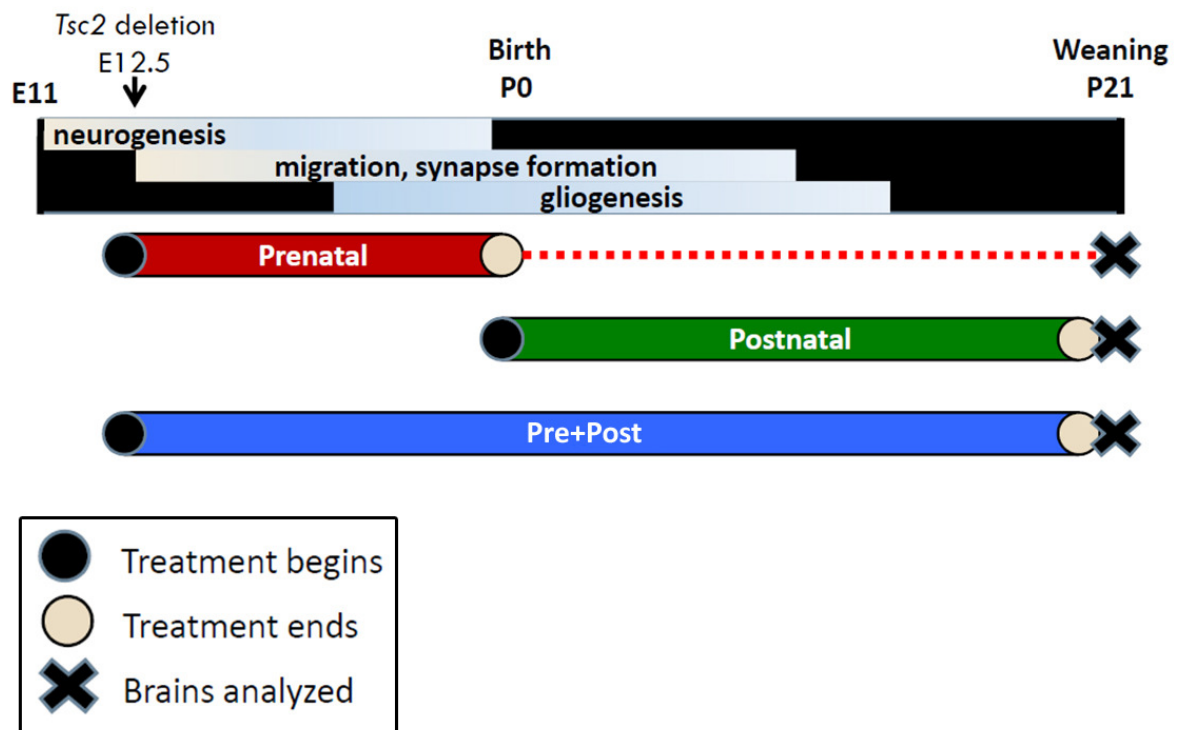


Fig. 4.1. Rapamycin treatment cohorts. Control (*Tsc2*^{flox/+}) and mutant (*Tsc2*^{flox/ko}; *hGFAP-Cre*) mice were divided into three treatment cohorts and treated intraperitoneally (IP) daily with 0.1 mg/kg rapamycin. “Prenatal” mice were treated *in utero* from embryonic day 12.5 (E12.5) to birth, at which point rapamycin was withdrawn. Resulting pups were monitored until P21, at which point they were taken for analysis. The “postnatal” group was treated from postnatal day 0 (P0) to weaning age at P21 and the “pre+post” cohort from E12.5-P21; both groups were analyzed at P21.

Materials and Methods

Mice and genotyping – See Chapter 3.

Rapamycin – Rapamycin was purchased from CalBioChem and solubilized in 100% methanol at 1.0 mg/ml for storage at -20°C for up to two months. Immediately before use, rapamycin was diluted with PBS and administered intraperitoneally (IP) at 0.1 mg/kg daily with a 30G½ needle from either 1) E12.5-birth (pre rap), 2) P0-P21 (post rap), or 3) E12.5-P21 (pre+post).

Histological studies – Histological studies were conducted as previously described in Chapter 3. Staining with antibody against Cre was used to verify genotype in some cases (data not shown).

Quantitative analysis – All analyses were conducted using a minimum of 3 control and mutant mouse pairs per comparison, in which 3 serial sections were used per mouse unless otherwise noted. Sections were stereotactically matched, with areas of analysis taken at similar distances from the midline. Count results were modified to correct for differences in total cortical size. For Cux1 analysis, all Cux1-labeled cells that spanned the thickness of the somatosensory cortex were counted. A line was then drawn to differentiate between Layers II-IV and Layers V-VI, with cells falling into the latter layers considered “ectopic.” Likewise, for assessment of hippocampal organization, a line was drawn between the organized pyramidal layer and the cells above it, with the latter being considered “ectopic”. For cell size analysis, sections were double-labeled with Cux1 and NeuN. Only cells that demonstrated colocalization of both markers in Layers II-IV were used for area

counting, to control for intrinsic differences in cell size between these and lower layers. Data was analyzed using a repeated-measures ANOVA in Microsoft Excel (Seattle, WA).

Immunoblotting – Mice were anaesthetized with 2.5% avertin in dH₂O before decapitation. Heads were immediately submerged in ice-cold artificial CSF (in mM: 10 HEPES, pH 7.2, 1.3 NaH₂PO₄·H₂O, 3 KCl, 10 glucose, 26 NaHCO₃, 2 MgCl₂·6H₂O, 124 NaCl) containing phosphatase inhibitors (2 NaF, 2 Na Molybdate, 1 Na Orthovanadate) until brain was extracted, quick-frozen in a dry ice/ethanol bath, and stored at -80°C until use. Cortex and hippocampus samples were homogenized on ice in 10x volume artificial CSF with 1% each of phosphatase inhibitor cocktails 1 and 2 and 1% mammalian protease inhibitor cocktail (Sigma) in a glass dounce homogenizer. Samples were sonicated on ice and centrifuged at 13,000 x g at 4°C for 10 min. Supernatant was isolated for protein concentration determination using a BCA reagent kit (Pierce, ThermoFisher Scientific, Rockford, IL). Samples were loaded on a 4-12% Bis-Tris gradient gel (Invitrogen) and transferred onto PVDF membrane. The membrane was blocked with 5% BSA in TBST for 1 hr at room temperature, cut into sections, and probed with primary antibody in 5% BSA in TBST for 3 hours at room temperature or overnight at 4°C. Horseradish peroxidase-conjugated secondary antibody was then applied for 1 hr at room temperature. Protein was visualized using an ECL reagent (Amersham) prior to exposure to X-ray film (CL-X Posure, Thermo). Blots were stripped using Restore Plus Western Blot Stripping Buffer for 15 minutes (Thermo) as necessary.

Antibodies – For immunohistochemistry, antibodies used were: Cux1 (1:50, Santa Cruz), GFAP (1:400, Sigma), NeuN (1:100) and MBP (1:200) (Millipore). Antibodies used for

immunoblotting were: tuberin (1:500), hamartin (1:500), S6 (1:500), and pS6 (S235/236) (1:500) from Cell Signaling.

Results

Low dosage of rapamycin is sufficient to attenuate mTORC1 activation in mutant mice to near-control levels

Zeng et al. (93) determined that 3.0 mg/kg of rapamycin was sufficient to “almost completely” inhibit activation of the mTORC1 pathway in control murine cortex, as demonstrated by phosphorylated S6 (pS6) expression in cortical lysates. A dosage of 1.0 mg/kg, however, was only able to decrease pS6 expression to about 75% of control level. Prior to conducting the pre- and postnatal rapamycin experiments, we optimized a rapamycin dosage that would not inhibit essential growth and development.

We began with a daily dose of 2.0 mg/kg starting at P0, which proved to be too high as all treated animals were runted compared to vehicle-treated control by P21 (data not shown). We therefore tested lower dosages (1.5, 1.0, and 0.5 mg/kg) using the same treatment scheme and found similar problems with growth inhibition. Our final test using a dosage of 0.1 mg/kg, however, resulted in healthy control and mutant mice that were both largely indistinguishable from vehicle controls. Lysates of the cortex and hippocampus of mutant and control animals treated with 0.1 mg/kg rapamycin demonstrated that this dosage was able to decrease mTORC1 activity in mutants to near-control levels as determined by pS6 expression (Fig. 4.2). Though other *in vivo* mouse studies have used as much as 3.0 - 6.0 mg/kg for their rapamycin dosages (93, 94), the reduction of pS6 to wild type levels suggest that 0.1 mg/kg would effectively inhibit mTORC1 activity when administered between P0 and P21.

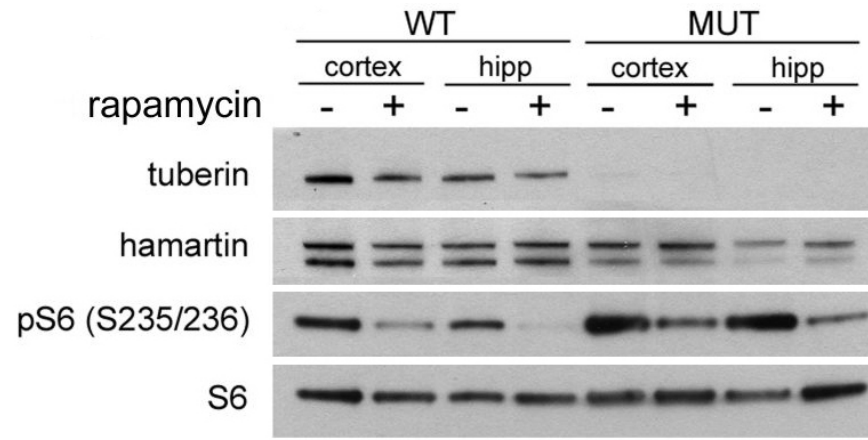


Fig 4.2. Postnatal rapamycin dosage of 0.1 mg/kg attenuates mTORC1 expression.

Western analysis was conducted using cortical and hippocampal lysates from P21 control and mutant mice that were either untreated or treated daily with 0.1 mg/kg rapamycin. Minimal tuberin expression is seen in all mutant samples, while hamartin is present in both control and mutant. Expression of phosphorylated S6 (pS6), a readout of mTORC1 activation, is increased in the cortex and hippocampus of the untreated mutant but is reduced in the mutant following rapamycin treatment. Activity of mTORC1 is also attenuated in control animals following treatment with rapamycin. Total S6 is used as a loading control.

Rapamycin treatment improves health, promotes weight gain, and extends lifespan

As previously reported (115), *Tsc2^{flox/ko}; hGFAP-Cre* mutant mice displayed a failure to thrive phenotype beginning P8, such that they were severely runted and sick-looking by weaning (Fig 4.3A). Following prenatal treatment with rapamycin, mutant mice achieved similar weights as their treated littermate controls until about P14 (Fig 4.3E), when their weight gain began to slow. By P21, these mice also appeared runted compared to controls, though to a lesser degree than the untreated mutant at the same timepoint (Fig 4.3B). In contrast, post rap and pre+post mutant mice were virtually indistinguishable from their littermate controls by weight or overall health throughout postnatal development (Fig 4.3C, D).

In addition to improving weight gain and health, rapamycin was also able to extend lifespan for all three treatment cohorts. Discontinuation of rapamycin, however, invariably resulted in seizures and subsequent death (Fig 4.3F). While the untreated *Tsc2^{flox/ko}; hGFAP-Cre* died at a median age of 23 days, the pre rap mutant lived until a median age of P31. Meanwhile, the post rap and pre+post mutants, whose treatments ended at P21, lived until P45 and P41, respectively. Following withdrawal of rapamycin, the latter two groups initially exhibited comparable weight gain to their littermate controls, though this gradually slowed and reversed within two weeks (data not shown). In their last week of life, several mice from these two groups were observed seizing before dying days later of seizures. Previous studies in our lab conducted using 2.0 mg/kg of rapamycin (administered from P10, 3x/week) showed that rapamycin was able to extend lifespan and maintain health until P150, when the study was discontinued (data not shown).

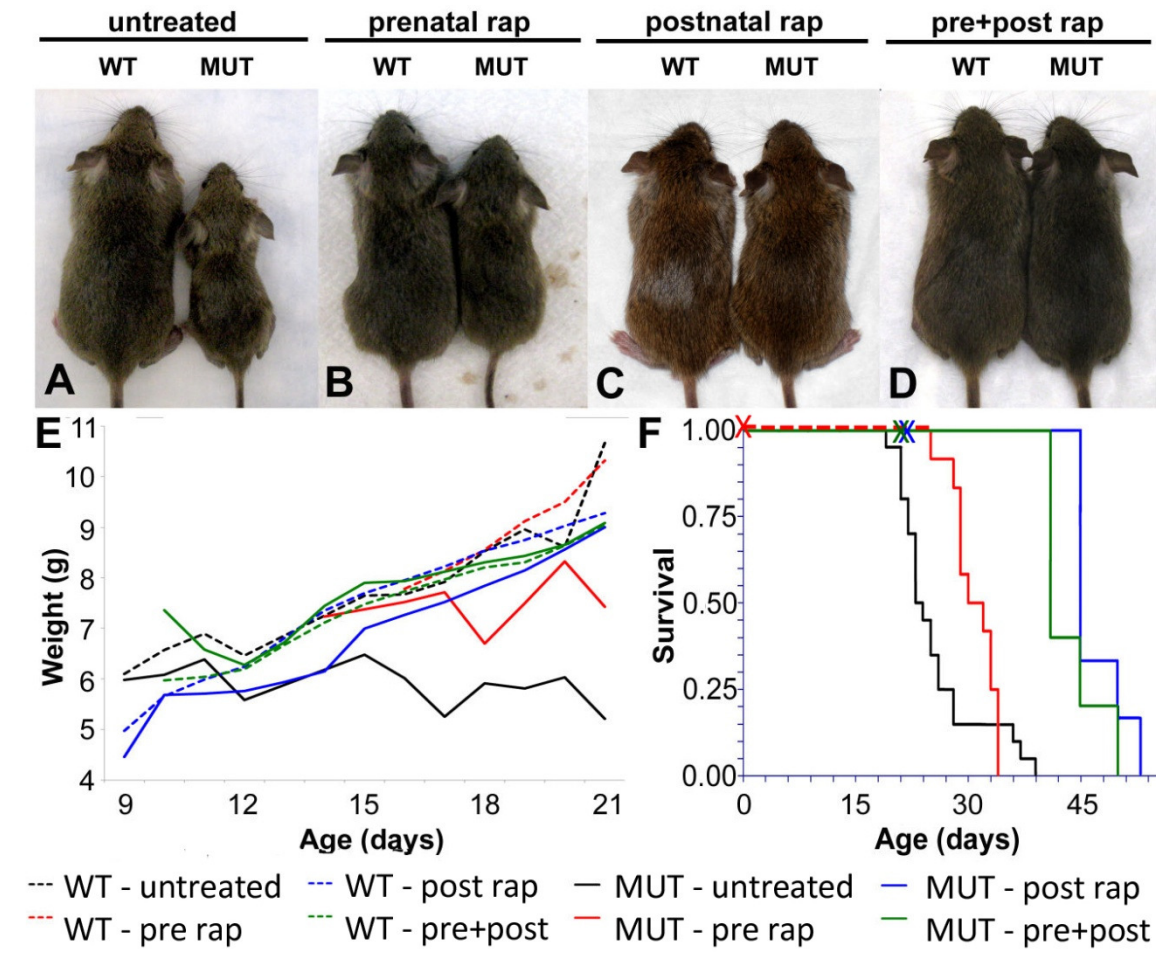


Fig 4.3. Comparison of rapamycin treatment cohorts. (A) By P21, the untreated mutant mouse is sick and runted compared to its littermate control. (B) Mutant mice are still smaller than controls following prenatal rapamycin treatment, though they appear healthier and larger than their untreated counterparts. (C, D) Postnatal and pre+post treatment results in mutant mice that are clinically indistinguishable from their littermate controls. (E) Weights of all four cohorts demonstrate that rapamycin does not have a noticeably negative effect on weight gain in control mice. Untreated mutants demonstrate a failure to thrive phenotype beginning P8. Pre rap mutants have similar weights as the control until around P14, at which point their weight gain plateaus. Post rap and pre+post mutants are similar in weight compared to controls. (F) Mutants of all cohorts die of seizures following withdrawal of rapamycin, denoted by the X. The median age of death for each cohort is: untreated, P23 (n=20); pre rap, P31 (n=12); post rap, P45 (n=6); pre+post, P41. (n=5).

Rapamycin alleviates megalencephaly and cell hypertrophy in the cortex

We examined the effect of rapamycin on cortical thickness and cell size using H&E-stained sections of each treatment cohort. In untreated *Tsc2^{fllox/ko}; hGFAP-Cre* mutant mice, we previously demonstrated a postnatal cerebral enlargement that resulted in a significantly thicker cortex than control mice by P21 (115) (Fig 4.4A). Interestingly, pre, post, and pre+post treatments all reduced cortical thickness to near-control levels (Fig 4.4B-D). Though the size of the control cortices were also decreased with each of these rapamycin treatments compared to the untreated control, the difference was not found to be significant (Fig 4.4I).

Neuronal hypertrophy was also demonstrated in the cortex of the untreated mutant. This was originally shown by comparing the average area of cells labeled with NeuN, a post-mitotic neuronal marker, in the mid-fifth section of mutant versus control cortices. To ensure that intrinsic differences between size of cells in Layers II-IV and Layer V did not influence our comparisons, we chose to calculate cell area of layer-specific cells by analyzing cells co-labeled with NeuN and Cux1, a Layer II-IV marker. Using this method of assessment, cortical neurons of the untreated mutant were still found to be significantly larger compared to the control (Fig 4.4E). However, following rapamycin treatment (Fig 4.4F-H), cell size was found to be significantly reduced in the mutant brains (Fig 4.4J). As mTORC1 is a known regulator of cell size, this finding served to validate the effectiveness of rapamycin treatment in these mice.

Combined pre+postnatal rapamycin treatment rescues lamination defects in mutant cortex

Defects in lamination were observed in the untreated mutant cortex, with noticeable blurring between the usually well-defined cortical layers (Fig 4.4A). This abnormality was particularly apparent in the marginal zone, the normally clearly-demarcated, cell-sparse layer adjacent to the pial surface, which is poorly delineated in the mutant (Fig 4.4A, white arrows). Postnatal treatment with rapamycin alone did not notably improve the definition of this layer, while prenatal treatment appeared to result in slight improvement of this defect. The combined pre+post treatment, however, resulted in a considerable degree of rescue, with a marginal zone similar to that of the untreated control (Fig 4.4D, yellow arrow). We investigated cortical lamination more closely using antibody against the transcription factor Cux1 to identify neurons of Layers II-IV (38). We had previously shown an excess of Cux1-labeled cells in cortical layers V and VI of the mutant animals, suggesting a defect in neuronal migration (115) (Fig 4.5A). Quantitative analysis of rapamycin-treated samples (Fig 4.5E) demonstrated that treatment with rapamycin prenatally resulted in a significant reduction of ectopic cells in the lower layers, whereas postnatal treatment alone showed no significant impact on ectopic cell number (Fig 4.5B-D). Mutant mice treated pre+postnatally therefore also demonstrated a significant degree of rescue in the number of ectopic Cux1-labeled cells in the cortex. These data suggest that rapamycin is able to rescue cortical migration defects that occur postnatal.

Combined pre+postnatal rapamycin treatment rescues lamination defects in mutant hippocampus

One of the most striking defects in the untreated mutant was found in the hippocampus, in which the usually tightly-organized pyramidal layer was severely disrupted, particularly in the CA1 and CA3 regions. Interestingly, ectopic cells in the CA1 region were

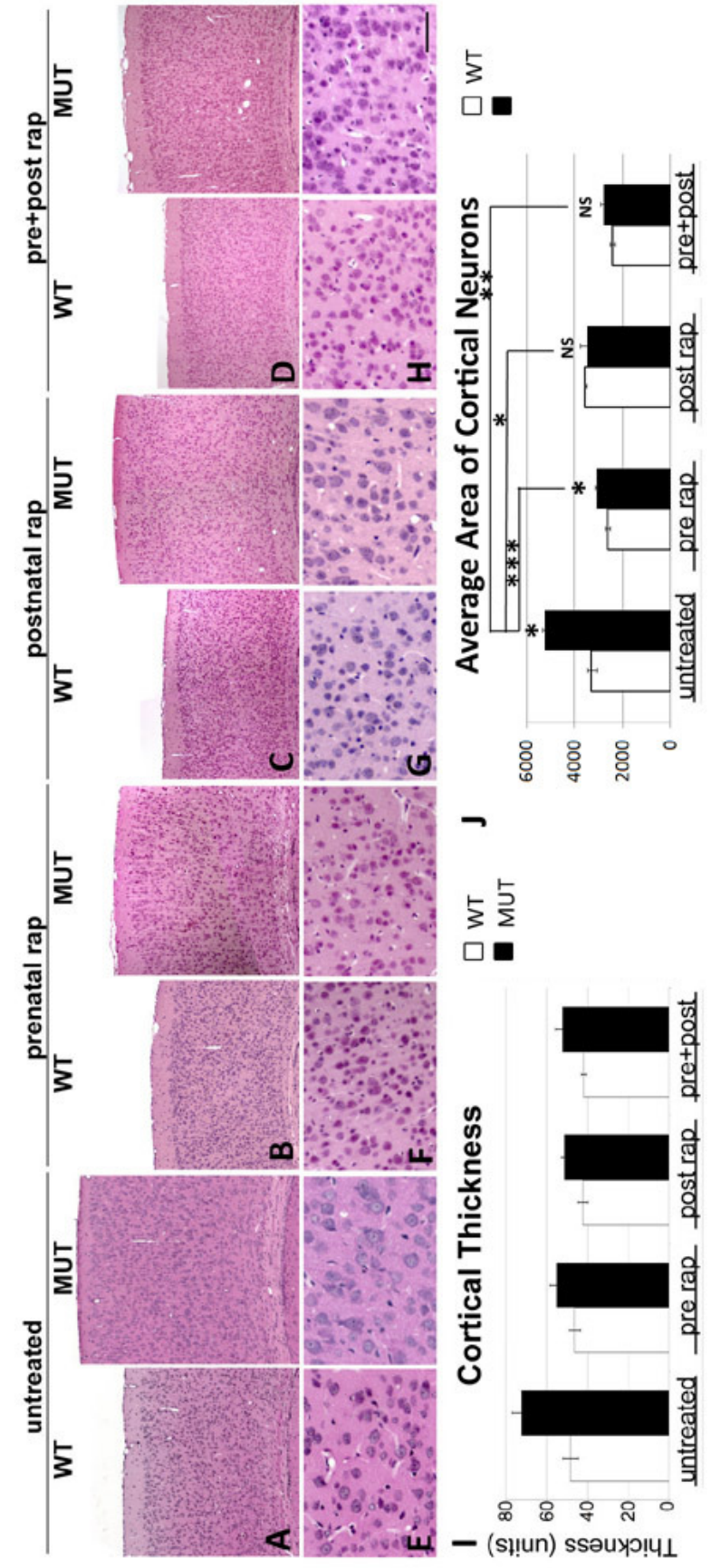


Fig 4.4. Rapamycin reduces cortical thickness, cell size, and alleviates lamination defects. (A) H&E analysis of cortical sections at P21 reveal that untreated *Tsc2^{flax/ko}; hGFAP-Cre* mice have significantly thicker cortices compared to control and an ill-defined marginal zone (white arrows). (B-D) Following rapamycin treatment, all three cohorts demonstrate a reduction of cortical thickness in the mutant, while the pre+post mutant also shows a well-demarcated marginal zone (yellow arrow). (E) Higher magnification of the cortices reveal enlarged, dysplastic cells in the mutant. (F-H) This enlargement is rescued by treatment with rapamycin. (I) Rapamycin treatment reduces cortical thickness in all three mutant cohorts to levels similar to the untreated control. (J) Cell area is also significantly reduced following rapamycin treatment.

not only enlarged but seemed to form a distinct layer above the hippocampus, suggesting a severe defect in lamination (115) (Fig 4.6A). Pre- or postnatal-only treatment with rapamycin did not appear to have a notable impact on this effect. The cortex of pre+post mice, however, showed a marked decrease in ectopic cells above the pyramidal layer of the hippocampus. Using NeuN-stained sections (Fig 4.6B), we quantitated the number of ectopic neurons in each cohort and found a significant reduction in the pre+post treated cohort compared to the untreated mutant (Fig 4.6C). These results indicate that the migration defect in these ectopic cells cannot be rescued by pre or postnatal rapamycin application alone, but requires continuous rapamycin presence.

We previously noted in Chapter 3 (Fig 3.4) the presence of a number of ring heterotopias in the SLM region of the mutant hippocampus by P10, which may have been formed from cells unable to migrate from the hippocampal fissure of the SO as shown by P5. Interestingly, no heterotopias were found in animals treated prenatally with rapamycin (n=5) or the combined pre+post treatment (n = 8). Postnatal treatment with rapamycin, however, still resulted in ring heterotopia formation (n = 7). Contrary to the conclusions above, these results suggest that prenatal rapamycin alone is able to alleviate the delayed migration of these ectopic cells, which cannot be rectified by postnatal treatment.

Postnatal rapamycin treatment rescues myelination defect and astrogliosis

We found an impairment of myelin progression in *Tsc2^{flox/ko}; hGFAP-Cre* mutant mice, where myelin was present in the corpus callosum yet largely absent in the cortex (115) (Fig 4.7A). We examined the effects of rapamycin on this defect using antibody against myelin basic protein (MBP) in P21 brain sections from each treatment cohort. Rapamycin treatment was effective in rescuing the myelination defect when given postnatally, as both post- and pre+post treated groups displayed an abundance of myelinated fibers in the lower

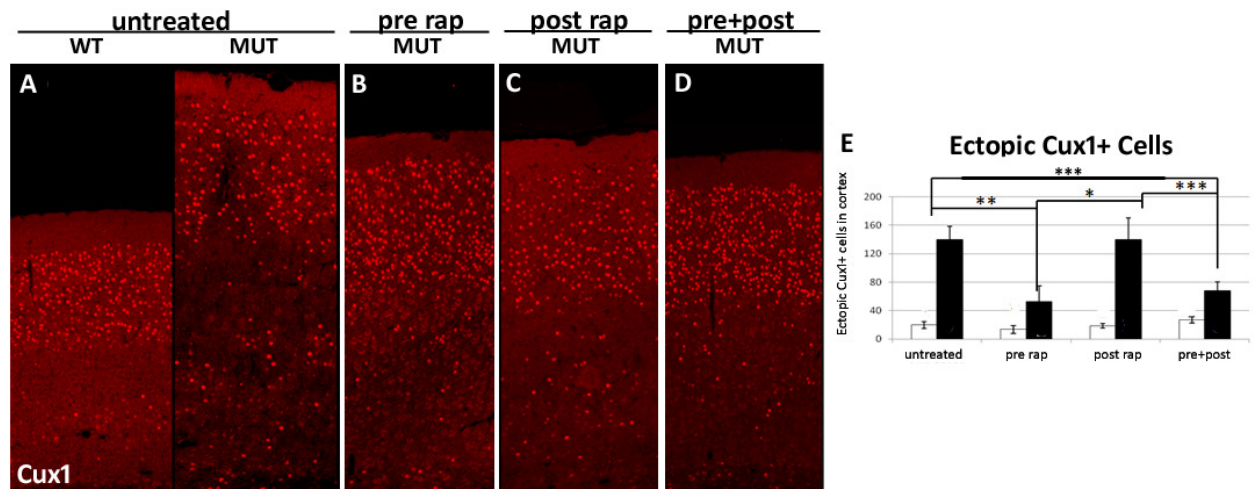


Fig 4.5. Prenatal rapamycin treatment alleviates cortical layer defect. (A) Untreated mutant sections stained for the cortical layer II-IV marker Cux1 demonstrated lamination defects, with significant numbers of ectopic cells in the lower layers as quantitated in (E). (B) Prenatal treatment with rapamycin rescues this migration defect, as significantly fewer ectopic cells are found in Layers V-VI (** $p < 0.005$). (C) Postnatal treatment did not appear to have an effect this migration defect, as they had similar numbers of Cux1 ectopic cells compared to the control. (D) The pre+post treatment demonstrated an even greater degree of rescue than that of the prenatally treated mouse (*** $P < 0.0005$). (E) Quantitation of Cux1+ ectopic cells in layers V-VI of the cortex.

cortex (Fig 4.7C, D). When given only prenatally, however, rapamycin did not appear to increase progression of myelin to the cortex (Fig 4.7B), confirming myelination as a postnatal process. Mutant mice were also found to exhibit an astrogliosis in both cortex and hippocampus, in which GFAP expression was strongly increased (Fig 4.7E). Similar to our findings regarding myelin, postnatal rapamycin was able to rescue the astrogliosis, while prenatal treatment alone resulted in an astrogliosis similar to that seen in the untreated mutant (Fig 4.6F,G). Combined pre+post treatment also resulted in prevention of the astrogliosis (Fig 4.6H), establishing the astrogliosis as a postnatal effect as well.

Discussion

With the establishment of the *Tsc2^{flox/ko}; hGFAP-Cre* mouse as a good model for TSC neuropathology (Chapter 3), we have chosen to use this mouse to explore the efficacy of rapamycin treatment in alleviating TSC defects. As TSC is largely a developmental disease, we sought to determine whether *in utero* treatment with rapamycin would be more effective in rescuing neurodevelopmental defects. However, as development does occur throughout the postnatal period, we also wanted to determine whether immediate rapamycin treatment might be more effective than later postnatal administration. We hence chose to systematically investigate these hypotheses by dividing our rapamycin treatments into three separate cohorts – pre rap, post rap, or pre+post.

Though we initially began with a rapamycin dosage of 2.0 mg/kg, we found that this amount runted wild type mice when administered postnatally. Following a dosage determination study, we lowered our dosage to 0.1 mg/kg, which not only had minimal clinical effect on wild type mice but also restored the ability of the mutant mice to gain weight. Analysis of postnatally treated brains showed that this dosage was enough to decrease pS6 expression, a readout of mTORC1 activation, to control levels. The impact of

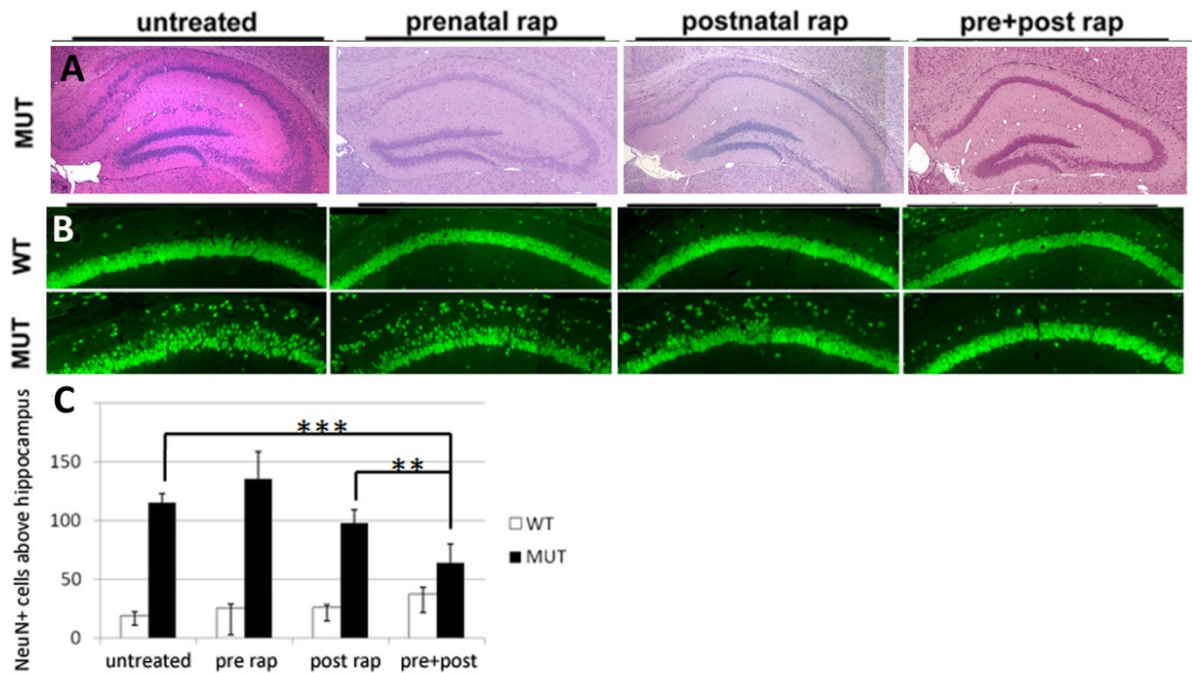


Fig 4.6. Pre+postnatal rapamycin treatment rescues lamination defects in the mutant. (A) H&E-stained sections of mutant mice of each treatment cohort demonstrate different degrees of lamination rescue, particularly notable in the pre+post treated mutant. (B) NeuN-stained sections were used to quantify lamination rescue by quantitating the number of ectopic cells above the pyramidal layer of the hippocampus. (C) Quantitation demonstrates that there are significantly fewer ectopic cells in the pre+post treated mutant compared to the untreated mutant ($***P < 0.0005$) and both pre and postnatally treated mutants ($**P < 0.005$).

this dosage is particularly interesting from a clinical perspective. Rapamycin is an FDA-approved immunosuppressant that is administered to transplant patients to achieve serum levels of 2-20 ng/ml (94), which translates to a maximum of 0.017 mg/kg in a 60 kg adult. Case studies using rapamycin in TSC patients at these levels have shown that rapamycin causes regression of SEGAs, though little effect on tubers is noted (146). Though studies in mouse models (93, 94) have demonstrated benefits of rapamycin treatment on defects characteristic of tubers such as cell size, they achieved this using dosages ranging from 3-6 mg/kg, several hundredfold of that given to humans. Though mouse and human pharmacokinetics differ, we were excited to establish in this study that a more patient-appropriate dosage of 0.1 mg/kg was still able to attenuate mTORC1 and rescue many TSC defects found in tubers. Given the wide range of side effects from rapamycin use, we felt it was important to determine that a lower dosage could result in similar clinical benefits. However, rapamycin serum levels in these mice will need to be examined to determine whether the mouse 0.1 mg/kg treatment is comparable to a similar dosage in humans.

We administered and withdrew rapamycin at different timepoints to elucidate effects of individual defects on overall health and survival of the mice. Interestingly, two characteristics were similarly altered among all treatments, cortical thickness and cell size. As noted in Chapter 3, megalencephaly is typically caused by abnormal proliferation of cells. However, we found no evidence of increased density of neurons, astrocytes, or interneurons in the untreated cortex of the mutant mouse, despite the seemingly sparser distribution of cells which suggested an increase in extracellular matrix. These results led us to conclude that the increase in cell size contributed significantly to the proportional increase in cortical size. Following rapamycin treatment, cortical thickness was decreased to control levels in all three treatment cohorts, while neuronal cell size significantly decreased as well. These results lend further support to our conclusion that increased cell

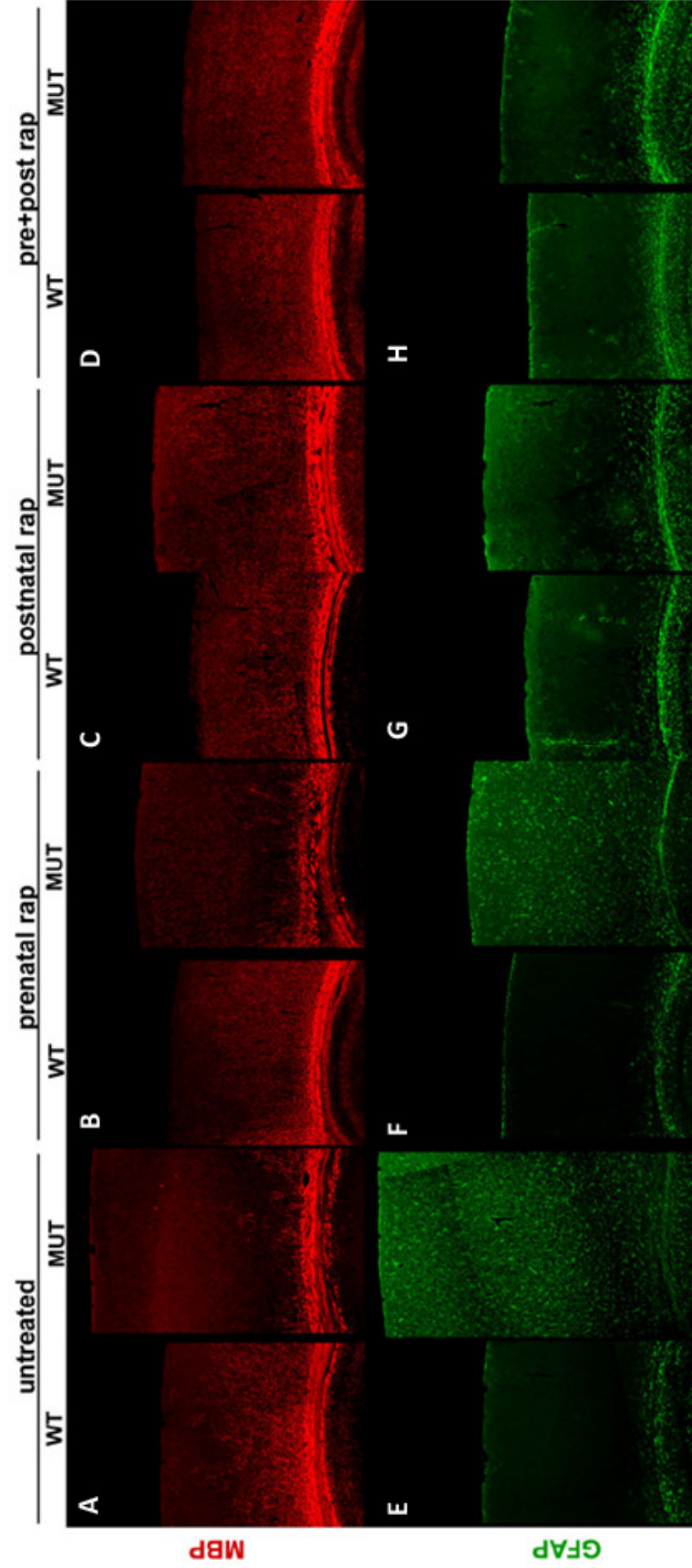


Fig 4.7. Postnatal rapamycin rescues myelin defect and astrogliosis. (A) Immunostaining with myelin basic protein (MBP) demonstrated a marked reduction of myelin in the lower cortex. MBP staining was present though patchy in the corpus callosum, suggesting a problem with myelin progression rather than formation. (B) Prenatal mutant mice exhibited similar myelination defects as the untreated mutants. (C, D) Postnatal treatment with rapamycin appears to fully rescue this defect. (F) Examination of astrocyte activity using GFAP reveals a notable increase in GFAP expression, indicative of an astrogliosis. (G) High expression of GFAP is still present despite prenatal treatment with rapamycin. (H, I) Postnatal treatment decreases GFAP expression to control levels.

size is a major factor in the development of megalencephaly.

However, though density of cells, a measure of total cell number divided by total cortex area, did not differ in the untreated control versus mutant, total cell counts were higher in the latter. As the mTORC1 pathway is important for translation, cell cycle, and microtubule dynamics (147), attenuation of this pathway via rapamycin provides a good opportunity to determine whether increased cell size does explain the cortical thickness in our mutant. This may be done by assessing whether total neuron and astrocyte counts for the rapamycin-treated mice differ compared to each other and the untreated mutant. For example, the rapamycin-treated mutants might have similar total cell populations as the untreated mutants and therefore have higher cell density, despite similar cell and cortical size as the untreated control. This result would suggest that the cortical thickness defect is unrelated to cellular hypertrophy, and that a proliferation defect did exist in the untreated mutant.

In addition, as overactivation of mTORC1 has been well-established to increase cell size (57), it is interesting that cell size seems uniformly decreased across all treated samples by P21. One would speculate that once rapamycin is withdrawn at birth in the prenatally treated mutant cortex, mTORC1 would be allowed to function uninhibited until sacrifice of these mice at P21. Despite the three week interval, however, prenatally treated mice do not have enlarged cells. In fact, closer examination of these cortical cells indicates that they are smaller than the untreated control and post or pre+post treated mutants. Some cells even appear pyknotic. As studies have shown that rapamycin may trigger apoptosis in some cell systems (91, 148-150) it is important to investigate cell death in our rapamycin-treated samples. It would also be informative to determine whether prenatal rapamycin may damage the inherent function of mTORC1 to increase cell size, or perhaps inhibit the ability of the cell itself to grow. On the other hand, characterization of the neuron-

specific TSC1 CKO mouse (94) showed that the benefits of rapamycin persist for several weeks following withdrawal of treatment. If this is the case, then perhaps increase in cell size could not occur within the short timeframe given before these mice were taken for study.

The persistence of rapamycin benefit for several weeks after withdrawal of treatment may explain the discrepancies between weight gain in the untreated versus treated cohorts. The post and pre+post mutants exhibited weight gain comparable to the littermate controls, as rapamycin was given throughout their postnatal life. Prenatally treated mice exhibited similar weight gain until around P14, when their weight plateaued. Though they also appeared somewhat runted by P21, they weighed more and looked more developed than untreated mutant mice. To better establish the relationship between weight gain benefits and rapamycin, observations of the postnatal health of prenatally-treated mice should be compared to rapamycin serum levels of corresponding days. In addition to possibly benefiting metabolism pathways, treatment with rapamycin may also be inhibiting seizure activity, resulting in more normal feeding and weight gain. As we have not investigated whether untreated and/or treated mice have subclinical seizures, data from EEG recordings of these mice might also be compared to rapamycin serum levels to determine whether there is a relationship between weight gain and seizure activity. These studies would also demonstrate how long benefits of rapamycin persist despite lowered serum levels following withdrawal of treatment. These results will contribute greatly to our knowledge regarding the role of mTORC1 in growth and development.

We found defects in myelin progression and an astrogliosis in the untreated mutant, which were still apparent in the prenatally-treated mutant. Postnatally administered rapamycin, however, rescued both of these defects, with wildtype-like progression of myelin fibers in the lower cortex and minimal evidence of astrogliosis in both post and pre+post

cohorts. In Chapter 3, I discussed the possibility that the hypomyelination observed was due to a reason independent of problems with the oligodendrocytes, such as axonal damage of the neurons in the lower cortex. This was in part based on findings in the neuron-specific TSC1 CKO in which hypomyelination was observed despite lack of Cre expression or differences in populations of the oligodendroglia (77). The lack of rescue in the prenatally-treated mice suggest that either (a) prenatal rapamycin was unable to rescue defective events that later resulted in hypomyelination, such as oligodendrocytes formation and subsequent maturation, (b) overexpression of mTORC1 following effective prenatal treatment is still sufficient to inhibit proper myelination, or (c) the defect in myelination in our mouse is due to a predominately postnatal effect, such as dendritic arborization and synapse formation of more newly-born neurons. More in-depth characterization of the myelin defect itself, such as myelin-thickness assessment, as well as investigation of axonal health and formation is necessary before further conclusions may be made. As astrogliosis was also not observed in the neuron-specific Tsc1 CKO (77) but was in the astrocyte-specific Tsc1 CKO (75), I also hypothesized that the astrogliosis in our mutant may not have been in response to axonal damage and was instead due to increased mTORC1 activity in the astroglia. The ability of rapamycin to inhibit the astrogliosis hence is logical.

One of the most striking defects found in the untreated *Tsc2^{flox/ko}; hGFAP-Cre* mutant involved aberrant lamination. Demarcation of the cortical layers and organization of the hippocampus were largely disrupted, and a number of ectopic cells stained with the upper layer marker Cux1 were found in lower layers. We also found a number of ring heterotopias within the hippocampus, possible indicators of abnormal neuronal migration. As migration occurs early in neurodevelopment (141) and studies suggest mTORC1 is highly involved in this process (137, 151), we hypothesized that prenatal rapamycin treatment would alleviate

most lamination defects compared to post or untreated. As expected, heterotopias were present in the post treated mutants and absent in the pre treated cohort. Fewer Cux1+ ectopic cells were also found in the pre versus post mutants, while the post and untreated groups exhibited similar numbers. However, no significant difference was found in the number of NeuN+ ectopic cells above the hippocampus between the untreated, pre, or post mutants. These results suggest that the timing and mechanisms of migration, as well as the involvement of mTORC1 in these mechanisms, may differ in different regions of the brain.

However, combined pre+post treatment resulted in almost full laminar rescue in the cortex and the hippocampus, resulting in a clearly demarcated Layer I of the cortex, significantly fewer Cux1 cells compared to the post or untreated mutants, and significantly fewer NeuN+ ectopic cells above the hippocampus than pre, post, or untreated mutants. Indeed, the pre+postnatally treated mutant is histologically similar to untreated control brains. These results indicate that mTORC1 activity is highly involved in neuronal migration, and tight regulation of its activity is needed both pre- and postnatally to ensure proper cellular migration. This may be further established by examination of prenatally-treated mutants at P0, which should show wildtype-like organization if this is the case.

Despite the high degree of rescue in the pre+post treated mutant, once taken off rapamycin, these mice only live an additional 4 weeks before they die of seizures, like the pre and post-treated mutants. We have not examined the brains of these mice following withdrawal of rapamycin. In their neuron-specific TSC1 CKO mouse, Meikle et al (94) found that mTORC1 was upregulated and cell size increased following removal of rapamycin, though rescued myelination did not regress. It is likely that we would find similar results in our treated mouse, though cell size might not increase in the prenatally treated mouse for reasons previously discussed. However, these studies make clear that despite seemingly

full histologic rescue, as seen in the pre+post mice, the presence of rapamycin must be constant to prevent recurrence of lesion formation.

By treating the *Tsc2^{flox/ko}; hGFAP-Cre* mice with rapamycin at different timepoints, we have been able to elucidate the impact of rapamycin on several prominent defects in TSC neuropathology. Pre, post, and pre+post treatments all restore cortical thickness and cell size to control levels. Postnatal treatment is able to rescue the hypomyelination and astrogliosis, while prenatal treatment seems to be more beneficial in rescuing some migrational defects. However, our studies show that correct migration in our mouse requires proper pre- and postnatal signaling, as a combination of pre+post treatment appears to more completely rescue migrational defects in both the cortex and hippocampus to a much greater degree than prenatal treatment alone. While further characterization is needed to fully understand the impact of the different treatments on TSC neuropathology, the astounding degree of rescue following pre+post treatment suggests that this combined treatment may provide the greatest benefit to patients in inhibiting TSC lesion formation. However, as histologic improvement does not always translate to functional improvement, we explored the degree of functional benefit the combined pre+postnatal rapamycin treatment has on the *Tsc2^{flox/ko}; hGFAP-Cre* mice in the following chapter.

Chapter Five:

Behavioral Testing of Rapamycin-Treated Tsc2^{flax/ko}; hGFAP-Cre Mice

Introduction

More than 95% of TSC patients exhibit brain manifestations, which have been associated with a wide range of neurologic morbidity such as mental retardation, behavioral problems, and learning difficulties (152). Even the approximately 50% of TSC patients who have a normal IQ of 80-130 are often affected with neuropsychological deficits (153), which include deficits in long-term and working memory (154, 155). Indeed, recent studies in mouse models have demonstrated that haploinsufficiency of either *Tsc1* (156) or *Tsc2* (157) result in impaired learning and memory, despite absence of cerebral lesions or seizures.

These findings underscore the importance of the TSC genes in learning and memory, which are thought to stem from their regulation of the mTORC1 pathway. Long-term learning and memory require the synthesis of new proteins, a process that mTORC1 tightly regulates in response to nutrients and growth factors (158). Stimulation of late long-term potentiation (L-LTP), used to measure memory at a cellular level, results in phosphorylation of mTORC1 downstream effectors such as 4E-BP1 and S6K1 (159). Studies in wild type rats both *in vitro* (160) and *in vivo* (161) have also demonstrated that inhibition of the mTORC1 kinase using rapamycin in the hippocampus results in impaired long term memory, providing further evidence of the importance of this pathway in learning and memory.

As established in Chapter 3, the *Tsc2^{flox/ko}; hGFAP-Cre* mouse models many characteristics of TSC neuropathology. Given this and the prevalence of learning and memory deficits in the TSC population, we hypothesized that our mutant mouse could be used to better understand these cognitive deficits. Unfortunately, the severity of defects in the untreated mutant results in sickness and death by P23, too young an age for most behavioral tests. As described in Chapter 4, however, a combination of pre+postnatal

rapamycin treatment in these mutants demonstrated nearly complete rescue of these defects, including weight gain, cortical thickness, cell size, cortical lamination, myelin progression, and an astrogliosis. Most striking, however, was the restoration of organization to the hippocampus, which appeared nearly indistinguishable from controls when analyzed with H&E and NeuN immunohistochemistry. This finding was particularly relevant given the importance of the hippocampus in long term learning and memory. As this treatment scheme seemed to restore the majority of histological defects we noted, particularly those in the hippocampus, we sought to assess whether the histologic rescue correlated with functional rescue of cognition and behavior. Control and mutant animals that had been treated with rapamycin were assessed with a battery of behavioral tests measuring learning and memory.

Since untreated mutants could not be used for comparison, we chose instead to test the postnatally-treated rapamycin cohort, which showed a lesser degree of histological rescue compared to the pre+post group. Comparisons of control and mutant mice of these two groups demonstrated not only whether histologic rescue translates to functional rescue, but whether combined pre+postnatal treatment with rapamycin improved learning and memory in this mouse model to a greater degree than postnatal treatment alone.

Materials and Methods

Mice – As described in Chapter 4, *Tsc2^{flox/ko}; hGFAP-Cre* (mutant) and *Tsc2^{flox/+}* (control) mice used for behavioral testing were treated with rapamycin either from birth (postnatal day 0, P0) (“postnatal treatment”) or beginning embryonic day 12.5 (E12.5) until adulthood (“pre+post treatment”). All mice were treated with rapamycin throughout behavioral testing, which began on average around P48. Control and mutant mice from both treatment cohorts were given coded IDs and randomly segregated into new groups for all behavioral testing,

which was done in collaboration with Natalia Rozas, a doctoral student in the laboratory of Pramod Dash, Ph.D. All testing and mouse handling was approved by the UT Animal Welfare Committee.

Rapamycin – Rapamycin preparation was the same as that described in Chapter 4.

Briefly, rapamycin was solubilized in 100% methanol and stored at a concentration of 1.0 mg/mL at -20°C for up to two months. Rapamycin was diluted with PBS immediately before use and administered IP at a dosage of 0.1 mg/kg daily with a 30G½ needle until P30-45 in both post rap and pre+post groups. Around this timepoint, mutant mice from both cohorts began to look sick, with one prenatally-treated and one pre+post treated mutant dying of seizures. This was likely due to decreased permeability of rapamycin through the blood brain barrier as mice aged, as studies have demonstrated decreased rapamycin concentration in the brain beyond P30 (Meikle 2008). Since previous experiments had shown that a dosage of 2 mg/kg administered three times a week was sufficient to extend lifespan and maintain health, all mice were switched to this treatment scheme at least one and a half weeks before behavioral testing began. Treatment continued at this dosage throughout behavioral testing.

Motor skills – To assess motor coordination, mice were tested on a Basile automated accelerating rotarod using a protocol set forth by Crawley and Paylor (162). Mice were trained for 90s at a constant 16 rpm before being tested for 300s at an accelerating 4-40 rpm. Mice were then allowed to rest in their home cages for 2 hours before being tested again for 300s at 4-40 rpm. Latency to fall for all trials was recorded.

Morris Water Maze – Spatial learning and memory was assessed using a standard version of the Morris water maze. Briefly, a tank (1.2 meters in diameter) located in a dimly-lit testing room was filled with water mixed with non-toxic white paint, rendering it opaque. A circular platform (11 cm in diameter) was submerged 2 cm below the surface of the water. Spatial cues, including lights as well as brightly colored shapes, were stationed on the walls around the tub. Before each trial, mice were taken from their home cage and individually placed in clean, diaper-lined cages with a heated water bottle for warmth. After 10 minutes of habituation, the trial began by placing a mouse into the tub from a random start location. Each mouse was given 60 s to locate the platform. If it could not within the 60 s, the blinded experimenter would guide it towards the platform and let it sit for 10 s. The mouse was then taken back to its bottle-heated cage to await the next trial, with a minimum inter-trial time of 4 minutes to rest. Activity of the mouse was tracked by an overhead camera, including swim speed, latency to platform, and swim direction.

Two variations of the Morris water maze were conducted in the order described below. Mice initially underwent mass training, in which they were given 12 consecutive trials in one day as described above, for 4 consecutive days. Twenty-four hours after the last trial, a probe trial was performed in which the platform was removed and mice were allowed to swim freely for 60 s. Latency to original platform location and number of times the mouse crossed the original platform location were recorded. Mice were then spaced trained, which consisted of 4 trials per day for 6 consecutive days. Twenty-four hours after the 6th day of training, a probe trial was conducted. The platform remained in the same location throughout both of these tests. Following all testing, the visual version of the Morris water maze was performed by placing a large painted brick on top of the platform. Latency to the visible platform and swim speed were recorded for each mouse and compared across groups.

Elevated Plus Maze (EPM) – EPM testing was conducted according to a protocol by Walf and Frye (163). Briefly, an EPM made of heavy white plastic and consisting of four arms (two open without walls and two enclosed by black plastic walls) was placed in the previously described Morris water maze tub in a brightly lit testing room. Each arm of the maze was attached to a thick plastic pipe to elevate the maze about 76 cm above the bottom of the drained tub. Two partitions hid the maze and tub from the rest of the testing room, where mouse cages were temporarily kept for testing.

All mouse testing was conducted between 11am and 4pm of the same day and the maze was thoroughly cleaned with 70% ethanol between each test. At the beginning of each test, mice were individually taken from their home cages and placed at the junction of the open and closed arms, facing towards an open arm and away from the experimenter. Mice were then observed for five minutes via an overhead camera by a blinded experimenter who was hidden behind the partition. Total time spent on open arms as well as entries into open and closed arms were manually assessed. Exploration into an arm was considered an entry when at least half the body of the mouse was on the arm. Data from mice that jumped off the maze was removed from the study (n=5, 3 WT and 2 postnatal treated KO mice).

Contextual Fear Conditioning – The fear conditioning test was modeled after a protocol described by Frankland et al. (164) in which the context of conditioning rather than an auditory cue is paired with a mild footshock as a method to assess learning and memory abilities. In our setup, the shock cage (Coulbourn Instruments) had a yellow and black-striped back wall and was scented with pineapple soap. The similarly-sized safe cage featured a blank white concave back wall that limited the floor space to a semicircle and was cleaned with ethanol. The floor of both cages contained a footshock grid. Cages were

placed side-by-side inside an internally-lit sound-proof box, though only one cage was used at any given time. Mice were individually taken from their home cages in a separate room and transported in a clean empty cage before each test. Each mouse was initially given 10 minutes to explore each cage, with no shock in either cage. The following day, mice were trained for 3 minutes in each cage, during which a 0.75 mA, 2s-long shock was given in the shock cage after 2 minutes and no shock was given in the safe cage. This experiment was repeated the next day and continued for 3 more days using the same setup. Freezing behavior was monitored in 2 s intervals throughout the 3 minutes in both cages by a blinded observer, though only data from the first 2 minutes (pre-shock time) was used. Mice were allowed a minimum of 3.5 hours between time in the shock cage and the safe cage (morning then afternoon, or vice versa) and groups were counterbalanced across cage testing order.

Object Recognition – Object recognition testing was carried out in two individual trials, modified from a protocol by Bevins and Besheer (1985). Briefly, mice were kept in their home cages in the dark testing room until testing began. Mice were then individually removed from their home cages and allowed to habituate for 10 minutes in an empty, approximately 15" x 15" x 18" (l x w x h) plastic-lined wooden box illuminated by a red light lamp. Differences in trials only began 24 hours after initial habituation in the empty box. In the long-term memory trial, mice were placed in the same box for 3 minutes with two identical sample objects (plastic hamburger buns) that were secured in two adjacent corners of the box with Velcro. Twenty-four hours later, one sample object was removed and replaced with a novel object (brass weight), which the mouse was allowed to explore for 3 minutes. In the short-term memory trial, mice were allowed to habituate with the two sample objects (golf balls) for 10 minutes. One hour later, one sample object was replaced with a novel

object (rubber stopper) and the mouse was allowed to explore for 3 minutes. In both trials, all object interactions were filmed and the placement of the sample and novel object was randomized between mice. All objects and the box were cleaned with 70% ethanol between trials. Scoring of total time with each object was initially conducted by one blinded observer and confirmed by a second blinded observer (Pearson's $r = 0.98$).

Results

Combined pre+postnatal rapamycin treatment impairs long-term spatial memory

By comparing cognitive function of the *Tsc2^{fllox/ko}; hGFAP-Cre* pre+post rapamycin treatment cohort to the postnatally treated cohort, we sought to determine whether the greater histological rescue we observed in the former group translated to greater functional rescue. As the most striking degree of histological improvement was found in the hippocampus, we chose to focus on learning and memory tests that were hippocampus-dependent. We began with the hidden-platform version of the Morris Water Maze (MWM), in which the mouse uses spatial cues (Fig 5.1A) to locate a submerged platform in a tub of opaque water (Fig 5.1B). The mice were initially placed through the more sensitive MWM test of mass training (see Methods & Materials) for 4 consecutive days (Fig 5.1C). However, mutant mice from both cohorts exhibited seizures and signs of exhaustion throughout the tests (as demonstrated by minimal cleaning behavior when placed back into the heated cage, labored breathing, and a hunched posture). As mutants from both groups found the platform in similar amounts of time by Day 4, we felt comfortable transitioning to a less stressful version of the MWM, which involved spaced training.

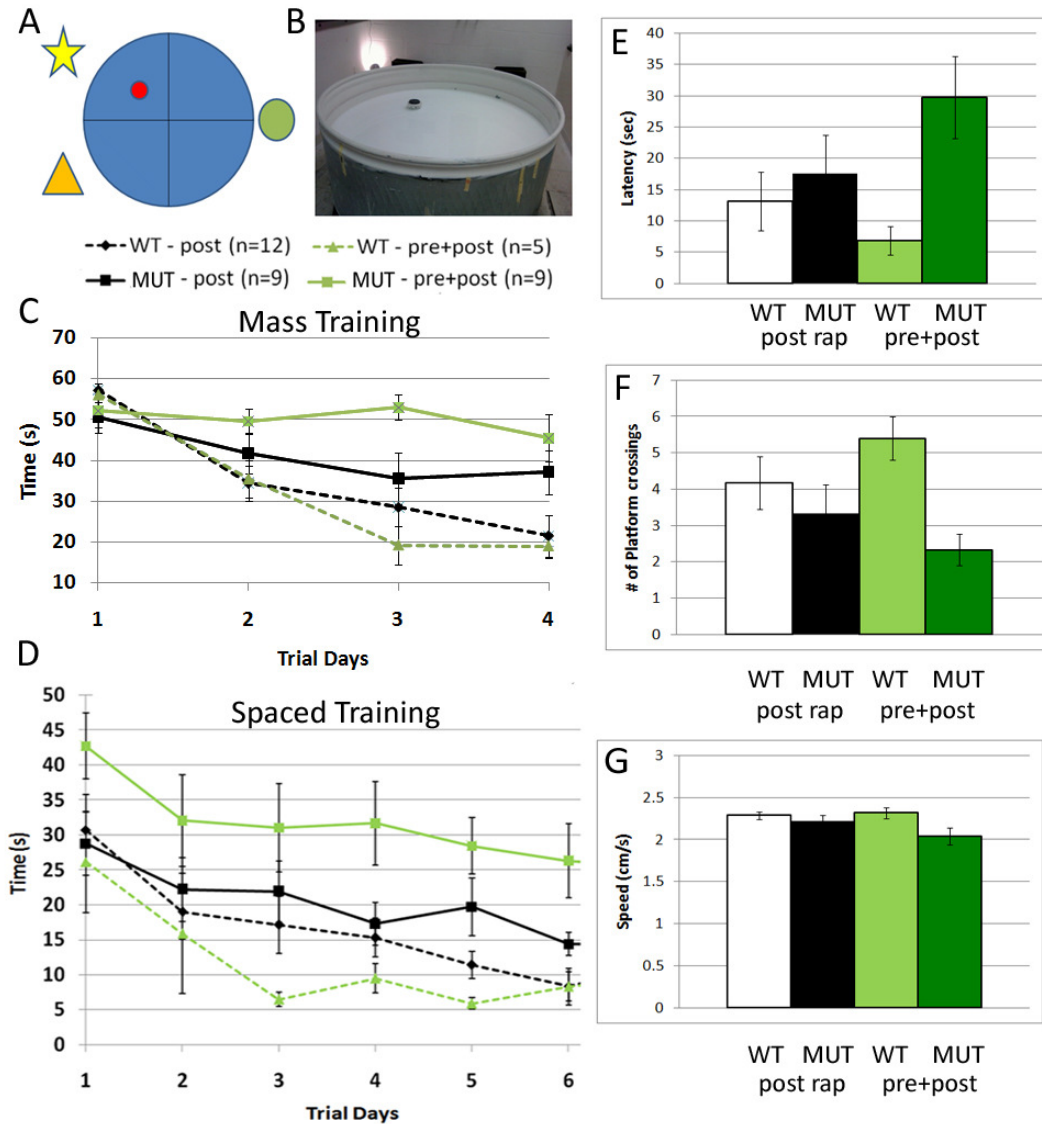


Fig 5.1. Combined pre+postnatal rapamycin treatment of *Tsc2^{flox/ko}; hGFAP-Cre* mice impairs spatial learning and memory. (A,B) Mice were trained in the Morris Water Maze, in which mice use spatial cues (A) around a tub of opaque water to find a submerged platform (B). (C) Post and pre+post rapamycin-treated mice were initially mass-trained over four days, though exhaustion and seizures in the mutants resulted in limited learning, as shown by the average time to find the platform by day 4 compared to controls. (D) Pre+post mutants took longer to find the platform compared to control and post mutants in the less-stressful spaced training task. Meanwhile the post mutants performed similarly to both post and pre+post treated controls. (E, F) 24 hours after day 6 of spaced training, the platform was removed and latency to find the platform location (E) and number of times the platform location was crossed was recorded (F). Pre+post mutants look significantly longer to find the platform and crossed it fewer times compared to control cohorts while post mutants performed similarly to their treated controls. (G) These results were not due to differences in swimming speed between groups, as measured using a visible platform.

In spaced training, mice were trained over the course of 6 days and the average time taken to find the platform, unmoved from mass training, was recorded per day (Fig 5.1D). No seizures or signs of exhaustion were observed during this test. Interestingly, though both pre+post and post rap mutants displayed similar latencies at the end of mass training, pre+post mutants took significantly longer to find the platform on Day 1 of spaced training compared to postnatally treated mutants. Though the average latency of pre+post mutants slightly decreased per day, their final time on Day 6 was still notably longer than that of the other cohorts. Meanwhile, the postnatally treated mutants consistently found the platform in a similar amount of time as the control groups. Twenty-four hours after their last trial on Day 6, we performed a probe trial in which the platform was removed. Pre+post mutants took significantly longer to locate the platform compared to the post rap mutants, who performed similarly to the control (Fig 5.1E). Pre+post mutants also crossed the platform fewer times on average than the post mutants (Fig 5.1F). These results were not due to differences in motor ability, as swim speeds were similar among all groups (Fig 5.1G) and prior rotarod testing showed no significant difference in latency to fall (data not shown). A visible-platform version of the MWM confirmed that discrepancies were also not due to visual impairment, as all mice were able to locate the platform in similar amounts of time in this case (data not shown).

Combined pre+postnatal rapamycin treatment impairs contextual discrimination and memory

To further investigate the apparent spatial learning and memory deficits of the pre+postnatally treated cohort, we tested the mice for context discrimination and memory abilities using contextual fear conditioning. This modified version of classical fear conditioning is more hippocampal-dependent as it tests the ability of the mice to

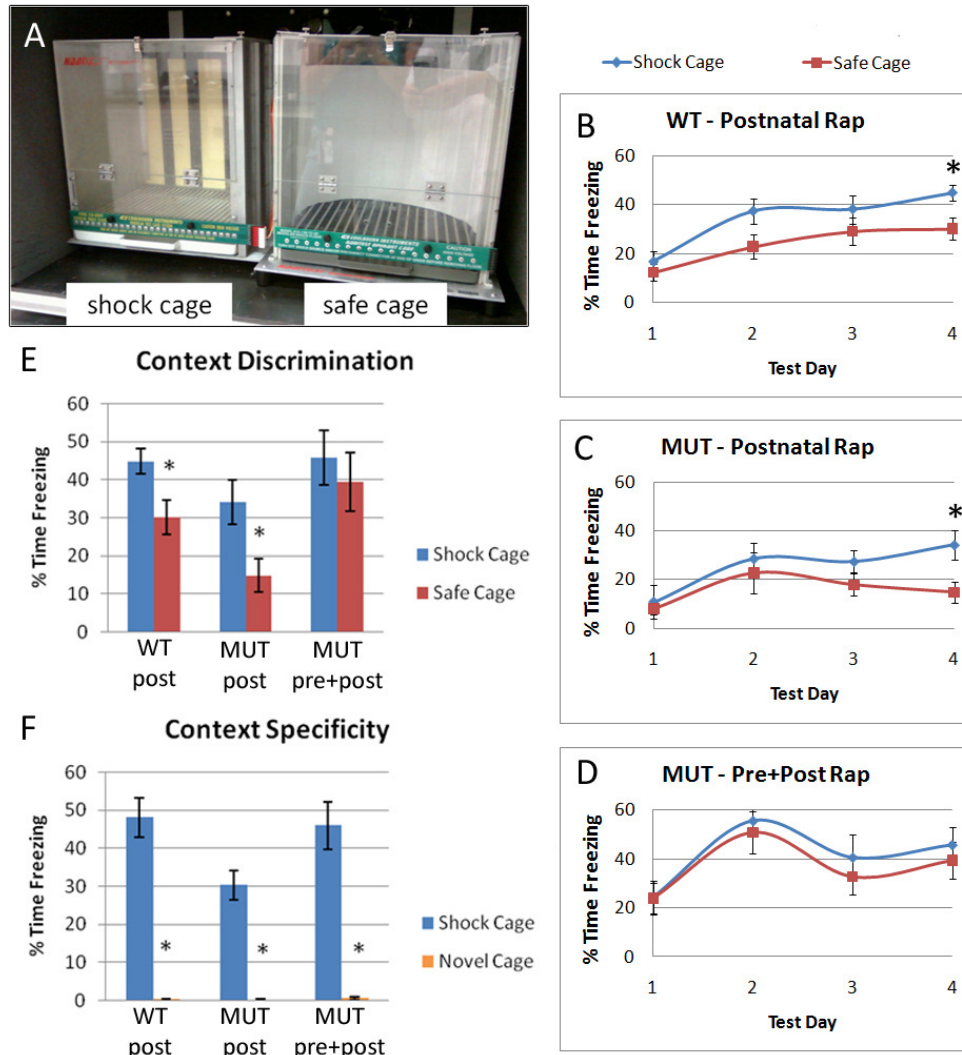


Fig 5.2. Combined pre+postnatal rapamycin treatment of *Tsc2*^{flox/ko}; *hGFAP-Cre* mice impairs contextual learning and memory. (A) Mice were tested for contextual memory, where the time spent freezing in a shock cage versus safe cage is measured. The two cages were located in a soundproof, darkened box as shown, with subtle differences including background, shape, and smells differentiating the two cages. One cage (shown on left) was always paired with the shock. (B-E) Over the course of 4 days, mice were measured for time spent freezing in either cage prior to shock. By Day 4, control mice (B) and postnatally treated mutants (C) froze longer in the shock cage versus safe cage, whereas pre+post mutants froze for similar amounts of time in both cages (D). Results from Day 4 are shown in bar graph in (E). (F) To demonstrate that freezing was not due to mere anxiety about a new environment, freezing behavior was measured in the shock cage and a completely novel context (cage in brightly lit room). All mice were able to distinguish between the two contexts. Post-treated control (n=12), post-treated mutant (n=8), pre+post treated mutant (n=9).

discriminate between two slightly similar contexts, one of which is paired with a shock and the other which is not (Fig 5.2A). Ability to discriminate is measured in percentage of time spent freezing in the shock cage versus the safe cage. Over the course of 4 days, time spent freezing in both cages was recorded (Fig 5.2B-D). By the fourth trial, postnatally treated mutant and control mice froze significantly longer in the shock cage than the safe cage, indicating they had learned to discriminate between contexts, whereas the freezing time of the pre+post treated mutant did not differ between either cage (Fig 5.2E). To determine whether mice were indeed remembering the shock and were not freezing due to anxiety from being moved or touched, we measured freezing behavior of the mice first in the shock cage and then in a novel, completely distinct cage. Both post and pre+post mutants were able to discriminate between these contexts (Fig 5.2F), indicating our findings were due to impaired contextual discrimination and memory in the pre+postnatally treated mutant.

Rapamycin-treated *Tsc2*^{flox/ko}; *hGFAP-Cre* mice display reduced anxiety-like behavior

Though the MWM and contextual fear conditioning are solid and informative tests to assess hippocampal functions of learning and memory (166, 167), both tests involve a large degree of stress. Results from other behavioral tests may hence be affected if certain subjects are more susceptible to stress or anxiety than others. We therefore sought to validate the last finding from our fear conditioning assay using another well-established test for anxiety, the elevated plus maze (EPM, see Methods). Often used to measure the anti-anxiety effects of new pharmacological agents, increased time or entrances on the open arms of the EPM are interpreted as indicators of alleviated anxiety (163). Post and pre+post mutant mice entered both the enclosed and open arms more often than the control mice (Fig 5.3A), indicating higher levels of activity. Interestingly, though they did not preferentially

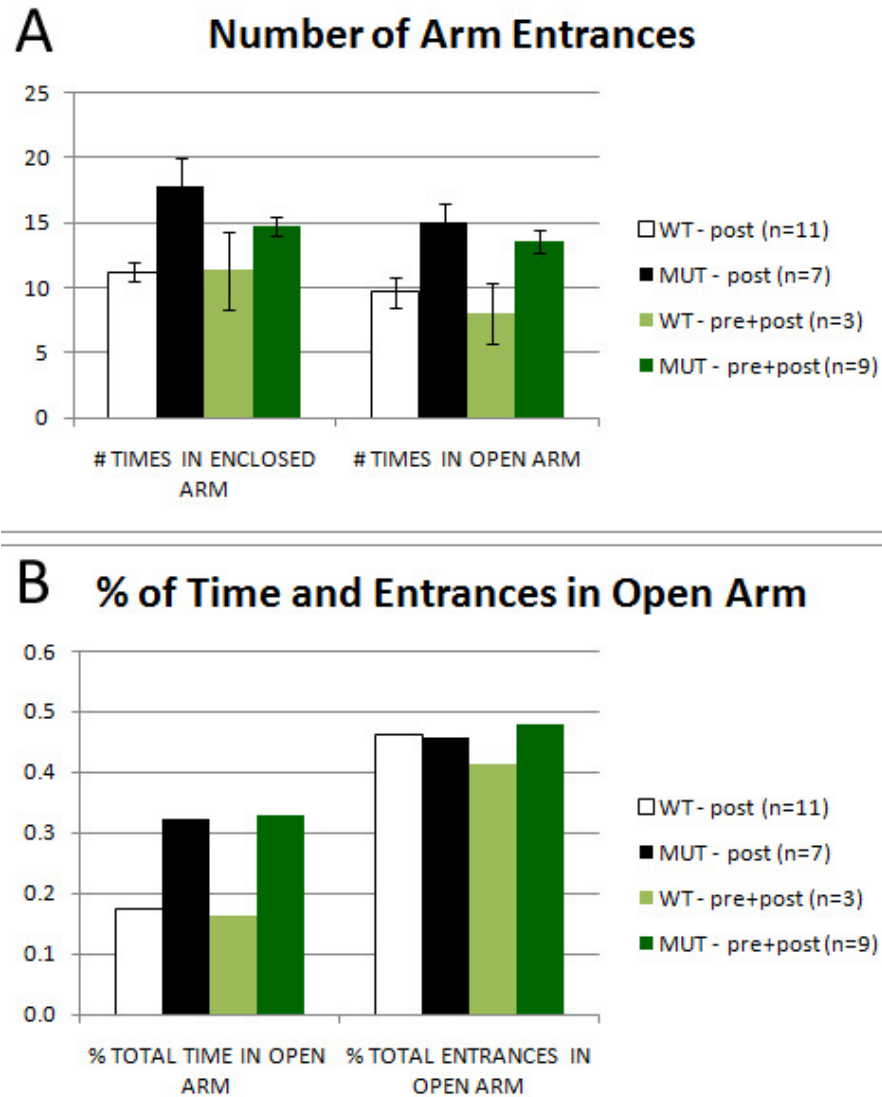


Fig 5.3. Rapamycin-treated *Tsc2*^{flox/ko}; *hGFAP-Cre* mice display anti-anxiety behavior. (A) Mice were tested for anxiety using the elevated plus maze, in which increased time or entrances on open arms demonstrate anti-anxiety. Both post and pre+post mutants entered the enclosed and open arms more frequently than controls, indicating higher levels of activity. (B) Though mutants did not preferentially enter the open arms compared to controls, they did spend more time on the open arms.

enter the open arm over the closed arm, they did spend significantly more time on the open arms than the control (Fig 5.3B). This finding suggests that the mutants of both treatment groups display less anxiety than their littermate controls.

Short-term memory is intact in all rapamycin-treated cohorts

To better understand why long-term learning and memory seemed to be disrupted in the pre+post mutant mice, we tested all groups for short-term memory using the object recognition test. This test makes use of the observation that mice preferentially interact with a previously unexplored object. Mice are hence exposed to two identical objects in phase one before one object is replaced with a novel object in phase two. Interaction time with each object is recorded. To test short-term memory, we allowed a one-hour interval between the two phases. Mutant and control mice from both treatment groups all interacted for a greater length of time with the novel object, demonstrating that short-term memory was not impaired in any group.

Discussion

In this study, we examined the functional effects of post and pre+post rapamycin treatment by testing the learning and memory abilities of treated *Tsc2^{flox/ko}; hGFAP-Cre* and control mice. We hypothesized that pre+post treated mutant animals would behave more like control animals since histologic rescue was most similar to control brains. Surprisingly, mutant mice treated pre+postnatally were impaired in spatial and contextual long-term learning and memory compared to postnatally treated mutant and control animals as demonstrated using the MWM and contextual fear conditioning tasks. Postnatally treated mutants, on the other hand, performed as well as post and pre+post treated controls. Both

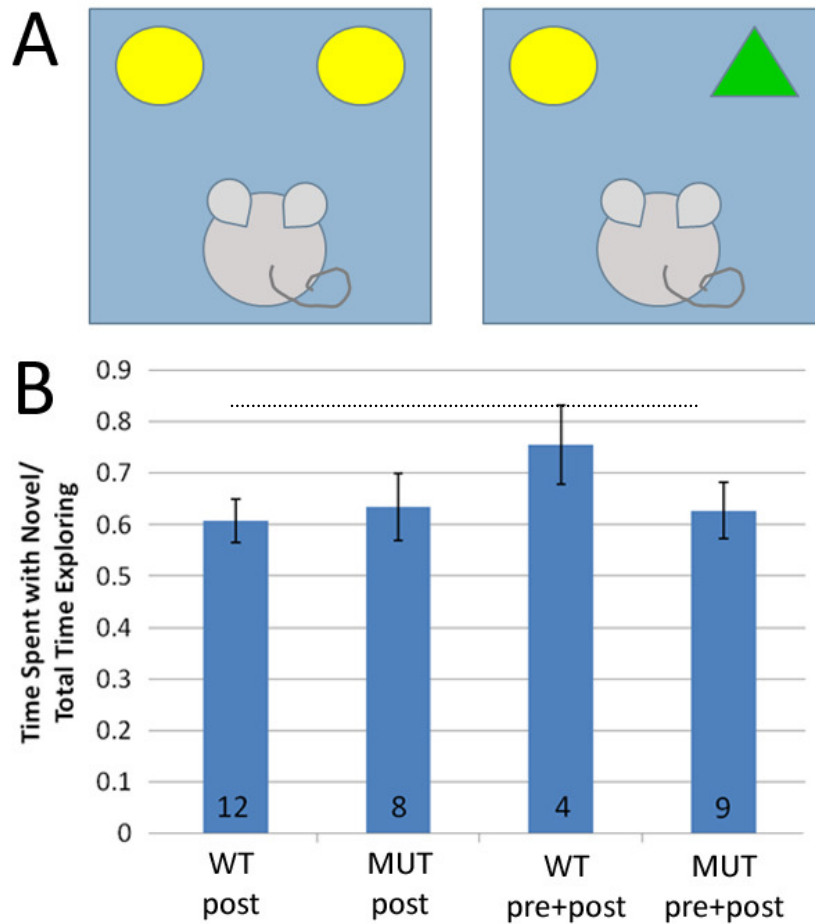


Fig 5.4. Short-term memory is intact in all rapamycin-treated cohorts. (A) The low-stress object recognition task was used to assess short-term memory. In this task, mice are habituated in a box then allowed to interact for 10 minutes with two identical objects (left). One hour later, one original object is replaced with a novel object and interaction with both objects is timed for 3 minutes. **(B)** All mice preferentially interacted with the novel object than the original, demonstrating intact short-term memory in all groups.

mutant groups also demonstrated reduced anxiety-like behavior in the elevated plus maze. Meanwhile, the short-term memory of all groups appeared intact as demonstrated by the object recognition task.

We originally hypothesized that the greater degree of histological rescue found in the pre+post mutants would translate to improved cognitive function compared to the post rap mutants, though this was demonstrated to be incorrect. Though post and pre+post mutants exhibited similar degrees of rescue of defects in cortical thickness, cell size, hypomyelination, and astrogliosis, pre+post mutants showed significantly improved lamination, an important factor in proper cognitive function. Despite their improved lamination, however, the pre+post mutants displayed significantly impaired learning and memory compared to post rap mutants. These results may be explained by considering the fact that while appropriate migration of cortical and hippocampal neurons is indeed critical to brain function (136), many other factors are involved in long term memory and learning, such as neurotransmitter homeostasis as well as dendrite and synapse formation and function (168). Studies in the astrocyte-specific *Tsc1* CKO mouse (93), for example, revealed abnormal glutamate homeostasis and subsequent impairments in MWM and fear conditioning results. Interestingly, the untreated *Tsc2^{flax/ko}; hGFAP-Cre* mouse has been found via Sholl analysis to have significantly increased dendritic branching, while dendritic spines appear round and mushroom-like (data not shown). Though our histologic analysis demonstrated rescue of some defects, we did not assess the impact of rapamycin on the increased dendritic arborization or many other factors that are important for proper brain function such as axon formation, neurotransmitter production and release, and neurotransmitter receptor density. Investigation of how prenatal versus postnatal rapamycin impacts these factors will be essential in helping us better understand the role of the mTORC1 pathway in cognitive function.

We consistently found that postnatally-treated mutant mice performed similarly to treated controls. This result suggests that postnatal treatment with rapamycin, when administered from birth, is able to restore learning and memory abilities in mutant mice. Our finding is similar to that shown by Ehninger et al. (2008), who demonstrated that rapamycin treatment was able to reverse spatial learning and contextual discrimination defects in 3-6 month old *Tsc2*^{+/-} mice compared to vehicle controls, using the MWM and same context discrimination task we chose. However, as our experiments did not include a naïve or vehicle-treated control group, we cannot conclusively determine whether postnatal treatment in the *Tsc2*^{flox/ko}; *hGFAP-Cre* mice rescued learning and memory abilities. As rapamycin has been shown to impair learning and memory *in vivo* (161), treated control mice might therefore also be impaired in their cognitive functions. We are currently testing untreated control mice to resolve this concern, as it is critical to understand whether rapamycin has detrimental effects on control animals. If impairment at this low dosage is minimal, then our results would indicate that postnatal treatment from birth can not only restore health, increase lifespan, and alleviate a number of histologic brain defects, but improve cognitive function as well. This would pave the way for exciting translational trials in neonates affected with TSC.

Chapter Six:
Significance and Future Directions

Introduction

Nearly a century and a half after Bourneville's initial account of TSC, much regarding its genetic etiology and relevant pathways has been discovered thanks to the efforts of generations of physicians, researchers, and patients. However, significant gaps still exist in our understanding of the pathophysiology of the disease, particularly in regard to the debilitating neurological manifestations. In this dissertation, we sought to address some of these unknowns through the creation, characterization, and rapamycin treatment of a novel brain-specific mouse model of TSC, *Tsc2^{flox/ko};hGFAP-Cre*. We hypothesized that deletion of *Tsc2* in radial glial cells would result in a mouse that recapitulated many aspects of TSC neuropathology. Using this mouse, we proposed to test the extent of mTORC1 involvement in TSC brain pathology formation by inhibiting mTORC1 with the macrolide rapamycin, while also demonstrating the therapeutic potential of this drug as a TSC treatment.

As described in previous chapters, the results of our study have yielded a number of novel findings. First, deletion of *Tsc2* in radial glial cells does indeed give rise to many TSC-like brain defects, indicating that these neuroglial progenitor cells may play a large role in TSC neuropathology. Second, loss of heterozygosity, as modeled in our mouse, leads to TSC-like brain pathology, lending support to the two-hit hypothesis for brain lesion formation in this disease. Third, inhibition of mTORC1 over-activity with rapamycin alleviates many TSC defects, demonstrating the high degree of involvement the mTORC1 pathway has in TSC pathology formation. Fourth, a low dosage of rapamycin is sufficient to effect histologic rescue in our mice, suggesting that the extremely high dosages used in other mouse studies may be unnecessary and/or lead to undesired side effects for translational studies. Fifth, combined prenatal and postnatal treatment with rapamycin resulted in the greatest histologic rescue of defects in neuronal migration compared to

individual prenatal or postnatal treatment, indicating that proper mTORC1 activity is required for correct migration throughout all stages of neurodevelopment. Sixth, prenatal rapamycin treatment is detrimental to learning and memory, suggesting that inhibition of mTORC1 activity may cause side effects during early development. Lastly, postnatal rapamycin administration in our model results in learning and memory abilities similar to those of treated control mice, a result that may support the novel treatment modality of rapamycin treatment in neonates with TSC.

The work described in this thesis has provided an excellent tool for the study of TSC in the brain and greatly enhanced understanding of the defects involved in TSC brain pathology. In addition, it has indicated a significant role of mTORC1 in TSC neuropathology formation, though much remains unknown regarding the downstream effectors and mechanisms by which this kinase induces lesion formation. The *Tsc2^{flox/ko};hGFAP-Cre* mouse model will be extremely useful in future studies that involve elucidating or verifying the mechanisms underlying formation of these defects. Below, I will discuss potential mechanisms that lead to two of the most prominent yet poorly understood defects found in TSC brain pathology, neuronal migration and myelination, and how these mechanisms might explain our findings in the *Tsc2^{flox/ko};hGFAP-Cre* mouse. In addition, I will propose future work to investigate these mechanisms and enhance our understanding of TSC neuropathology formation.

mTOR and Neuronal Migration

As previously discussed, cellular migration is a highly regulated process that is essential to proper brain function. As described in the discussion section of Chapter 3, the defects in migration in TSC brain lesions are so severe that the disease may be considered

a neuronal migration disorder (16). We also found significant defects in neuronal migration in the cortex and hippocampus in the untreated *Tsc2^{flox/ko};hGFAP-Cre* mouse, as indicated by poorly defined cortical layers, the presence of cells stained with an upper-layer marker in the lower layers of the cortex, and ring heterotopias and an ectopic layer of cells above the pyramidal layer of the hippocampus. Prenatal rapamycin treatment resulted in alleviated cortical migration defects, though hippocampal abnormalities were not significantly affected, while our analysis demonstrated that postnatal rapamycin treatment had no significant effect on migration. A combination of prenatal and postnatal treatment, however, resulted in significant rescue of both cortical and hippocampal migration defects. These results indicate the need for proper mTORC1 function during both prenatal and postnatal neurodevelopment for correct neuronal migration.

A. Migration and the Cell Cycle

A1. Cell cycle progression and cell size

Several studies have implicated the impact of mTORC1 on cell cycle progression as a major mechanism by which the kinase is involved in migration. Laminar organization in the cortex requires precise coordination between the timing of cell cycle exit of progenitor cells and the determination of their laminar fate, which occurs during the S phase of the last cell division (169). Fingar et al. (170, 171) established *in vitro* that S6K1 and 4E-BP1, well-established downstream effectors of mTORC1, were responsible for mTORC1's control of G₁-phase progression. They hypothesized that their results might indicate a model in which cell growth and cell cycle are closely coupled, such that mTORC1 primarily drives cell growth via macromolecular biosynthesis, with progression of the cell cycle being a secondary consequence. However, they also noted a rapamycin-insensitive and therefore

mTORC1-independent aspect of G₁-phase progression and suggested a possible role for the mammalian orthologue of a yeast protein, TORC2, known at the time to mediate both rapamycin-sensitive and -insensitive signals. Later studies confirmed the presence of mTORC2 (96), a rapamycin-insensitive second kinase complex of mTOR, which is activated by the TSC complex (95) and activates Akt via phosphorylation (172, 173). Though FKBP12-rapamycin cannot bind directly to mTORC2, prolonged presence of rapamycin allows it to bind to free mTOR and thereby inhibit mTORC2 assembly and consequently Akt activity (100). Rosner et al. (174) later demonstrated in primary non-transformed, non-immortalized human fibroblasts that mTORC1 was able to control the cell cycle via the aforementioned downstream effectors independently of mTORC2 activity. However, mTORC2 was also able to regulate cell size and the cell cycle through its activation of mTORC1 via Akt/Tsc2/Rheb. These studies indicate the critical role of mTORC1 and mTORC2 in controlling cell size as well as cell cycle progression, which is closely tied to migration.

A2. Cell cycle progression and cyclin-dependent kinase inhibitor p27^{Kip1}

Another method of regulation of the cell cycle by the mTOR complexes, independent of S6K1 and 4E-BP1 translational activity, was recently proposed in which mTOR promotes the phosphorylation and therefore targeted degradation of p27^{Kip1}, a Cip/Kip cyclin-dependent kinase inhibitor (CKI) highly involved in brain development (175). p27^{Kip1} promotes cell cycle exit at the G₁ restriction point by blocking the catalytic activity of cyclin E/A and cdk2 (cyclin dependent kinase 2) (176), inhibiting phosphorylation of pRb (retinoblastoma protein) and halting transcription of genes required for transition from G₁ to S phase (Koff, Polyak, 1995, Cell Cycle Res). p27^{Kip1} is therefore particularly involved in

determining the length of the cell cycle and the probability of cell cycle exit (Lukaszewicz, Savatier, 2005, Neuron), and therefore the birth date of projection neurons. Increased mTOR activity hence enhances cell cycle progression through degradation of p27^{Kip1} (177). Accordingly, p27^{Kip1} knockout mice demonstrate increased cell proliferation and enlarged brains, particularly as a result of thicker upper cortical layers at the expense of lower layers (178). This finding of enlarged brains and decreased lower layer neuron population is similarly found in the *Tsc2^{flox/ko};hGFAP-Cre* mouse model, in which overexpression of mTOR may be leading to increased degradation of p27^{Kip1}. These findings suggest that p27^{Kip1} may play a role in the formation of TSC brain pathology.

A3. Future examination of the cell cycle

With the similarities between the *Tsc2^{flox/ko};hGFAP-Cre* mouse model and p27^{Kip1} knockout mice, it is important to investigate the activity of p27^{Kip1} as well as the contributions of the cell cycle to the phenotype found in our model. Direct visualization of phosphorylated and unphosphorylated p27^{Kip1} expression via immunohistochemical staining or immunoblotting may be easily conducted during mid-neurogenesis timepoints, such as E13.5 and E16.5. As mTOR activity is highly increased in the mouse model, p27^{Kip1} presence should be decreased, and therefore increase of G₁ to S cell cycle progression should be noted. Unchecked protein synthesis via upregulated mTORC1 activity may also disrupt the cell cycle and contribute to the observed migration defects. Basic analysis of cell cycle progression should therefore be conducted, and may be quickly performed using immunohistochemical labeling and quantitation of cells with cell-cycle markers such as anti-pH3, a marker of cells undergoing mitosis, which might be conducted at E12.5, E14.5, E16.5, and E18.5 to compare differences in M phase activity between the control and

mutant mice. Comparison of number of cells exiting the cell cycle may also be analyzed using co-labeling of BrdU, an S-phase marker, and Ki67, a cell cycle marker. This experiment involves injecting pregnant dams with BrdU, waiting 24 hours for a full cell cycle then co-labeling with anti-BrdU and anti-Ki67 antibodies, and quantitating cells that are BrdU+ but Ki67-. This experiment might also be conducted at a variety of embryonic timepoints to investigate cell cycle progression and regulation in the mouse model. We have currently initiated analysis of expression arrays from cortical samples taken at E14.5, E16.5, and P10. Investigation of these samples and additional proteomic array analysis at these timepoints will further establish presence of relevant cell cycle components. Repetition of these studies using *Tsc2^{flox/ko};hGFAP-Cre* mice undergoing concurrent rapamycin treatment, in which we see improvement of migration defects, might determine whether cell cycle components, and in particular p27^{Kip1}, play a significant role in formation of these defects.

B. Migration and the Rho Family Small GTPases

B1. The Rho family small GTPases

The Rho family of small GTPases, most notably RhoA, Rac1, and Cdc42, are crucial regulators of cellular migration that cycle between an inactive GDP-bound form and an active GTP-bound form. RhoA advances the formation of actin stress fibers and focal adhesions (Ridley, 1992, Cell; Amano, 1997, Science) while controlling actin-myosin contractility, which is important for translocation of the cell body and retraction of the rear of the cell (179). Rac1 promotes formation and extension of lamellipodia, whereas Cdc42 stimulates formation of filopodia (180). Proper cellular migration particularly requires a balanced polarity between Rac1 and RhoA, with higher Rac1 activity present at the leading

edge of the cell and higher RhoA activity at the rear of the cell (Woods, 2010, Cell Cycle). Disruption of this balance disrupts migration and impacts other morphological events such as growth-cone motility and axon guidance in the cell (181) .

B2. p27^{Kip1} and RhoA

In a function distinct from its regulation of the cell cycle, p27^{Kip1} has been shown to play a more direct role in migration by modulating RhoA activation. p27^{Kip1} was found by Besson et al (182) to inhibit RhoA via direct binding to prevent its interaction with its guanine-nucleotide exchange factors (GEFs), which exchange GDP for GTP and thereby activate RhoA (183)(Schmidt & Hall, 2002, Genes Dev). Mouse embryonic fibroblasts (MEFs) derived from p27^{Kip1} knockout mice had impaired mobility, increased numbers of stress fibers, and increased numbers of focal adhesions (182), likely due to the imbalance between RhoA and Rac1. In a separate experiment, prolonged but not acute treatment with rapamycin *in vitro* caused an increase in p27^{Kip1} presence and also impaired RhoA activity and cell migration, results of which could be mimicked by mTORC2 siRNA inhibition, implicating the specific role of mTORC2 in negatively regulating p27^{Kip1} (175) and underlining the delicateness of RhoA/Rac1 balance. As the loss of the TSC complex has been shown to impair mTORC2 kinase activity *in vitro* (95), loss of Tsc2 in the *Tsc2^{flox/ko};hGFAP-Cre* mouse likely also results in impaired mTORC2 activity. According to the results discussed above, this would lead to reduced degradation of p27^{Kip1}, greater inhibition of RhoA, and consequent decrease in cell motility, which may explain the migration defects found in the model. However, prolonged treatment with rapamycin at our dosage alleviated these migration defects rather than exacerbated them, suggesting that alternate mechanisms in regulation of migration need to be explored.

B3. S6K1, 4E-BP1, and the Rho family small GTPases

The involvement of mTOR in regulating RhoA, Rac1, and Cdc42 was further confirmed in a recent study by Liu et al. (184), in which rapamycin treatment was found to inhibit protein synthesis and the activity of the three GTPases *in vitro*. While this study makes no mention of p27^{Kip1}, it instead implicates a different set of regulators of RhoA, Rac1, and Cdc42 - the downstream effectors of mTORC1, S6K1 and 4E-BP1. By disrupting mTORC1 or mTORC2 by down-regulating raptor or rictor, respectively, the authors were able to conclude that mTORC1 was involved in inhibiting the protein synthesis of the three GTPases, whereas mTORC2 mainly inhibited their activity, as measured by decreased GTP-bound forms of the GTPases. Prolonged rapamycin treatment, however, mainly suppressed RhoA, Rac1, and Cdc42 activity and therefore cell motility by inhibiting the protein expression of the small GTPases. Meanwhile, rapamycin inhibition could be overcome by overexpression of RhoA but not the other proteins, suggesting that rapamycin inhibits cell motility at least in part through attenuation of RhoA protein expression. These results indicate a larger role of mTORC1 in migration than the aforementioned studies implied. It is therefore possible that overactivation of mTORC1 in the *Tsc2^{flox/ko};hGFAP-Cre* mouse and the resulting migration defect is attenuated through rapamycin treatment, which results in restored balance to RhoA levels and subsequent appropriate migration.

B5. Future examination of the Rho family small GTPases

The relationship between the mTOR complexes and RhoA, Rac1, and Cdc42 as described above suggest that the Rho family of small GTPases may play an important role in the migration defects found in TSC pathology. Though these *in vitro* studies show that prolonged rapamycin inhibits migration through these proteins at least in some part, it is

unclear how the small GTPases are impacted by treatment following the removal of Tsc2, particularly in an *in vivo* system. Characterization of the activity of RhoA, Rac1, and Cdc42 as well as the phosphorylation status of the two mTOR complexes in the *Tsc2^{flox/ko};hGFAP-Cre* mouse will therefore be very useful in investigating this question. Phosphorylation status and protein presence may be measured using immunoblot analysis of embryo cortex and hippocampal lysates throughout corticogenesis, for example at E13.5, E15.5, E17.5, and P0. Activity of the small GTPases may be more specifically measured using affinity binding assays to pull down GTP-bound RhoA, Rac1, and Cdc42 before immunoblot analysis. Investigation of these and other migration-linked effectors via expression and proteomic arrays may further establish the roles of these and other proteins in the formation of TSC defects. For example, analysis of E16.5 cortical samples by expression array in our lab has demonstrated a significant increase in expression of Pak1 in the *Tsc2^{flox/ko};hGFAP-Cre* mouse compared to a littermate control. As Pak1, a downstream effector of Rac1 and Cdc42, is an important regulator of neuronal polarity, morphology, migration, and synaptic function (Nikolic 2008 Mol Neurobiol), investigation of why this protein is so highly upregulated following Tsc2 deletion will provide direct insight into TSC pathology formation.

mTOR and Myelination

A. Myelination and Migration

In addition to neuronal migration, the *Tsc2^{flox/ko};hGFAP-Cre* mouse is also characterized by defective myelination. Developmental studies, as described in Chapter 3, indicated that the hypomyelination observed in the adult was due to aberrant progression of myelin into the lower cortical layers, rather than as a result of demyelination. Though myelin presence, as visualized by immunohistochemistry using MBP as a marker, appears slightly

patchy in the corpus callosum, actual formation of myelin does not seem to be severely affected. Our investigation of mature oligodendrocytes using antibodies against CC1 demonstrated in the *Tsc2^{flox/ko};hGFAP-Cre* mouse an increased number of oligodendrocytes in which mTORC1 was also upregulated. Whether increase in mTORC1 activity or increase in cell number affects the ability of oligodendrocytes to myelinate remains to be studied. The neuron-specific *Tsc1* CKO mouse, however, demonstrates similar myelination defects as our model, without evidence of increase in or aberrant distribution of oligodendrocytes (77), indicating that these particular characteristics may play a lesser role in the hypomyelination phenotype. Before alternate hypotheses may be studied, however, we must first establish that oligodendrocytes are correctly distributed throughout the cortex in the *Tsc2^{flox/ko};hGFAP-Cre* mouse. Oligodendrocyte precursor cells (OPCs) move using saltatory migration (185), in which the leading edge of the cell orients towards the pial surface with alternating stationary and fast-moving phases, including dramatic shape changes (186). This method of movement resembles formation of axonal growth cones, a process which incorporate signals from the previously mentioned RhoA and its related effectors (187). Given that RhoA signaling is likely highly altered in the *Tsc2^{flox/ko};hGFAP-Cre* mouse, OPC migration to a position appropriate for myelination may also be compromised. Use of immunohistochemical markers such as Olig2, MOG, and CC1 to visualize and quantitate OPC and mature oligodendrocytes should be sufficient to establish proper placement of these cells for myelination.

B. Myelination and Axonal Surface Molecules

As characterization of the neuron-specific *Tsc1* CKO did not yield differences in OPC distribution or number, the authors instead suggested that hypomyelination was seen

as loss of Tsc1 in neurons might inhibit the induction of myelination (77). This hypothesis is quite plausible, given that myelination of individual axons by oligodendrocytes may be heavily regulated by extracellular ligands and secreted molecules present on the surface of the axon itself (188). As support, Meikle et al (2007) cite high expression of the growth-associated protein GAP-43 in the P21 mouse model. GAP-43 has a distinct inverse relationship with myelin (189) and is usually expressed during axonal outgrowth before P7 (190), indicating that neurons may be more responsible than oligodendrocytes in causing the hypomyelination defect observed. Initial effort might therefore focus on investigating aberrant neuronal signaling to oligodendrocytes in the *Tsc2^{flox/ko};hGFAP-Cre* mouse. A number of well-characterized axonally expressed ligands may be studied for this purpose, such as Jagged, PSA-NCAM, and LINGO-1, all of which inhibit the differentiation of OPCs or myelination (191-193).

B. Myelination and Neuronal Activity

Deletion of Tsc2 and subsequent mTORC1 activation in the *Tsc2^{flox/ko};hGFAP-Cre* mouse may also alter electrical activity of the axons, which in turn may influence myelination (194, 195). Aberrant neuronal activity may alter expression of the previously mentioned surface ligands. Unregulated release of neurotransmitters such as adenosine by active axons might also inhibit or disrupt OPC differentiation and subsequent myelination (196). Investigation of neurotransmitters *in vivo* may be conducted via microdialysis or direct electrochemical methods, while detection of individual neuronal activity can be achieved via patch clamping of cultured brain slices.

Model Summary

Though TSC neuropathology is characterized by a number of defects, aberrant neuronal migration and hypomyelination are two of the most cardinal and poorly understood traits. As these characteristics are also well-recapitulated in the *Tsc2^{flox/ko};hGFAP-Cre* mouse model, I have focused on them in this discussion to better guide future investigation into the formation of these defects. Neuronal migration may be controlled by a number of factors, most prominently release of the cell from the cell cycle and physical ability of the cell to move. The important roles of p27^{Kip1} and mTORC1's downstream effectors S6K1 and 4E-BP1 in controlling the cell cycle as well as Rho family small GTPases have therefore been discussed, with future study emphasizing the relative levels of these proteins at different developmental timepoints. Myelination may be highly affected by inhibited OPC movement or altered neuronal induction, whether by surface molecule or neurotransmitter signaling. Investigation of OPC/oligodendrocyte positioning and electrical/biochemical signaling to determine what is causing the aberrant myelin progression is therefore relevant. The results of these proposed studies will provide much-needed insight into the neuronal migration and hypomyelination defects seen in TSC pathology. I will now discuss additional future studies which may also enhance our understanding of TSC neuropathology formation.

Additional Future Studies

A. Creation of a tuber-based mouse model

One of the main criticisms of our model, as well as that of the Eker rat and TSC1 CKO models, has been the absence of focal tubers, a defining characteristic of TSC neuropathology. In a TSC Investigator's Meeting workshop, participants felt that:

The relevance of all of these results [from animal models] to human TSC remains to be established... [participants] remained cautious of direct correlation to human TSC. Despite the variety of neuropathology in these models, none expressed typical cortical tubers (197).

In response to this critique, Wong (198) correctly pointed out that a number of findings derived from “tuberfree” animal models have already impacted understanding of human TSC. He cites as examples the discovery of the role of the TSC complex in the mTORC1 pathway, originally found in *Drosophila* (52, 199) and now the basis for rapamycin treatments, as well as abnormalities in astrocyte glutamate transporters, found in the astrocyte-specific TSC1 CKO (200) and now verified in human TSC tissue (201). He concludes that while caution is always appropriate when interpreting animal data, data from these models have already been found to have direct clinical applications to TSC.

While study of models that do not display focal tubers has indeed been extremely informative, it is also important to note that though we do not see focal tubers per se, many of the characteristics found throughout the *Tsc2*^{flox/ko}; *hGFAP-Cre* brain model those of tubers. It is thought that tubers form from a single progenitor (202). By deleting *Tsc2* in all radial glial progenitor cells, we have recapitulated much of the disease and in many respects created a “holotuber.” Some aspects of TSC, such as seizures and cognitive disabilities, may admittedly be much more severe in this mouse due to the presence of tuber-like defects throughout the entire brain rather than in an isolated area surrounded by normal tissue. Other characteristic defects such as migration problems or giant cells, however, are likely similar to those found in isolated lesions.

Now that we have defined and examined these characteristics in our mouse model, future experiments may satisfy critics of our “tuberless” model relatively easily by deleting

Tsc2 in only a few radial glial cells. This may be achieved most efficiently using an *hGFAP-Cre* retrovirus, which if delivered at low titer and directly to the ventricles of *Tsc2^{flox/ko}* embryos, may result in focal deletion of *Tsc2* in dividing radial glial cells. This experiment would validate whether tubers can originate from radial glial cells, as well as elucidate the contributions of a haploinsufficient environment to the localized tuber by comparing its characteristics with those of our original *Tsc2^{flox/ko}; hGFAP-Cre* mouse. Though inherent differences between the mouse and human brain, such as the lissencephalic nature of the mouse brain, may prevent actual tuber formation, results of this experiment would be very informative and perhaps more appealing to human-centric investigators.

B. Further investigation of differentiation and proliferation defects

Though the *Tsc2^{flox/ko};hGFAP-Cre* mouse does recapitulate the majority of characteristics found in TSC brain lesions, we see little evidence of the prominent defects of abnormal differentiation and proliferation. While one explanation might be that radial glial cells (RGCs) only partially contribute to the TSC brain phenotype and therefore these particular defects are not present in our model, several findings indicate otherwise. Ring heterotopias in the hippocampus reveal cells that do not stain for post-mitotic neuronal or glial markers, suggestive of a problem with differentiation into one or the other cell line. Meanwhile, embryonic analysis demonstrated aberrant populations of neural progenitor pools, indicating either aberrant differentiation into post-mitotic neurons or basal progenitor cells (BPCs), or possibly a proliferation defect in one progenitor pool. Future work might focus on characterizing these defects more thoroughly, prenatally as well as postnatally, in these mice.

For example, though we did not find aberrant proliferation in the mutant embryos using our methods as described in Chapter 3, proliferation is often the most common explanation for a greater number of cells. Other experiments must therefore be conducted to validate our initial findings that aberrant proliferation of RGCs and BPCs did not occur. While cell counts at a certain timepoint are useful, they do not distinguish between (1) lack of a proliferation defect, which we originally concluded, (2) a proliferative event followed closely by cell death, and (3) a proliferative event immediately followed by differentiation into other cell types, such as post-mitotic neurons or BPCs, which would not stain for the original cell marker and therefore not be counted. As altered progenitor pools are found by E14.5 and *Tsc2* deletion only occurs two days prior, evidence of cell death should be easy to detect around E13.5 should it exist. Immunohistochemistry with antibodies against a cell death marker such as CC3 or TUNEL staining would therefore be useful. Though we investigated proliferation using BrdU, we were unable to distinguish between RGCs and BPCs undergoing S phase based on location alone, due to the interkinetic nuclear oscillations of RGCs during synthesis towards the subventricular zone where BPCs reside (139). By double-labeling with the robust BPC marker *Tbr2* and BrdU, we will be able to determine whether more RGCs are undergoing S phase in the mutant compared to control. To identify whether cells are leaving the cell cycle to become post-mitotic neurons, we may inject BrdU, wait 24 hours for completion of a cell cycle, and double label with BrdU and Ki67, a general marker of mitosis. An increase of cells that are BrdU+/Ki67- in the mutant would suggest that cells were undergoing synthesis but then leaving the cell cycle. Together, these three experiments would clarify whether proliferation plays a role in the altered progenitor pool defect rather, or in addition to, differentiation.

Postnatal analysis must also be conducted more thoroughly to establish whether these two defects are present in our mouse model. Our experiments thus far have used markers

that identify post-mitotic neurons or glia for our cell counts, rather than markers that investigate immature cells. Crino et al (203) showed that tubers contained cells stained with nestin, an embryonic intermediate filament protein, PCNA (proliferating cell nuclear antigen), and Ki-67. These markers are expressed during embryonic development but not by mature neurons after migration, demonstrating that many cells in tubers are developmentally retarded. Repeating this experiment in our mutant mouse at P0, P5, P10, and P15 might therefore reveal defects in proliferation and differentiation better than cell counts alone.

C. Characterization of seizure phenotype

Epilepsy is one of the most common neurological manifestations of TSC, as well as one of the most devastating (204). Nonfatal seizures have been routinely observed in both TSC1 CKO mouse models throughout their lifespan (93, 94). Our mutant mice, however, do not exhibit a clinical seizure phenotype until P23, when seizures consistently end in a fatal tonic phase. It is unclear how the seizure phenotype in our mouse compares to those of the other mouse models. This question is particularly interesting given that our mouse demonstrates more severe histologic defects than either mouse. Investigation of the underlying seizure phenotype of our mutant may therefore elucidate the importance of certain TSC defects to seizure events.

Additionally, we have observed several nonfatal seizures in our mice following rapamycin treatment. As rapamycin has been shown to alleviate seizures in both TSC1 CKO mice as well, it would be interesting to see what impact our lower dosage of rapamycin might have on seizure activity. Measuring differences between seizure

phenotype in our pre, post, and pre+post rapamycin treated cohorts would also be useful in establishing which treatment might be more beneficial for this aspect.

The standard method of seizure assessment is via video-EEG recordings. In mice, this requires surgical implantation of epidural screw electrodes and a monitoring setup, which our lab is currently not equipped for. However, such an experiment would be particularly useful for our mice, as this method would not only measure seizures but also provide a background EEG. As we see low frequency of seizures in the treated mice, interictal EEG activity would provide adequate data regarding the impact of different rapamycin treatments on brain functioning, perhaps enough to determine whether prenatal treatment was more beneficial for seizure management.

As our lab is currently best suited for histological study, however, characterization of seizure activity via Timm staining may be more appropriate. The Timm stain allows visualization of zinc deposits that accumulate along mossy fibers that are produced by hilar cells of the hippocampus. While it is unclear whether mossy fiber sprouting is a cause or effect of seizures (Koyama & Ikegaya 2004, Curr Neurovasc Res), Timm staining is frequently used to assess the seizure phenotype. In fact, rapamycin has been shown to decrease mossy fiber sprouting (Buckmaster 2009, J Neurosci). Though this data was not coupled with EEG recordings, it provides support that Timm staining in our mice might provide a more practical method of assessing variation between benefits of rapamycin administered at different timepoints.

Conclusion

This dissertation describes the creation, characterization, and treatment of a novel, *Tsc2*-based radial glial model of TSC brain pathology in the mouse, *Tsc2^{flox/ko};hGFAP-Cre*,

which recapitulates many features of TSC neuropathology. Our studies with this mouse have yielded a number of significant and novel findings. We have confirmed the radial glial cell as a likely source of TSC brain pathology formation, gathered evidence to support LOH as a mode of brain lesion formation, and established a significant role for mTOR in regulating brain size, neuronal size and migration, myelination, astrogliosis, and learning and memory. This work has provided an excellent tool for the study of TSC in the brain, while characterization of this model has also greatly enhanced the understanding of the defects involved in TSC neuropathology. Using this model, additional studies may also be conducted to elucidate the currently poorly understood mechanisms by which TSC brain pathology forms. Moreover, our investigations of rapamycin treatment of this mouse model at different time points may establish precedent for novel treatment modalities in the clinic, further establishing the high impact the *Tsc2^{flox/ko};hGFAP-Cre* mouse has and will continue to have on increasing our understanding of TSC.

References

1. Gomez, M.R. (1999) History of Tuberous Sclerosis Complex. In Gomez, M.R. (ed.), *Tuberous Sclerosis Complex*. 3rd ed. Oxford University Press, New York.
2. Osborne, J.P., Fryer, A. and Webb, D. (1991) Epidemiology of tuberous sclerosis. *Ann N Y Acad Sci*, **615**, 125-7.
3. Roach, E.S., Gomez, M.R. and Northrup, H. (1998) Tuberous sclerosis complex consensus conference: revised clinical diagnostic criteria. *J Child Neurol*, **13**, 624-8.
4. Crino, P.B., Nathanson, K.L. and Henske, E.P. (2006) The tuberous sclerosis complex. *N Engl J Med*, **355**, 1345-56.
5. Jozwiak, S., Schwartz, R.A., Janniger, C.K., Michalowicz, R. and Chmielik, J. (1998) Skin lesions in children with tuberous sclerosis complex: their prevalence, natural course, and diagnostic significance. *Int J Dermatol*, **37**, 911-7.
6. Harding, C.O. and Pagon, R.A. (1990) Incidence of tuberous sclerosis in patients with cardiac rhabdomyoma. *Am J Med Genet*, **37**, 443-6.
7. Farooki, Z.Q., Ross, R.D., Paridon, S.M., Humes, R.A., Karpawich, P.P. and Pinsky, W.W. (1991) Spontaneous regression of cardiac rhabdomyoma. *Am J Cardiol*, **67**, 897-9.
8. Smythe, J.F., Dyck, J.D., Smallhorn, J.F. and Freedom, R.M. (1990) Natural history of cardiac rhabdomyoma in infancy and childhood. *Am J Cardiol*, **66**, 1247-9.
9. Chorianopoulos, D. and Stratakis, G. (2008) Lymphangioleiomyomatosis and tuberous sclerosis complex. *Lung*, **186**, 197-207.
10. Shepherd, C.W., Gomez, M.R., Lie, J.T. and Crowson, C.S. (1991) Causes of death in patients with tuberous sclerosis. *Mayo Clin Proc*, **66**, 792-6.

11. O'Hagan, A.R., Ellsworth, R., Secic, M., Rothner, A.D. and Brouhard, B.H. (1996) Renal manifestations of tuberous sclerosis complex. *Clin Pediatr (Phila)*, **35**, 483-9.
12. Orlova, K.A. and Crino, P.B. The tuberous sclerosis complex. *Ann N Y Acad Sci*, **1184**, 87-105.
13. Asato, M.R. and Hardan, A.Y. (2004) Neuropsychiatric problems in tuberous sclerosis complex. *J Child Neurol*, **19**, 241-9.
14. Ess, K.C. (2009) Tuberous sclerosis complex: everything old is new again. *J Neurodevelopmental Disord*, **1**, 141-149.
15. Napolioni, V., Moavero, R. and Curatolo, P. (2009) Recent advances in neurobiology of Tuberous Sclerosis Complex. *Brain Dev*, **31**, 104-13.
16. DiMario, F.J., Jr. (2004) Brain abnormalities in tuberous sclerosis complex. *J Child Neurol*, **19**, 650-7.
17. Zaroff, C.M., Barr, W.B., Carlson, C., LaJoie, J., Madhavan, D., Miles, D.K., Nass, R. and Devinsky, O. (2006) Mental retardation and relation to seizure and tuber burden in tuberous sclerosis complex. *Seizure*, **15**, 558-62.
18. Kossoff, E.H. Infantile spasms. *Neurologist*, **16**, 69-75.
19. Curatolo, P., Seri, S., Verdecchia, M. and Bombardieri, R. (2001) Infantile spasms in tuberous sclerosis complex. *Brain Dev*, **23**, 502-7.
20. Zaroff, C.M., Devinsky, O., Miles, D. and Barr, W.B. (2004) Cognitive and behavioral correlates of tuberous sclerosis complex. *J Child Neurol*, **19**, 847-52.
21. Crino, P.B. and Henske, E.P. (1999) New developments in the neurobiology of the tuberous sclerosis complex. *Neurology*, **53**, 1384-90.
22. Gomez, M.R. (1999) Natural History of Cerebral Tuberous Sclerosis. In Gomez, M.R. (ed.), *Tuberous Sclerosis Complex*. 3rd ed. Oxford University Press, New York

23. Northrup, H. and Au, K.-S. (1999) The TSC1 Gene: Part 1 - Gene Mapping. In Gomez, M.R. (ed.), *Tuberous Sclerosis Complex*. 3rd ed. Oxford University Press, New York.
24. van Slegtenhorst, M., de Hoogt, R., Hermans, C., Nellist, M., Janssen, B., Verhoef, S., Lindhout, D., van den Ouweland, A., Halley, D., Young, J. *et al.* (1997) Identification of the tuberous sclerosis gene TSC1 on chromosome 9q34. *Science*, **277**, 805-8.
25. Consortium, T.E.C.T.S. (1993) Identification and characterization of the tuberous sclerosis gene on chromosome 16. *Cell*, **75**, 1305-15.
26. Kwiatkowski, D.J. (1999) The TSC1 Gene: Part 2 - Identification, Mutations, and Mosaicism. In Gomez, M.R. (ed.), *Tuberous Sclerosis Complex*. 3rd ed. Oxford University Press, New York.
27. Knudson, A.G., Jr. (1971) Mutation and cancer: statistical study of retinoblastoma. *Proc Natl Acad Sci U S A*, **68**, 820-3.
28. Henske, E.P., Wessner, L.L., Golden, J., Scheithauer, B.W., Vortmeyer, A.O., Zhuang, Z., Klein-Szanto, A.J., Kwiatkowski, D.J. and Yeung, R.S. (1997) Loss of tuberin in both subependymal giant cell astrocytomas and angiomyolipomas supports a two-hit model for the pathogenesis of tuberous sclerosis tumors. *Am J Pathol*, **151**, 1639-47.
29. Knowles, M.A., Habuchi, T., Kennedy, W. and Cuthbert-Heavens, D. (2003) Mutation spectrum of the 9q34 tuberous sclerosis gene TSC1 in transitional cell carcinoma of the bladder. *Cancer Res*, **63**, 7652-6.
30. Chan, J.A., Zhang, H., Roberts, P.S., Jozwiak, S., Wieslawa, G., Lewin-Kowalik, J., Kotulska, K. and Kwiatkowski, D.J. (2004) Pathogenesis of tuberous sclerosis subependymal giant cell astrocytomas: biallelic inactivation of TSC1 or TSC2 leads to mTOR activation. *J Neuropathol Exp Neurol*, **63**, 1236-42.

31. Henske, E.P., Scheithauer, B.W., Short, M.P., Wollmann, R., Nahmias, J., Hornigold, N., van Slegtenhorst, M., Welsh, C.T. and Kwiatkowski, D.J. (1996) Allelic loss is frequent in tuberous sclerosis kidney lesions but rare in brain lesions. *Am J Hum Genet*, **59**, 400-6.
32. Niida, Y., Stemmer-Rachamimov, A.O., Logrip, M., Tapon, D., Perez, R., Kwiatkowski, D.J., Sims, K., MacCollin, M., Louis, D.N. and Ramesh, V. (2001) Survey of somatic mutations in tuberous sclerosis complex (TSC) hamartomas suggests different genetic mechanisms for pathogenesis of TSC lesions. *Am J Hum Genet*, **69**, 493-503.
33. Ma, L., Chen, Z., Erdjument-Bromage, H., Tempst, P. and Pandolfi, P.P. (2005) Phosphorylation and functional inactivation of TSC2 by Erk implications for tuberous sclerosis and cancer pathogenesis. *Cell*, **121**, 179-93.
34. Han, S., Santos, T.M., Puga, A., Roy, J., Thiele, E.A., McCollin, M., Stemmer-Rachamimov, A. and Ramesh, V. (2004) Phosphorylation of tuberin as a novel mechanism for somatic inactivation of the tuberous sclerosis complex proteins in brain lesions. *Cancer Res*, **64**, 812-6.
35. Govindarajan, B., Mizesko, M.C., Miller, M.S., Onda, H., Nunnelley, M., Casper, K., Brat, D., Cohen, C. and Arbiser, J.L. (2003) Tuberous sclerosis-associated neoplasms express activated p42/44 mitogen-activated protein (MAP) kinase, and inhibition of MAP kinase signaling results in decreased in vivo tumor growth. *Clin Cancer Res*, **9**, 3469-75.
36. Ma, L., Teruya-Feldstein, J., Bonner, P., Bernardi, R., Franz, D.N., Witte, D., Cordon-Cardo, C. and Pandolfi, P.P. (2007) Identification of S664 TSC2 phosphorylation as a marker for extracellular signal-regulated kinase mediated mTOR activation in tuberous sclerosis and human cancer. *Cancer Res*, **67**, 7106-12.
37. Sancak, O., Nellist, M., Goedbloed, M., Elfferich, P., Wouters, C., Maat-Kievit, A., Zonnenberg, B., Verhoef, S., Halley, D. and van den Ouweland, A. (2005) Mutational

- analysis of the TSC1 and TSC2 genes in a diagnostic setting: genotype--phenotype correlations and comparison of diagnostic DNA techniques in Tuberous Sclerosis Complex. *Eur J Hum Genet*, **13**, 731-41.
38. Jones, A.C., Shyamsundar, M.M., Thomas, M.W., Maynard, J., Idziaszczyk, S., Tomkins, S., Sampson, J.R. and Cheadle, J.P. (1999) Comprehensive mutation analysis of TSC1 and TSC2- and phenotypic correlations in 150 families with tuberous sclerosis. *Am J Hum Genet*, **64**, 1305-15.
 39. Jones, A.C., Daniells, C.E., Snell, R.G., Tachataki, M., Idziaszczyk, S.A., Krawczak, M., Sampson, J.R. and Cheadle, J.P. (1997) Molecular genetic and phenotypic analysis reveals differences between TSC1 and TSC2 associated familial and sporadic tuberous sclerosis. *Hum Mol Genet*, **6**, 2155-61.
 40. van Slegtenhorst, M., Verhoef, S., Tempelaars, A., Bakker, L., Wang, Q., Wessels, M., Bakker, R., Nellist, M., Lindhout, D., Halley, D. *et al.* (1999) Mutational spectrum of the TSC1 gene in a cohort of 225 tuberous sclerosis complex patients: no evidence for genotype-phenotype correlation. *J Med Genet*, **36**, 285-9.
 41. Dabora, S.L., Jozwiak, S., Franz, D.N., Roberts, P.S., Nieto, A., Chung, J., Choy, Y.S., Reeve, M.P., Thiele, E., Egelhoff, J.C. *et al.* (2001) Mutational analysis in a cohort of 224 tuberous sclerosis patients indicates increased severity of TSC2, compared with TSC1, disease in multiple organs. *Am J Hum Genet*, **68**, 64-80.
 42. Rosner, M., Hanneder, M., Siegel, N., Valli, A. and Hengstschlager, M. (2008) The tuberous sclerosis gene products hamartin and tuberin are multifunctional proteins with a wide spectrum of interacting partners. *Mutat Res*, **658**, 234-46.
 43. Young, J. and Povey, S. (1998) The genetic basis of tuberous sclerosis. *Mol Med Today*, **4**, 313-9.

44. van Slegtenhorst, M., Nellist, M., Nagelkerken, B., Cheadle, J., Snell, R., van den Ouweland, A., Reuser, A., Sampson, J., Halley, D. and van der Sluijs, P. (1998) Interaction between hamartin and tuberlin, the TSC1 and TSC2 gene products. *Hum Mol Genet*, **7**, 1053-7.
45. Plank, T.L., Yeung, R.S. and Henske, E.P. (1998) Hamartin, the product of the tuberous sclerosis 1 (TSC1) gene, interacts with tuberlin and appears to be localized to cytoplasmic vesicles. *Cancer Res*, **58**, 4766-70.
46. Benvenuto, G., Li, S., Brown, S.J., Braverman, R., Vass, W.C., Cheadle, J.P., Halley, D.J., Sampson, J.R., Wienecke, R. and DeClue, J.E. (2000) The tuberous sclerosis-1 (TSC1) gene product hamartin suppresses cell growth and augments the expression of the TSC2 product tuberlin by inhibiting its ubiquitination. *Oncogene*, **19**, 6306-16.
47. Chong-Kopera, H., Inoki, K., Li, Y., Zhu, T., Garcia-Gonzalo, F.R., Rosa, J.L. and Guan, K.L. (2006) TSC1 stabilizes TSC2 by inhibiting the interaction between TSC2 and the HERC1 ubiquitin ligase. *J Biol Chem*, **281**, 8313-6.
48. Tee, A.R., Manning, B.D., Roux, P.P., Cantley, L.C. and Blenis, J. (2003) Tuberous sclerosis complex gene products, Tuberlin and Hamartin, control mTOR signaling by acting as a GTPase-activating protein complex toward Rheb. *Curr Biol*, **13**, 1259-68.
49. Inoki, K., Li, Y., Xu, T. and Guan, K.L. (2003) Rheb GTPase is a direct target of TSC2 GAP activity and regulates mTOR signaling. *Genes Dev*, **17**, 1829-34.
50. Wullschleger, S., Loewith, R. and Hall, M.N. (2006) TOR signaling in growth and metabolism. *Cell*, **124**, 471-84.
51. Bai, X., Ma, D., Liu, A., Shen, X., Wang, Q.J., Liu, Y. and Jiang, Y. (2007) Rheb activates mTOR by antagonizing its endogenous inhibitor, FKBP38. *Science*, **318**, 977-80.

52. Gao, X., Zhang, Y., Arrazola, P., Hino, O., Kobayashi, T., Yeung, R.S., Ru, B. and Pan, D. (2002) Tsc tumour suppressor proteins antagonize amino-acid-TOR signalling. *Nat Cell Biol*, **4**, 699-704.
53. Smith, E.M., Finn, S.G., Tee, A.R., Browne, G.J. and Proud, C.G. (2005) The tuberous sclerosis protein TSC2 is not required for the regulation of the mammalian target of rapamycin by amino acids and certain cellular stresses. *J Biol Chem*, **280**, 18717-27.
54. Guertin, D.A. and Sabatini, D.M. (2007) Defining the role of mTOR in cancer. *Cancer Cell*, **12**, 9-22.
55. Manning, B.D. and Cantley, L.C. (2003) United at last: the tuberous sclerosis complex gene products connect the phosphoinositide 3-kinase/Akt pathway to mammalian target of rapamycin (mTOR) signalling. *Biochem Soc Trans*, **31**, 573-8.
56. Inoki, K., Li, Y., Zhu, T., Wu, J. and Guan, K.L. (2002) TSC2 is phosphorylated and inhibited by Akt and suppresses mTOR signalling. *Nat Cell Biol*, **4**, 648-57.
57. Huang, J. and Manning, B.D. (2008) The TSC1-TSC2 complex: a molecular switchboard controlling cell growth. *Biochem J*, **412**, 179-90.
58. Ma, W. and Quirion, R. (2005) The ERK/MAPK pathway, as a target for the treatment of neuropathic pain. *Expert Opin Ther Targets*, **9**, 699-713.
59. Shaw, R.J., Bardeesy, N., Manning, B.D., Lopez, L., Kosmatka, M., DePinho, R.A. and Cantley, L.C. (2004) The LKB1 tumor suppressor negatively regulates mTOR signaling. *Cancer Cell*, **6**, 91-9.
60. Laderoute, K.R., Amin, K., Calaoagan, J.M., Knapp, M., Le, T., Orduna, J., Foretz, M. and Viollet, B. (2006) 5'-AMP-activated protein kinase (AMPK) is induced by low-oxygen and glucose deprivation conditions found in solid-tumor microenvironments. *Mol Cell Biol*, **26**, 5336-47.

61. Inoki, K., Zhu, T. and Guan, K.L. (2003) TSC2 mediates cellular energy response to control cell growth and survival. *Cell*, **115**, 577-90.
62. Liu, L., Cash, T.P., Jones, R.G., Keith, B., Thompson, C.B. and Simon, M.C. (2006) Hypoxia-induced energy stress regulates mRNA translation and cell growth. *Mol Cell*, **21**, 521-31.
63. Reiling, J.H. and Hafen, E. (2004) The hypoxia-induced paralogs Scylla and Charybdis inhibit growth by down-regulating S6K activity upstream of TSC in *Drosophila*. *Genes Dev*, **18**, 2879-92.
64. DeYoung, M.P., Horak, P., Sofer, A., Sgroi, D. and Ellisen, L.W. (2008) Hypoxia regulates TSC1/2-mTOR signaling and tumor suppression through REDD1-mediated 14-3-3 shuttling. *Genes Dev*, **22**, 239-51.
65. Sarbassov, D.D., Ali, S.M. and Sabatini, D.M. (2005) Growing roles for the mTOR pathway. *Curr Opin Cell Biol*, **17**, 596-603.
66. Wang, L., Rhodes, C.J. and Lawrence, J.C., Jr. (2006) Activation of mammalian target of rapamycin (mTOR) by insulin is associated with stimulation of 4EBP1 binding to dimeric mTOR complex 1. *J Biol Chem*, **281**, 24293-303.
67. Thomas, B.J., Gunning, D.A., Cho, J. and Zipursky, L. (1994) Cell cycle progression in the developing *Drosophila* eye: roughex encodes a novel protein required for the establishment of G1. *Cell*, **77**, 1003-14.
68. Ito, N. and Rubin, G.M. (1999) gigas, a *Drosophila* homolog of tuberous sclerosis gene product-2, regulates the cell cycle. *Cell*, **96**, 529-39.
69. Potter, C.J., Huang, H. and Xu, T. (2001) *Drosophila* Tsc1 functions with Tsc2 to antagonize insulin signaling in regulating cell growth, cell proliferation, and organ size. *Cell*, **105**, 357-68.

70. Gao, X. and Pan, D. (2001) TSC1 and TSC2 tumor suppressors antagonize insulin signaling in cell growth. *Genes Dev*, **15**, 1383-92.
71. Kwiatkowski, D.J., Zhang, H., Bandura, J.L., Heiberger, K.M., Glogauer, M., el-Hashemite, N. and Onda, H. (2002) A mouse model of TSC1 reveals sex-dependent lethality from liver hemangiomas, and up-regulation of p70S6 kinase activity in Tsc1 null cells. *Hum Mol Genet*, **11**, 525-34.
72. Onda, H., Lueck, A., Marks, P.W., Warren, H.B. and Kwiatkowski, D.J. (1999) Tsc2(+/-) mice develop tumors in multiple sites that express gelsolin and are influenced by genetic background. *J Clin Invest*, **104**, 687-95.
73. Kobayashi, T., Minowa, O., Kuno, J., Mitani, H., Hino, O. and Noda, T. (1999) Renal carcinogenesis, hepatic hemangiomatosis, and embryonic lethality caused by a germ-line Tsc2 mutation in mice. *Cancer Res*, **59**, 1206-11.
74. Uhlmann, E.J., Apicelli, A.J., Baldwin, R.L., Burke, S.P., Bajenaru, M.L., Onda, H., Kwiatkowski, D. and Gutmann, D.H. (2002) Heterozygosity for the tuberous sclerosis complex (TSC) gene products results in increased astrocyte numbers and decreased p27-Kip1 expression in TSC2+/- cells. *Oncogene*, **21**, 4050-9.
75. Uhlmann, E.J., Wong, M., Baldwin, R.L., Bajenaru, M.L., Onda, H., Kwiatkowski, D.J., Yamada, K. and Gutmann, D.H. (2002) Astrocyte-specific TSC1 conditional knockout mice exhibit abnormal neuronal organization and seizures. *Ann Neurol*, **52**, 285-96.
76. Bajenaru, M.L., Zhu, Y., Hedrick, N.M., Donahoe, J., Parada, L.F. and Gutmann, D.H. (2002) Astrocyte-specific inactivation of the neurofibromatosis 1 gene (NF1) is insufficient for astrocytoma formation. *Mol Cell Biol*, **22**, 5100-13.
77. Meikle, L., Talos, D.M., Onda, H., Pollizzi, K., Rotenberg, A., Sahin, M., Jensen, F.E. and Kwiatkowski, D.J. (2007) A mouse model of tuberous sclerosis: neuronal loss of Tsc1 causes

- dysplastic and ectopic neurons, reduced myelination, seizure activity, and limited survival. *J Neurosci*, **27**, 5546-58.
78. Park, S.H., Pepkowitz, S.H., Kerfoot, C., De Rosa, M.J., Poukens, V., Wienecke, R., DeClue, J.E. and Vinters, H.V. (1997) Tuberous sclerosis in a 20-week gestation fetus: immunohistochemical study. *Acta Neuropathol*, **94**, 180-6.
 79. Wei, J., Li, P., Chiriboga, L., Mizuguchi, M., Yee, H., Miller, D.C. and Greco, M.A. (2002) Tuberous sclerosis in a 19-week fetus: immunohistochemical and molecular study of hamartin and tuberin. *Pediatr Dev Pathol*, **5**, 448-64.
 80. Ess, K.C., Kamp, C.A., Tu, B.P. and Gutmann, D.H. (2005) Developmental origin of subependymal giant cell astrocytoma in tuberous sclerosis complex. *Neurology*, **64**, 1446-9.
 81. Ess, K.C., Uhlmann, E.J., Li, W., Li, H., Declue, J.E., Crino, P.B. and Gutmann, D.H. (2004) Expression profiling in tuberous sclerosis complex (TSC) knockout mouse astrocytes to characterize human TSC brain pathology. *Glia*, **46**, 28-40.
 82. Noctor, S.C., Flint, A.C., Weissman, T.A., Dammerman, R.S. and Kriegstein, A.R. (2001) Neurons derived from radial glial cells establish radial units in neocortex. *Nature*, **409**, 714-20.
 83. Zhuo, L., Theis, M., Alvarez-Maya, I., Brenner, M., Willecke, K. and Messing, A. (2001) hGFAP-cre transgenic mice for manipulation of glial and neuronal function in vivo. *Genesis*, **31**, 85-94.
 84. Malatesta, P., Hack, M.A., Hartfuss, E., Kettenmann, H., Klinkert, W., Kirchhoff, F. and Gotz, M. (2003) Neuronal or glial progeny: regional differences in radial glia fate. *Neuron*, **37**, 751-64.

85. Brown, E.J., Albers, M.W., Shin, T.B., Ichikawa, K., Keith, C.T., Lane, W.S. and Schreiber, S.L. (1994) A mammalian protein targeted by G1-arresting rapamycin-receptor complex. *Nature*, **369**, 756-8.
86. Chiu, M.I., Katz, H. and Berlin, V. (1994) RAPT1, a mammalian homolog of yeast Tor, interacts with the FKBP12/rapamycin complex. *Proc Natl Acad Sci U S A*, **91**, 12574-8.
87. Chang, J.Y., Sehgal, S.N. and Bansbach, C.C. (1991) FK506 and rapamycin: novel pharmacological probes of the immune response. *Trends Pharmacol Sci*, **12**, 218-23.
88. Sabatini, D.M., Erdjument-Bromage, H., Lui, M., Tempst, P. and Snyder, S.H. (1994) RAFT1: a mammalian protein that binds to FKBP12 in a rapamycin-dependent fashion and is homologous to yeast TORs. *Cell*, **78**, 35-43.
89. Chen, J., Zheng, X.F., Brown, E.J. and Schreiber, S.L. (1995) Identification of an 11-kDa FKBP12-rapamycin-binding domain within the 289-kDa FKBP12-rapamycin-associated protein and characterization of a critical serine residue. *Proc Natl Acad Sci U S A*, **92**, 4947-51.
90. Kobayashi, T., Hirayama, Y., Kobayashi, E., Kubo, Y. and Hino, O. (1995) A germline insertion in the tuberous sclerosis (Tsc2) gene gives rise to the Eker rat model of dominantly inherited cancer. *Nat Genet*, **9**, 70-4.
91. Kenerson, H.L., Aicher, L.D., True, L.D. and Yeung, R.S. (2002) Activated mammalian target of rapamycin pathway in the pathogenesis of tuberous sclerosis complex renal tumors. *Cancer Res*, **62**, 5645-50.
92. Kenerson, H., Dundon, T.A. and Yeung, R.S. (2005) Effects of rapamycin in the Eker rat model of tuberous sclerosis complex. *Pediatr Res*, **57**, 67-75.
93. Zeng, L.H., Xu, L., Gutmann, D.H. and Wong, M. (2008) Rapamycin prevents epilepsy in a mouse model of tuberous sclerosis complex. *Ann Neurol*, **63**, 444-53.

94. Meikle, L., Pollizzi, K., Egnor, A., Kramvis, I., Lane, H., Sahin, M. and Kwiatkowski, D.J. (2008) Response of a neuronal model of tuberous sclerosis to mammalian target of rapamycin (mTOR) inhibitors: effects on mTORC1 and Akt signaling lead to improved survival and function. *J Neurosci*, **28**, 5422-32.
95. Huang, J., Dibble, C.C., Matsuzaki, M. and Manning, B.D. (2008) The TSC1-TSC2 complex is required for proper activation of mTOR complex 2. *Mol Cell Biol*, **28**, 4104-15.
96. Jacinto, E., Loewith, R., Schmidt, A., Lin, S., Ruegg, M.A., Hall, A. and Hall, M.N. (2004) Mammalian TOR complex 2 controls the actin cytoskeleton and is rapamycin insensitive. *Nat Cell Biol*, **6**, 1122-8.
97. Arimura, N. and Kaibuchi, K. (2005) Key regulators in neuronal polarity. *Neuron*, **48**, 881-4.
98. Yoshimura, T., Arimura, N., Kawano, Y., Kawabata, S., Wang, S. and Kaibuchi, K. (2006) Ras regulates neuronal polarity via the PI3-kinase/Akt/GSK-3beta/CRMP-2 pathway. *Biochem Biophys Res Commun*, **340**, 62-8.
99. Harrington, L.S., Findlay, G.M., Gray, A., Tolkacheva, T., Wigfield, S., Rebholz, H., Barnett, J., Leslie, N.R., Cheng, S., Shepherd, P.R. *et al.* (2004) The TSC1-2 tumor suppressor controls insulin-PI3K signaling via regulation of IRS proteins. *J Cell Biol*, **166**, 213-23.
100. Sarbassov, D.D., Ali, S.M., Sengupta, S., Sheen, J.H., Hsu, P.P., Bagley, A.F., Markhard, A.L. and Sabatini, D.M. (2006) Prolonged rapamycin treatment inhibits mTORC2 assembly and Akt/PKB. *Mol Cell*, **22**, 159-68.
101. Yeung, R.S., Katsetos, C.D. and Klein-Szanto, A. (1997) Subependymal astrocytic hamartomas in the Eker rat model of tuberous sclerosis. *Am J Pathol*, **151**, 1477-86.
102. Onda, H., Crino, P.B., Zhang, H., Murphey, R.D., Rastelli, L., Gould Rothberg, B.E. and Kwiatkowski, D.J. (2002) Tsc2 null murine neuroepithelial cells are a model for human tuber giant cells, and show activation of an mTOR pathway. *Mol Cell Neurosci*, **21**, 561-74.

103. Hernandez, O., Way, S., McKenna, J., 3rd and Gambello, M.J. (2007) Generation of a conditional disruption of the Tsc2 gene. *Genesis*, **45**, 101-6.
104. Rodriguez, C.I., Buchholz, F., Galloway, J., Sequerra, R., Kasper, J., Ayala, R., Stewart, A.F. and Dymecki, S.M. (2000) High-efficiency deleter mice show that FLPe is an alternative to Cre-loxP. *Nat Genet*, **25**, 139-40.
105. Meyers, E.N., Lewandoski, M. and Martin, G.R. (1998) An Fgf8 mutant allelic series generated by Cre- and Flp-mediated recombination. *Nat Genet*, **18**, 136-41.
106. Mohn, A.R., Gainetdinov, R.R., Caron, M.G. and Koller, B.H. (1999) Mice with reduced NMDA receptor expression display behaviors related to schizophrenia. *Cell*, **98**, 427-36.
107. Partanen, J., Schwartz, L. and Rossant, J. (1998) Opposite phenotypes of hypomorphic and Y766 phosphorylation site mutations reveal a function for Fgfr1 in anteroposterior patterning of mouse embryos. *Genes Dev*, **12**, 2332-44.
108. White, J.K., Auerbach, W., Duyao, M.P., Vonsattel, J.P., Gusella, J.F., Joyner, A.L. and MacDonald, M.E. (1997) Huntingtin is required for neurogenesis and is not impaired by the Huntington's disease CAG expansion. *Nat Genet*, **17**, 404-10.
109. Jansen, A.C., Sancak, O., D'Agostino, M.D., Badhwar, A., Roberts, P., Gobbi, G., Wilkinson, R., Melanson, D., Tampieri, D., Koeneke, R. *et al.* (2006) Unusually mild tuberous sclerosis phenotype is associated with TSC2 R905Q mutation. *Ann Neurol*, **60**, 528-39.
110. Khare, L., Strizheva, G.D., Bailey, J.N., Au, K.S., Northrup, H., Smith, M., Smalley, S.L. and Henske, E.P. (2001) A novel missense mutation in the GTPase activating protein homology region of TSC2 in two large families with tuberous sclerosis complex. *J Med Genet*, **38**, 347-9.

111. O'Connor, S.E., Kwiatkowski, D.J., Roberts, P.S., Wollmann, R.L. and Huttenlocher, P.R. (2003) A family with seizures and minor features of tuberous sclerosis and a novel TSC2 mutation. *Neurology*, **61**, 409-12.
112. Coevoets, R., Arican, S., Hoogeveen-Westerveld, M., Simons, E., van den Ouweland, A., Halley, D. and Nellist, M. (2009) A reliable cell-based assay for testing unclassified TSC2 gene variants. *Eur J Hum Genet*, **17**, 301-10.
113. Pollizzi, K., Malinowska-Kolodziej, I., Doughty, C., Betz, C., Ma, J., Goto, J. and Kwiatkowski, D.J. (2009) A hypomorphic allele of Tsc2 highlights the role of TSC1/TSC2 in signaling to AKT and models mild human TSC2 alleles. *Hum Mol Genet*, **18**, 2378-87.
114. Rakic, P. (1972) Mode of cell migration to the superficial layers of fetal monkey neocortex. *J Comp Neurol*, **145**, 61-83.
115. Way, S.W., McKenna, J., 3rd, Mietzsch, U., Reith, R.M., Wu, H.C. and Gambello, M.J. (2009) Loss of Tsc2 in radial glia models the brain pathology of tuberous sclerosis complex in the mouse. *Hum Mol Genet*, **18**, 1252-65.
116. Green, A.J., Smith, M. and Yates, J.R. (1994) Loss of heterozygosity on chromosome 16p13.3 in hamartomas from tuberous sclerosis patients. *Nat Genet*, **6**, 193-6.
117. Boer, K., Jansen, F., Nellist, M., Redeker, S., van den Ouweland, A.M., Spliet, W.G., van Nieuwenhuizen, O., Troost, D., Crino, P.B. and Aronica, E. (2008) Inflammatory processes in cortical tubers and subependymal giant cell tumors of tuberous sclerosis complex. *Epilepsy Res*, **78**, 7-21.
118. Englund, C., Fink, A., Lau, C., Pham, D., Daza, R.A., Bulfone, A., Kowalczyk, T. and Hevner, R.F. (2005) Pax6, Tbr2, and Tbr1 are expressed sequentially by radial glia, intermediate progenitor cells, and postmitotic neurons in developing neocortex. *J Neurosci*, **25**, 247-51.

119. Sosunov, A.A., Wu, X., Weiner, H.L., Mikell, C.B., Goodman, R.R., Crino, P.D. and McKhann, G.M., 2nd (2008) Tuberous sclerosis: a primary pathology of astrocytes? *Epilepsia*, **49 Suppl 2**, 53-62.
120. Crino, P.B. (2004) Molecular pathogenesis of tuber formation in tuberous sclerosis complex. *J Child Neurol*, **19**, 716-25.
121. Nieto, M., Monuki, E.S., Tang, H., Imitola, J., Haubst, N., Khoury, S.J., Cunningham, J., Gotz, M. and Walsh, C.A. (2004) Expression of Cux-1 and Cux-2 in the subventricular zone and upper layers II-IV of the cerebral cortex. *J Comp Neurol*, **479**, 168-80.
122. Frotscher, M., Chai, X., Bock, H.H., Haas, C.A., Forster, E. and Zhao, S. (2009) Role of Reelin in the development and maintenance of cortical lamination. *J Neural Transm*, **116**, 1451-5.
123. Wojtowicz, J.M. and Kee, N. (2006) BrdU assay for neurogenesis in rodents. *Nat Protoc*, **1**, 1399-405.
124. Hisaoka, T., Nakamura, Y., Senba, E. and Morikawa, Y. The forkhead transcription factors, Foxp1 and Foxp2, identify different subpopulations of projection neurons in the mouse cerebral cortex. *Neuroscience*, **166**, 551-63.
125. Ma, X.M. and Blenis, J. (2009) Molecular mechanisms of mTOR-mediated translational control. *Nat Rev Mol Cell Biol*, **10**, 307-18.
126. Noctor, S.C., Martinez-Cerdeno, V., Ivic, L. and Kriegstein, A.R. (2004) Cortical neurons arise in symmetric and asymmetric division zones and migrate through specific phases. *Nat Neurosci*, **7**, 136-44.
127. Zhang, D., Hu, X., Qian, L., O'Callaghan, J.P. and Hong, J.S. Astrogliosis in CNS pathologies: is there a role for microglia? *Mol Neurobiol*, **41**, 232-41.

128. Boer, K., Troost, D., Jansen, F., Nellist, M., van den Ouweland, A.M., Geurts, J.J., Spliet, W.G., Crino, P. and Aronica, E. (2008) Clinicopathological and immunohistochemical findings in an autopsy case of tuberous sclerosis complex. *Neuropathology*, **28**, 577-90.
129. Griffiths, P.D., Bolton, P. and Verity, C. (1998) White matter abnormalities in tuberous sclerosis complex. *Acta Radiol*, **39**, 482-6.
130. Makki, M.I., Chugani, D.C., Janisse, J. and Chugani, H.T. (2007) Characteristics of abnormal diffusivity in normal-appearing white matter investigated with diffusion tensor MR imaging in tuberous sclerosis complex. *AJNR Am J Neuroradiol*, **28**, 1662-7.
131. Mason, J.L., Xuan, S., Dragatsis, I., Efstratiadis, A. and Goldman, J.E. (2003) Insulin-like growth factor (IGF) signaling through type 1 IGF receptor plays an important role in remyelination. *J Neurosci*, **23**, 7710-8.
132. Narayanan, S.P., Flores, A.I., Wang, F. and Macklin, W.B. (2009) Akt signals through the mammalian target of rapamycin pathway to regulate CNS myelination. *J Neurosci*, **29**, 6860-70.
133. Ronnett, G.V., Hester, L.D., Nye, J.S., Connors, K. and Snyder, S.H. (1990) Human cortical neuronal cell line: establishment from a patient with unilateral megalencephaly. *Science*, **248**, 603-5.
134. Cooke, R.J. Catch-up growth: implications for the preterm and term infant. *Eur J Clin Nutr*, **64 Suppl 1**, S8-S10.
135. Maya-Monteiro, C.M. and Bozza, P.T. (2008) Leptin and mTOR: partners in metabolism and inflammation. *Cell Cycle*, **7**, 1713-7.
136. Metin, C., Vallee, R.B., Rakic, P. and Bhide, P.G. (2008) Modes and mishaps of neuronal migration in the mammalian brain. *J Neurosci*, **28**, 11746-52.

137. Larson, Y., Liu, J., Stevens, P.D., Li, X., Li, J., Evers, B.M. and Gao, T. Tuberous sclerosis complex 2 (TSC2) regulates cell migration and polarity through activation of CDC42 and RAC1. *J Biol Chem*, **285**, 24987-98.
138. Tsai, J.W., Chen, Y., Kriegstein, A.R. and Vallee, R.B. (2005) LIS1 RNA interference blocks neural stem cell division, morphogenesis, and motility at multiple stages. *J Cell Biol*, **170**, 935-45.
139. Taverna, E. and Huttner, W.B. Neural progenitor nuclei IN motion. *Neuron*, **67**, 906-14.
140. Vallee, R.B. and Tsai, J.W. (2006) The cellular roles of the lissencephaly gene LIS1, and what they tell us about brain development. *Genes Dev*, **20**, 1384-93.
141. Gupta, A., Tsai, L.H. and Wynshaw-Boris, A. (2002) Life is a journey: a genetic look at neocortical development. *Nat Rev Genet*, **3**, 342-55.
142. Sofroniew, M.V. (2009) Molecular dissection of reactive astrogliosis and glial scar formation. *Trends Neurosci*, **32**, 638-47.
143. Deng, W. Neurobiology of injury to the developing brain. *Nat Rev Neurol*, **6**, 328-36.
144. Rogawski, M.A. (2005) Astrocytes get in the act in epilepsy. *Nat Med*, **11**, 919-20.
145. Tian, G.F., Azmi, H., Takano, T., Xu, Q., Peng, W., Lin, J., Oberheim, N., Lou, N., Wang, X., Zielke, H.R. *et al.* (2005) An astrocytic basis of epilepsy. *Nat Med*, **11**, 973-81.
146. Franz, D.N., Leonard, J., Tudor, C., Chuck, G., Care, M., Sethuraman, G., Dinopoulos, A., Thomas, G. and Crone, K.R. (2006) Rapamycin causes regression of astrocytomas in tuberous sclerosis complex. *Ann Neurol*, **59**, 490-8.
147. Swiech, L., Perycz, M., Malik, A. and Jaworski, J. (2008) Role of mTOR in physiology and pathology of the nervous system. *Biochim Biophys Acta*, **1784**, 116-32.

148. Huang, S., Liu, L.N., Hosoi, H., Dilling, M.B., Shikata, T. and Houghton, P.J. (2001) p53/p21(CIP1) cooperate in enforcing rapamycin-induced G(1) arrest and determine the cellular response to rapamycin. *Cancer Res*, **61**, 3373-81.
149. Thimmaiah, K.N., Easton, J., Huang, S., Veverka, K.A., Germain, G.S., Harwood, F.C. and Houghton, P.J. (2003) Insulin-like growth factor I-mediated protection from rapamycin-induced apoptosis is independent of Ras-Erk1-Erk2 and phosphatidylinositol 3'-kinase-Akt signaling pathways. *Cancer Res*, **63**, 364-74.
150. Lieberthal, W., Fuhro, R., Andry, C.C., Rennke, H., Abernathy, V.E., Koh, J.S., Valeri, R. and Levine, J.S. (2001) Rapamycin impairs recovery from acute renal failure: role of cell-cycle arrest and apoptosis of tubular cells. *Am J Physiol Renal Physiol*, **281**, F693-706.
151. Hernandez-Negrete, I., Carretero-Ortega, J., Rosenfeldt, H., Hernandez-Garcia, R., Calderon-Salinas, J.V., Reyes-Cruz, G., Gutkind, J.S. and Vazquez-Prado, J. (2007) P-Rex1 links mammalian target of rapamycin signaling to Rac activation and cell migration. *J Biol Chem*, **282**, 23708-15.
152. Prather, P. and de Vries, P.J. (2004) Behavioral and cognitive aspects of tuberous sclerosis complex. *J Child Neurol*, **19**, 666-74.
153. Joinson, C., O'Callaghan, F.J., Osborne, J.P., Martyn, C., Harris, T. and Bolton, P.F. (2003) Learning disability and epilepsy in an epidemiological sample of individuals with tuberous sclerosis complex. *Psychol Med*, **33**, 335-44.
154. Harrison, J.E., O'Callaghan, F.J., Hancock, E., Osborne, J.P. and Bolton, P.F. (1999) Cognitive deficits in normally intelligent patients with tuberous sclerosis. *Am J Med Genet*, **88**, 642-6.
155. Ridler, K., Suckling, J., Higgins, N.J., de Vries, P.J., Stephenson, C.M., Bolton, P.F. and Bullmore, E.T. (2007) Neuroanatomical correlates of memory deficits in tuberous sclerosis complex. *Cereb Cortex*, **17**, 261-71.

156. Goorden, S.M., van Woerden, G.M., van der Weerd, L., Cheadle, J.P. and Elgersma, Y. (2007) Cognitive deficits in Tsc1+/- mice in the absence of cerebral lesions and seizures. *Ann Neurol*, **62**, 648-55.
157. Ehninger, D., Han, S., Shilyansky, C., Zhou, Y., Li, W., Kwiatkowski, D.J., Ramesh, V. and Silva, A.J. (2008) Reversal of learning deficits in a Tsc2+/- mouse model of tuberous sclerosis. *Nat Med*, **14**, 843-8.
158. Costa-Mattioli, M., Sossin, W.S., Klann, E. and Sonenberg, N. (2009) Translational control of long-lasting synaptic plasticity and memory. *Neuron*, **61**, 10-26.
159. Hou, L. and Klann, E. (2004) Activation of the phosphoinositide 3-kinase-Akt-mammalian target of rapamycin signaling pathway is required for metabotropic glutamate receptor-dependent long-term depression. *J Neurosci*, **24**, 6352-61.
160. Tang, S.J., Reis, G., Kang, H., Gingras, A.C., Sonenberg, N. and Schuman, E.M. (2002) A rapamycin-sensitive signaling pathway contributes to long-term synaptic plasticity in the hippocampus. *Proc Natl Acad Sci U S A*, **99**, 467-72.
161. Dash, P.K., Orsi, S.A. and Moore, A.N. (2006) Spatial memory formation and memory-enhancing effect of glucose involves activation of the tuberous sclerosis complex-Mammalian target of rapamycin pathway. *J Neurosci*, **26**, 8048-56.
162. Crawley, J.N. and Paylor, R. (1997) A proposed test battery and constellations of specific behavioral paradigms to investigate the behavioral phenotypes of transgenic and knockout mice. *Horm Behav*, **31**, 197-211.
163. Walf, A.A. and Frye, C.A. (2007) The use of the elevated plus maze as an assay of anxiety-related behavior in rodents. *Nat Protoc*, **2**, 322-8.

164. Frankland, P.W., Cestari, V., Filipkowski, R.K., McDonald, R.J. and Silva, A.J. (1998) The dorsal hippocampus is essential for context discrimination but not for contextual conditioning. *Behav Neurosci*, **112**, 863-74.
165. Bevins, R.A. and Besheer, J. (2006) Object recognition in rats and mice: a one-trial non-matching-to-sample learning task to study 'recognition memory'. *Nat Protoc*, **1**, 1306-11.
166. Brandeis, R., Brandys, Y. and Yehuda, S. (1989) The use of the Morris Water Maze in the study of memory and learning. *Int J Neurosci*, **48**, 29-69.
167. Wehner, J.M. and Radcliffe, R.A. (2004) Cued and contextual fear conditioning in mice. *Curr Protoc Neurosci*, **Chapter 8**, Unit 8 5C.
168. Pang, P.T. and Lu, B. (2004) Regulation of late-phase LTP and long-term memory in normal and aging hippocampus: role of secreted proteins tPA and BDNF. *Ageing Res Rev*, **3**, 407-30.
169. McConnell, S.K. and Kaznowski, C.E. (1991) Cell cycle dependence of laminar determination in developing neocortex. *Science*, **254**, 282-5.
170. Fingar, D.C., Salama, S., Tsou, C., Harlow, E. and Blenis, J. (2002) Mammalian cell size is controlled by mTOR and its downstream targets S6K1 and 4EBP1/eIF4E. *Genes Dev*, **16**, 1472-87.
171. Fingar, D.C., Richardson, C.J., Tee, A.R., Cheatham, L., Tsou, C. and Blenis, J. (2004) mTOR controls cell cycle progression through its cell growth effectors S6K1 and 4E-BP1/eukaryotic translation initiation factor 4E. *Mol Cell Biol*, **24**, 200-16.
172. Guertin, D.A., Stevens, D.M., Thoreen, C.C., Burds, A.A., Kalaany, N.Y., Moffat, J., Brown, M., Fitzgerald, K.J. and Sabatini, D.M. (2006) Ablation in mice of the mTORC components raptor, rictor, or mLST8 reveals that mTORC2 is required for signaling to Akt-FOXO and PKCalpha, but not S6K1. *Dev Cell*, **11**, 859-71.

173. Jacinto, E., Facchinetti, V., Liu, D., Soto, N., Wei, S., Jung, S.Y., Huang, Q., Qin, J. and Su, B. (2006) SIN1/MIP1 maintains rictor-mTOR complex integrity and regulates Akt phosphorylation and substrate specificity. *Cell*, **127**, 125-37.
174. Rosner, M., Siegel, N., Valli, A., Fuchs, C. and Hengstschlager, M. mTOR phosphorylated at S2448 binds to raptor and rictor. *Amino Acids*, **38**, 223-8.
175. Moss, S.C., Lightell, D.J., Jr., Marx, S.O., Marks, A.R. and Woods, T.C. Rapamycin regulates endothelial cell migration through regulation of the cyclin-dependent kinase inhibitor p27Kip1. *J Biol Chem*, **285**, 11991-7.
176. Sherr, C.J. and Roberts, J.M. (1999) CDK inhibitors: positive and negative regulators of G1-phase progression. *Genes Dev*, **13**, 1501-12.
177. Woods, T.C. Regulation of cell migration by mTOR is mediated through changes in p27(Kip1) phosphorylation. *Cell Cycle*, **9**.
178. Goto, T., Mitsuhashi, T. and Takahashi, T. (2004) Altered patterns of neuron production in the p27 knockout mouse. *Dev Neurosci*, **26**, 208-17.
179. Ridley, A.J. and Hall, A. (1992) The small GTP-binding protein rho regulates the assembly of focal adhesions and actin stress fibers in response to growth factors. *Cell*, **70**, 389-99.
180. Heasman, S.J. and Ridley, A.J. (2008) Mammalian Rho GTPases: new insights into their functions from in vivo studies. *Nat Rev Mol Cell Biol*, **9**, 690-701.
181. Koh, C.G. (2006) Rho GTPases and their regulators in neuronal functions and development. *Neurosignals*, **15**, 228-37.
182. Besson, A., Gurian-West, M., Schmidt, A., Hall, A. and Roberts, J.M. (2004) p27Kip1 modulates cell migration through the regulation of RhoA activation. *Genes Dev*, **18**, 862-76.

183. Schmidt, S., Diriong, S., Mery, J., Fabbrizio, E. and Debant, A. (2002) Identification of the first Rho-GEF inhibitor, TRIPalpha, which targets the RhoA-specific GEF domain of Trio. *FEBS Lett*, **523**, 35-42.
184. Liu, L., Luo, Y., Chen, L., Shen, T., Xu, B., Chen, W., Zhou, H., Han, X. and Huang, S. Rapamycin inhibits cytoskeleton reorganization and cell motility by suppressing RhoA expression and activity. *J Biol Chem*, **285**, 38362-73.
185. Klambt, C. (2009) Modes and regulation of glial migration in vertebrates and invertebrates. *Nat Rev Neurosci*, **10**, 769-79.
186. Tsai, H.H., Macklin, W.B. and Miller, R.H. (2009) Distinct modes of migration position oligodendrocyte precursors for localized cell division in the developing spinal cord. *J Neurosci Res*, **87**, 3320-30.
187. Wu, K.Y., Hengst, U., Cox, L.J., Macosko, E.Z., Jeromin, A., Urquhart, E.R. and Jaffrey, S.R. (2005) Local translation of RhoA regulates growth cone collapse. *Nature*, **436**, 1020-4.
188. Emery, B. Regulation of oligodendrocyte differentiation and myelination. *Science*, **330**, 779-82.
189. Kapfhammer, J.P. and Schwab, M.E. (1994) Inverse patterns of myelination and GAP-43 expression in the adult CNS: neurite growth inhibitors as regulators of neuronal plasticity? *J Comp Neurol*, **340**, 194-206.
190. Erzurumlu, R.S., Jhaveri, S. and Benowitz, L.I. (1990) Transient patterns of GAP-43 expression during the formation of barrels in the rat somatosensory cortex. *J Comp Neurol*, **292**, 443-56.
191. Wang, S., Sdrulla, A.D., diSibio, G., Bush, G., Nofziger, D., Hicks, C., Weinmaster, G. and Barres, B.A. (1998) Notch receptor activation inhibits oligodendrocyte differentiation. *Neuron*, **21**, 63-75.

192. Charles, P., Hernandez, M.P., Stankoff, B., Aigrot, M.S., Colin, C., Rougon, G., Zalc, B. and Lubetzki, C. (2000) Negative regulation of central nervous system myelination by polysialylated-neural cell adhesion molecule. *Proc Natl Acad Sci U S A*, **97**, 7585-90.
193. Mi, S., Miller, R.H., Lee, X., Scott, M.L., Shulag-Morskaya, S., Shao, Z., Chang, J., Thill, G., Levesque, M., Zhang, M. *et al.* (2005) LINGO-1 negatively regulates myelination by oligodendrocytes. *Nat Neurosci*, **8**, 745-51.
194. Demerens, C., Stankoff, B., Logak, M., Anglade, P., Allinquant, B., Couraud, F., Zalc, B. and Lubetzki, C. (1996) Induction of myelination in the central nervous system by electrical activity. *Proc Natl Acad Sci U S A*, **93**, 9887-92.
195. Barres, B.A. and Raff, M.C. (1993) Proliferation of oligodendrocyte precursor cells depends on electrical activity in axons. *Nature*, **361**, 258-60.
196. Stevens, B., Porta, S., Haak, L.L., Gallo, V. and Fields, R.D. (2002) Adenosine: a neuron-glial transmitter promoting myelination in the CNS in response to action potentials. *Neuron*, **36**, 855-68.
197. Holmes, G.L. and Stafstrom, C.E. (2007) Tuberous sclerosis complex and epilepsy: recent developments and future challenges. *Epilepsia*, **48**, 617-30.
198. Wong, M. (2007) The utility of tuberless models of tuberous sclerosis. *Epilepsia*, **48**, 1629-30; author reply 1632-4.
199. Potter, C.J., Pedraza, L.G. and Xu, T. (2002) Akt regulates growth by directly phosphorylating Tsc2. *Nat Cell Biol*, **4**, 658-65.
200. Wong, M., Ess, K.C., Uhlmann, E.J., Jansen, L.A., Li, W., Crino, P.B., Mennerick, S., Yamada, K.A. and Gutmann, D.H. (2003) Impaired glial glutamate transport in a mouse tuberous sclerosis epilepsy model. *Ann Neurol*, **54**, 251-6.

201. Wu, X., Sosunov, A.A., Tikoo, R., Weiner, H.L., Crino, P.B. and McKhann, G.M., 2nd (2005) Glutamate transport is impaired in the human tuberous sclerosis tissue. . *Epilepsia*, **46**
202. Franz, D.N. (2007) mTOR in tuberous sclerosis and other neurological disorders. *Epilepsia*, **48**, 1630-1; author reply 1632-4.
203. Crino, P.B., Trojanowski, J.Q., Dichter, M.A. and Eberwine, J. (1996) Embryonic neuronal markers in tuberous sclerosis: single-cell molecular pathology. *Proc Natl Acad Sci U S A*, **93**, 14152-7.
204. Thiele, E.A. (2004) Managing epilepsy in tuberous sclerosis complex. *J Child Neurol*, **19**, 680-6.

VITA

Sharon Win Way was born in Taipei, Taiwan in 1983. Her family moved to Tucson, Arizona, for 7 years before moving back to Taiwan, when Sharon was 9. After graduating from National Experimental High School in Hsinchu, Taiwan, she attended Rice University and received her Bachelor of Arts in Biosciences and her Bachelor of Arts in Psychology in May 2005. She then pursued a doctorate in Human Molecular Genetics from the University of Texas Health Science Center at Houston, which was awarded December 17, 2010.